Table 5-3 Eigenvectors and Eigenvalues of Chip Samples

| | Z( 1) | Z( 2) | Z( 3) | Z( 4) | Z( 5) | Z( 6) | Z( 7) | Z( 8) | Z( 9) | Z(10) | Z(11) | Z(12) |
|---|---|---|---|---|---|---|---|---|---|---|---|---|
| Au | 0.13296 | 0.25362 | -0.38583 | 0.57564 | -0.09516 | -0.56050 | 0.00974 | -0.08479 | 0.07414 | -0.30575 | -0.03739 | 0.08303 |
| Cu | 0.41340 | -0.07698 | 0.04077 | -0.26982 | -0.23074 | -0.08134 | -0.17575 | -0.07352 | 0.25652 | -0.34873 | 0.28467 | -0.61976 |
| Mo | 0.11845 | 0.43518 | -0.13145 | -0.43709 | 0.51640 | 0.07545 | 0.20235 | -0.08334 | 0.04655 | -0.44220 | -0.23873 | 0.11539 |
| Pb | 0.27341 | 0.31919 | -0.26090 | 0.25729 | -0.00472 | 0.53897 | 0.24994 | 0.05353 | -0.19309 | 0.08728 | 0.53677 | -0.01513 |
| Zn | 0.36605 | -0.18793 | -0.20534 | -0.35111 | -0.16565 | -0.11983 | -0.33416 | -0.17620 | -0.19572 | 0.00420 | 0.23231 | 0.62326 |
| Ag | 0.01938 | 0.51802 | 0.18267 | -0.03755 | -0.46781 | 0.19355 | -0.29200 | 0.40570 | 0.32167 | -0.03197 | -0.18680 | 0.22572 |
| As | 0.37830 | 0.18412 | -0.34123 | -0.09373 | 0.05555 | -0.05014 | -0.12708 | -0.10131 | 0.00131 | 0.64715 | -0.41545 | -0.27265 |
| Se | 0.36126 | -0.01458 | 0.26863 | -0.04316 | 0.15824 | -0.36025 | 0.17874 | 0.68609 | -0.36385 | 0.05131 | 0.04753 | -0.02211 |
| Hg | 0.23460 | 0.24879 | 0.59342 | 0.05380 | 0.04498 | -0.22258 | 0.27867 | -0.43232 | 0.26912 | 0.27220 | 0.18982 | 0.17133 |
| F | 0.25229 | -0.39690 | -0.13330 | 0.17492 | 0.34469 | 0.14519 | 0.03027 | 0.27526 | 0.68402 | 0.04927 | 0.01848 | 0.20792 |
| Ba | 0.29862 | -0.04154 | 0.35868 | 0.40831 | 0.28735 | 0.27960 | -0.51599 | -0.16329 | -0.25580 | -0.20243 | -0.23027 | -0.02554 |
| Tl | 0.32679 | -0.28208 | 0.03773 | 0.05525 | -0.43954 | 0.22391 | 0.52513 | -0.10787 | -0.09666 | -0.20435 | -0.46833 | 0.08944 |
| Eigenvalue | 3.85860 | 2.15094 | 1.16862 | 1.05814 | 0.74918 | 0.70649 | 0.51249 | 0.47030 | 0.45158 | 0.34391 | 0.29399 | 0.23578 |
| *Proportion* | *0.32155* | *0.17925* | *0.09739* | *0.08818* | *0.06243* | *0.05887* | *0.04271* | *0.03919* | *0.03763* | *0.02866* | *0.02450* | *0.01965* |
| Accum. Prop. | 0.32155 | 0.50079 | 0.59818 | 0.68636 | 0.74879 | 0.80766 | 0.85037 | 0.88956 | 0.92719 | 0.95585 | 0.98035 | 1.00000 |

# CHAPTER 5 DRILLING SURVEY

## 5-1 Outline of the Diamond Drilling

### 5-1-1 Objective of Diamond Drilling

As a result of geological and geochemical surveys carried out in the initial phase of the project, an epithermal-gold-type ore deposit was expected as a promising target for future exploration in the Piren Hill Area. In the second phase, a drilling survey consisting of two holes (total hole length 300m) was *planned and successively carried out in order to explore underground* emplacement of the epithermal-gold-type ore deposit, and to investigate and unravel the relationship between the emplacement conditions of the ore deposit and the results of geological and geochemical surveys.

The purpose of each hole is as follows;

MJTC-1 : exploration of gold mineralized area (Davulgılı Hill) discovered on the surface.

MJTC-2 : exploration of gold mineralized area (Davulgılı Hill) and gold anomalous area as found by geochemical survey on the surface.

### 5-1-2 Outline of Drilling Operation

(1) Location of drill holes

| No. | X | Y | Z [m sea level] | Direction | Dip |
|---|---|---|---|---|---|
| MJTC-1 | 79150 | 20760 | 364 | N40° E | -50° |
| MJTC-2 | 79580 | 20920 | 382 | S40° W | -50° |

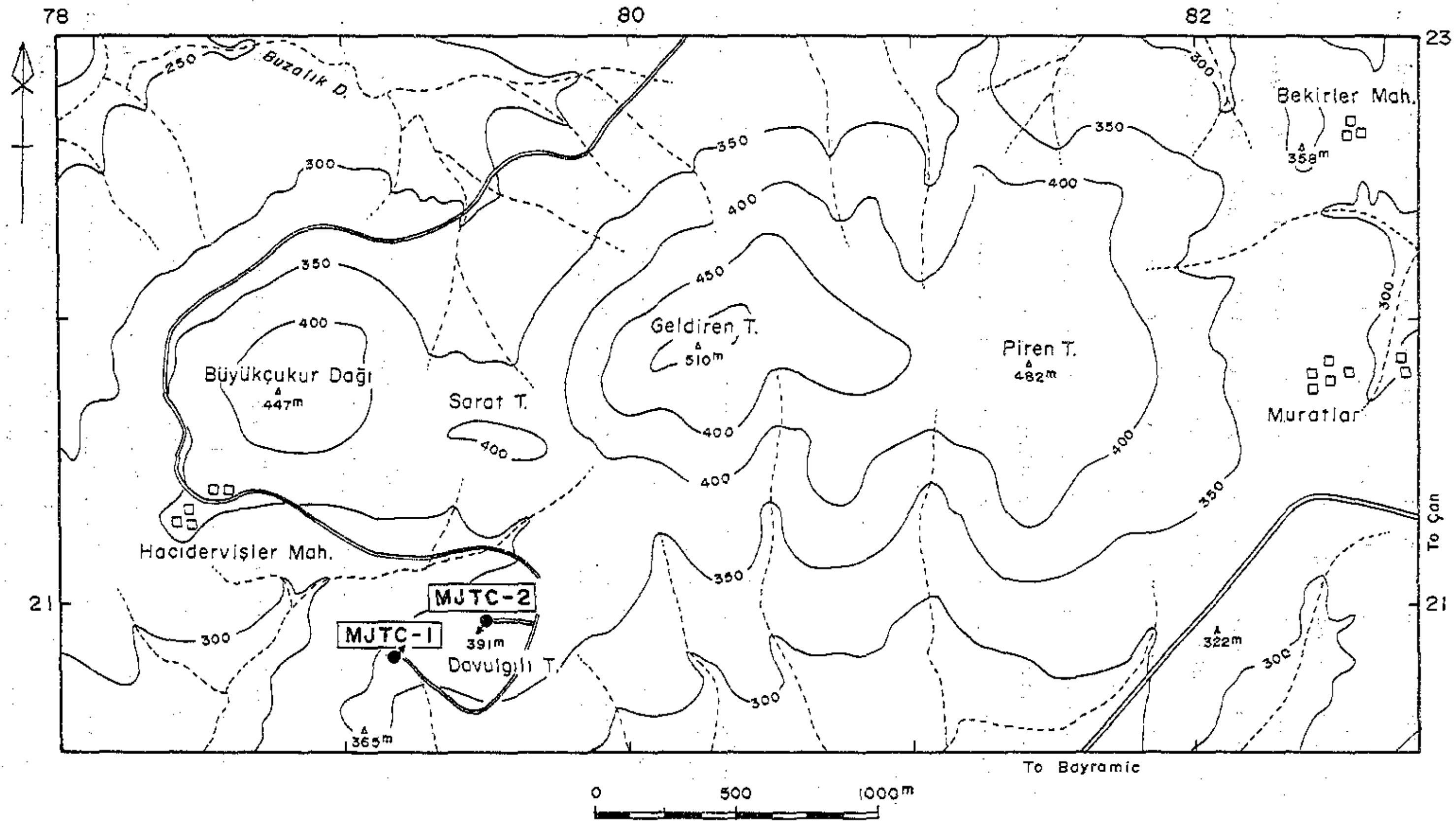


Fig. 5-4 Location Map of Drill Holes in the Piren Tepe Area

(2) Drilling operation method

The wire line drilling method using an NQ-type diamond bit as far as possible was applied. Drill inclinations were inlined -50°.

(3) Core survey

A geological columnar section 1/200 in scale was complied, and colour photographs of all collected drill cores were taken.

(4) Chemical assay of drilling cores

Whole collected cores were split along the core extension, and half-pieces of the split core were chemically assayed to detect gold and silver content for the enter section, while selected samples were analyzed for gold, silver, copper, lead, zinc, antimony, mercury and molybdenum content.

(5) Laboratory studies of the core

Microscope observations of rock thin sections and ore polished specimens, measurement of homogenization temperature and salinity of fluid inclusions, and detection of altered minerals by X-ray diffraction meter were performed.

5-1-3 Holes Drilled

Drill Holes Performed

| No. | Length Drilled | Surface Soil | Core Length | Core Recovery | Period |
|---|---|---|---|---|---|
| MJTC-1 | 151.00m | 0.00m | 145.75m | 96.5% | Aug.14~Sep.12 |
| MJTC-2 | 151.00m | 0.00m | 130.05m | 86.1% | Aug.14~Sep.19 |

5-2 Drilling Operation

5-2-1 Drilling Method

The drilling operation was performed by means of the wire line method using a diamond drilling bit of NQ size at MJTC-1 and MJTC-2 sites which had exposed bedrock at the surface.

Bentonite mud water was circulated during drilling in order to reduce torque resistance caused by collapse in the hole.

Geology of the Piren Hill Area consists of silicified and argillized andesite. At the predominantly alterated sections of rocks in the hole, the rocks are soft and brittle and have many well-developed cracks and fissures which often cause loss of circulating mud water and much flash water. On the other hand, strongly silicified rock is very hard to drill.

5-2-2 Drilling Machine, Equipment and Consumables

Longyear L-38 and Acker were used for the drilling operation. Types and specifications of the machines, engines, pumps and equipment, and amount of consumables are shown in Table 2-5, 2-6 and 2-7.

5-2-3 Operation Members and Shifts

The operation of move-in and move-out from site to site, and preparation work in the site were performed by a shift-per-day system, while the actual drilling operation was carried out by three shifts per day with eight working hours per shift. One drilling shift consisted of five members, a Japanese driller, a Turkish assistant driller [MTA] and three Turkish workers.

5-2-4 Transportation and Road Construction

The drilling machines, equipment and consumables were transported from the Northwest Anadol Regional Office of MTA located in Balıkesir to a place near these drilling sites by a large truck, and then to the drilling sites by a small truck. As there was no access road, a new 0.75km road for MJTC-1 and MJTC-2 was constructed by bulldozer.

5-2-5 Water Supply

The water necessary for the drilling operation was carry by two tractors from a nearby well.

5-2-6 Withdrawal

After completion of the drilling survey at Piren Hill, the drilling machines and equipment were transported to the MJTC-5 and MJTC-6 sites at Arlık Stream.

5-3 Results of Diamond Drilling

5-3-1 MJTC-1

As altered andesite of the Şapçı Volcanics was exposed at the surface of the site, the hole was drilled using an NQ diamond bit, and circulating mud water, and was reamed with HW and NX casing shoe bits. HW and NX casing pipes were inserted through the argillized zones to 3.1m and 9.30m. Below 9.30m, an NQ wire line method, and bentonite mud water were used for the drilling operation. The drilling was completed at 151.00m.

The lithology of this drill hole consists of strongly argillized rocks (0～73.00m), silicified and argillized andesite (73.00～119.10m), and fractured andesite (119.10～151.00m).

Table 5-4 Record of the Drilling Operation at MJTC-1

| | Drilling length | | | Total | | Shift | | Working men | |
|---|---|---|---|---|---|---|---|---|---|
| | Shift 1 | Shift 2 | Shift 3 | Drilling | Core length | Drilling | Total | Engineer | Worker |
| | m | m | m | m | m | shift | shift | man | man |
| 13 Aug | Holiday | | | | | | | | |
| 14 Aug | Prds | | | | | | 1 | 2 | 4 |
| 15 Aug | Prds | | | | | | 2 | 2 | 4 |
| 16 Aug | Prds | | | | | | 3 | 2 | 4 |
| 17 Aug | Prds | | | | | | 4 | 2 | 4 |
| 18 Aug | Prds | | | | | | 5 | 2 | 4 |
| 19 Aug | 4.05 | | | 4.05 | 3.85 | 1 | 6 | 1 | 4 |
| 20 Aug | Holiday | | | | | | | | |
| 21 Aug | 6.90 | | | 10.95 | 10.75 | 1 | 7 | 2 | 4 |
| 22 Aug | 2.95 | | | 13.90 | 13.10 | 1 | 8 | 2 | 4 |
| 23 Aug | 9.15 | | | 23.05 | 22.25 | 1 | 9 | 2 | 4 |
| 24 Aug | 9.15 | | | 32.20 | 30.05 | 1 | 10 | 2 | 4 |
| 25 Aug | 10.60 | | | 42.80 | 39.30 | 1 | 11 | 2 | 4 |
| 26 Aug | 7.00 | | | 49.80 | 44.80 | 1 | 12 | 2 | 4 |
| 27 Aug | Holiday | | | | | | | | |
| 28 Aug | 6.30 | | | 56.10 | 51.10 | 1 | 13 | 2 | 4 |
| 29 Aug | MW | 6.70 | | 62.80 | 57.80 | 2 | 15 | 2 | 4 |
| 30 Aug | 5.80 | 3.35 | | 71.95 | 66.95 | 2 | 17 | 2 | 4 |
| 31 Aug | 1.95 | 7.20 | | 81.10 | 76.10 | 2 | 19 | 2 | 4 |
| 1 Sep | 3.40 | 3.85 | 1.90 | 90.25 | 85.25 | 3 | 22 | 2 | 4 |
| 2 Sep | 5.20 | 3.95 | | 99.40 | 94.40 | 2 | 24 | 2 | 4 |
| 3 Sep | Holiday | | | | | | | | |
| 4 Sep | 3.05 | 4.20 | 5.80 | 112.45 | 107.45 | 3 | 27 | 3 | 12 |
| 5 Sep | 3.20 | 5.10 | 3.70 | 124.45 | 119.45 | 3 | 30 | 3 | 12 |
| 6 Sep | 2.40 | 3.05 | 6.10 | 136.00 | 131.00 | 3 | 33 | 3 | 12 |
| 7 Sep | 2.35 | Reco | 5.35 | 143.70 | 138.45 | 3 | 36 | 3 | 12 |
| 8 Sep | 3.70 | 1.95 | 1.65 | 151.00 | 145.75 | 3 | 39 | 3 | 12 |
| 9 Sep | Dism | | | | | | 40 | 1 | 4 |
| 10 Sep | Holiday | | | | | | | | |
| 11 Sep | Dism | | | | | | 41 | 1 | 8 |
| 12 Sep | Dism | | | | | | 42 | 1 | 8 |
| Total | 87.15 | 39.35 | 24.50 | 151.00 | 145.75 | 34 | 42 | 53 | 152 |

Abbreviations

Roco ; Road construction

Prds ; Preparation for drilling site

Tran ; Transportation

TRRE ; Transportation and Reassemblage

MW ; Preparation of mud water

Dism ; Dismantlement

Reco ; Recovering work

INCP ; Inserting casing pipe

OUCP ; Retrieving casing pipe

Table 5-5 Record of the Drilling Operation at MJTC-2

| | Drilling length | | | Total | | Shift | | Working men | |
|---|---|---|---|---|---|---|---|---|---|
| | Shift 1 | Shift 2 | Shift 3 | Drilling | Core length | Drilling | Total | Engineer | Worker |
| | m | m | m | m | m | shift | shift | man | man |
| 13 Aug | Holiday | | | | | | | | |
| 14 Aug | Prds | | | | | | 1 | 2 | 4 |
| 15 Aug | Prds | | | | | | 2 | 2 | 4 |
| 16 Aug | 3.10 | | | 3.10 | 1.35 | 1 | 3 | 2 | 4 |
| 17 Aug | 0.15 | | | 3.25 | 1.50 | 1 | 4 | 2 | 4 |
| 18 Aug | 1.15 | | | 4.40 | 2.35 | 1 | 5 | 2 | 4 |
| 19 Aug | 1.60 | | | 6.00 | 3.60 | 1 | 6 | 2 | 4 |
| 20 Aug | Holiday | | | | | | | | |
| 21 Aug | INCP | Reco | | 6.00 | 3.60 | 2 | 8 | 2 | 8 |
| 22 Aug | Reco | Reco | | 6.00 | 3.60 | 2 | 10 | 2 | 8 |
| 23 Aug | Reco | 3.05 | | 9.05 | 4.10 | 2 | 12 | 2 | 8 |
| 24 Aug | 0.80 | - | | 9.85 | 4.40 | 2 | 14 | 2 | 8 |
| 25 Aug | Reco | - | | 9.85 | 4.40 | 1 | 15 | 2 | 8 |
| 26 Aug | Reco | 1.15 | | 11.00 | 4.60 | 2 | 17 | 2 | 8 |
| 27 Aug | Holiday | | | | | | | | |
| 28 Aug | Reco | INCP | | 11.00 | 4.60 | 2 | 19 | 2 | 8 |
| 29 Aug | Reco | Reco | | 11.00 | 4.60 | 2 | 21 | 2 | 8 |
| 30 Aug | Reco | 4.95 | | 15.95 | 7.95 | 2 | 23 | 2 | 8 |
| 31 Aug | 2.05 | 13.90 | | 31.90 | 18.85 | 2 | 25 | 2 | 8 |
| 1 Sep | INCP | 4.90 | | 36.80 | 20.95 | 2 | 27 | 2 | 8 |
| 2 Sep | 4.25 | 2.35 | | 43.40 | 24.70 | 2 | 29 | 2 | 8 |
| 3 Sep | Holiday | | | | | | | | |
| 4 Sep | 1.50 | 1.30 | | 46.20 | 27.20 | 2 | 31 | 2 | 8 |
| 5 Sep | 2.25 | 1.25 | | 49.70 | 30.80 | 2 | 33 | 2 | 8 |
| 6 Sep | 4.50 | 1.80 | | 56.00 | 35.05 | 2 | 35 | 2 | 8 |
| 7 Sep | 1.65 | - | | 57.65 | 36.70 | 1 | 36 | 1 | 4 |
| 8 Sep | 2.85 | - | | 60.50 | 39.55 | 1 | 37 | 1 | 4 |
| 9 Sep | 2.20 | 6.60 | | 69.30 | 48.35 | 2 | 39 | 2 | 8 |
| 10 Sep | Holiday | | | | | | | | |
| 11 Sep | 5.30 | 6.10 | 5.80 | 86.50 | 65.55 | 3 | 42 | 3 | 12 |
| 12 Sep | 5.50 | 4.15 | 4.50 | 100.65 | 79.70 | 3 | 45 | 3 | 12 |
| 13 Sep | 4.05 | 7.60 | 4.90 | 117.20 | 96.55 | 3 | 48 | 3 | 12 |
| 14 Sep | 4.95 | 6.35 | 3.05 | 131.55 | 110.60 | 3 | 51 | 3 | 12 |
| 15 Sep | 2.75 | 3.80 | 5.40 | 143.50 | 122.95 | 3 | 54 | 3 | 12 |
| 16 Sep | 5.35 | 2.15 | | 151.00 | 130.05 | 2 | 56 | 2 | 8 |
| 17 Sep | Holiday | | | | | | | | |
| 18 Sep | Dism | | | | | | 57 | 2 | 8 |
| 19 Sep | Dism | | | | | | 58 | 2 | 8 |
| Total | 55.95 | 71.40 | 23.65 | 151.00 | 130.05 | 54 | 58 | 63 | 244 |

Abbreviations

Prds ; Preparation for drilling site
Reco ; Recovering work
INCP ; Inserting casing pipe
Dism ; Dismantlement
MW ; Preparation of mud water
OUCP ; Retrieving casing pipe

Table 5-6 Summary of the Drilling Operation of MJTC-1

| Operation | Survey period: Period | Days | Work day days | Off day days | Total men: Engineer man | Total men: Worker man |
|---|---|---|---|---|---|---|
| Preparation | 14 ~ 18 August | 5 | 5 | – | 10 | 20 |
| Drilling | 19 August~8 Sep | 21 | Drilling 18<br>Recovering | 3 | 40 | 112 |
| Removing | 9 ~ 12 September | 4 | 3 | 1 | 3 | 20 |
| Total | 14 August~12 Sep | 30 | 26 | 4 | 53 | 152 |

| Drilling length | | | |
|---|---|---|---|
| Length planned | 150.00m | Over-burden | – m |
| Increase or Decrease in length | 151.00m | Core length | 145.75m |
| Length drilled | 151.00m | Core recovery | 96.5 % |

Core recovery of 50 m hole

| Depth of hole (m) | Core recovery (%) | Core recovery cumulated (%) |
|---|---|---|
| 0~ 50 | 90 | 90 |
| 50~ 100 | 100 | 95 |
| 100~ 151 | 99 | 96.5 |

| Working hours | h | % | % |
|---|---|---|---|
| Drilling | 152 | 54 | 44 |
| Other work | 120 | 42 | 35 |
| Recovering | 8 | 4 | 2 |
| Total | 280 | 100 | 81 |
| Reassemblage | 40 | | 12 |
| Dismantlement | 24 | | 7 |
| Water transportation | | | |
| Road construction and others | | | |
| G.Total | 344 | | 100 |

Efficiency of drilling

| | |
|---|---|
| Total m/work period (m/day) | 151.00m/18 days (8.39m/day) |
| Total m/total shift (m/shift) | 151.00m/34 shifts (4.44m/shift) |

Drilling length/bit (each sized bit)

| Bit size | HW | NX | NQ |
|---|---|---|---|
| Drilled length (m) | 3.10 | 9.30 | 151.00 |
| Core length (m) | | | 145.75 |

Casing pipe inserted

| Size | Meterage (m) | Drilling x100 / length (%) | Meterage recovery (%) |
|---|---|---|---|
| HW | 3.10 | 2 | 100 |
| NX | 9.30 | 6 | 100 |
| BQ | | | |

Direction: N40°E Incline: -50°

Table 5-7 Summary of the Drilling Operation of MJTC-2

| Operation | Survey period: Period | Days | Work day (days) | Off day (days) | Total men: Engineer (man) | Total men: Worker (man) |
|---|---|---|---|---|---|---|
| Preparation | 14 ~ 15 August | 2 | 2 | - | 2 | 8 |
| Drilling | 16 August~ 16 Sep | 32 | Drilling 28 Recovering | 4 | 59 | 220 |
| Removing | 18 ~ 19 September | 3 | 2 | 1 | 2 | 16 |
| Total | 14 August~ 19 Sep | 37 | 32 | 5 | 63 | 244 |

| Drilling length | | | |
|---|---|---|---|
| Length planned | 150.00m | Over-burden | - m |
| Increase or Decrease in length | 151.00m | Core length | 130.05m |
| Length drilled | 151.00m | Core recovery | % 86 |

Core recovery of 50 m hole

| Depth of hole (m) | Core recovery (%) | Core recovery cumulated (%) |
|---|---|---|
| 0~ 50 | 62 | 62 |
| 50~ 100 | 96 | 79 |
| 100~ 151 | 100 | 86 |

| Working hours | h | % | % |
|---|---|---|---|
| Drilling | 202 | 47 | 44 |
| Other work | 190 | 44 | 41 |
| Recovering | 40 | 9 | 9 |
| Total | 432 | 100 | |
| Reassemblage | 16 | | 3 |
| Dismantlement | 16 | | 3 |
| Water transportation | | | |
| Road construction and others | | | |
| G.Total | 464 | | 100 |

Efficiency of drilling

| | |
|---|---|
| Total m/work period(m/day) | 151.00m/28 days (5.39 m/day) |
| Total m/total shift (m/shift) | 151.00m/54 shifts (2.80 m/shift) |

Drilling length/bit(each sized bit)

| Bit size | HW | NX | NQ |
|---|---|---|---|
| Drilled length(m) | - | 61.0 | 151.00 |
| Core length(m) | | | 130.05 |

Casing pipe inserted

| Size | Meterage (m) | Meterage / Drilling length X100 (%) | Meterage recovery (%) |
|---|---|---|---|
| HW | | | |
| NX | 61.00 | 40.00 | 100 |
| BQ | | | |

Direction: S40° W Incline:-50°

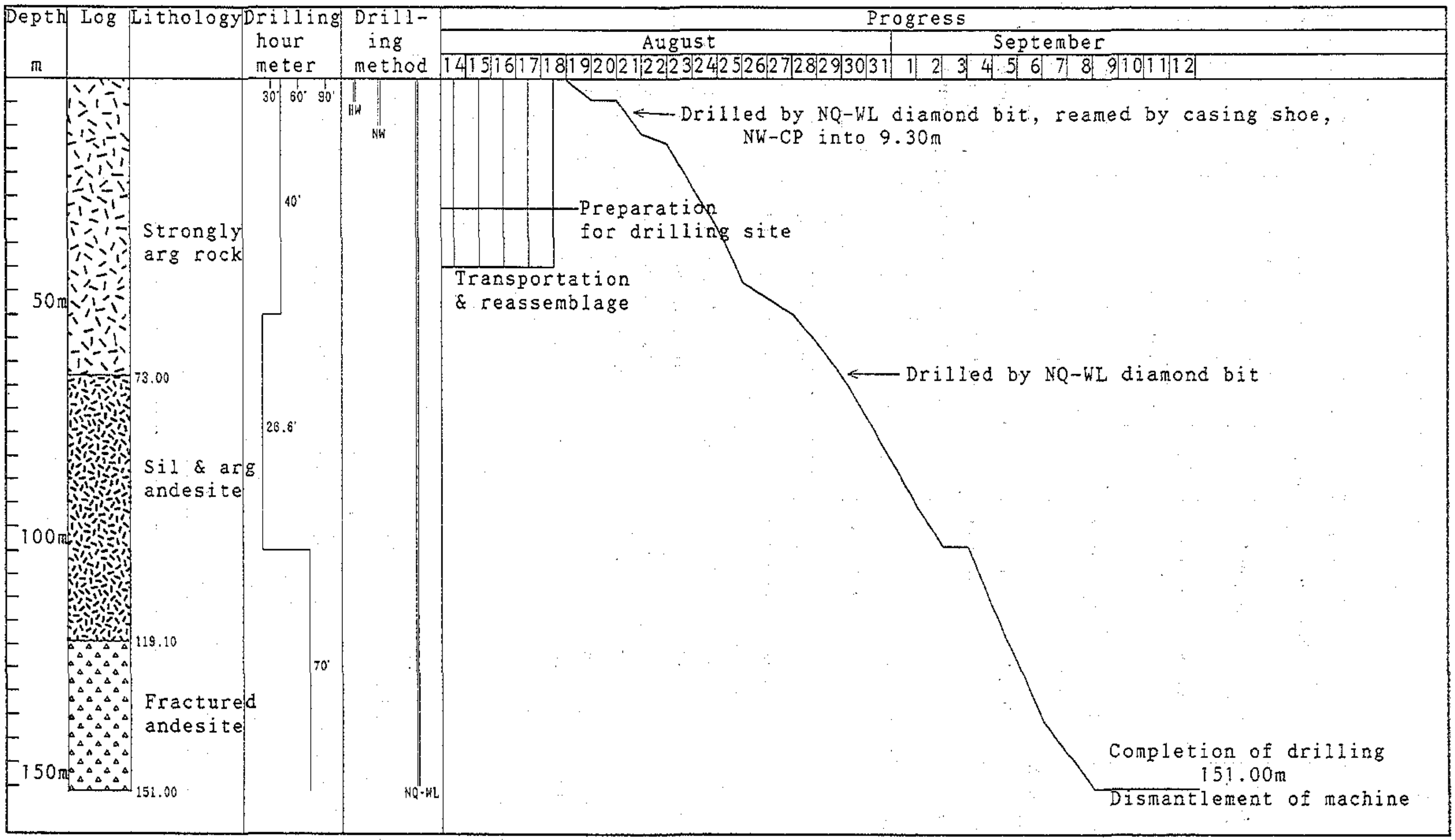


Fig.5-5 Drilling Progress of MJTC-1

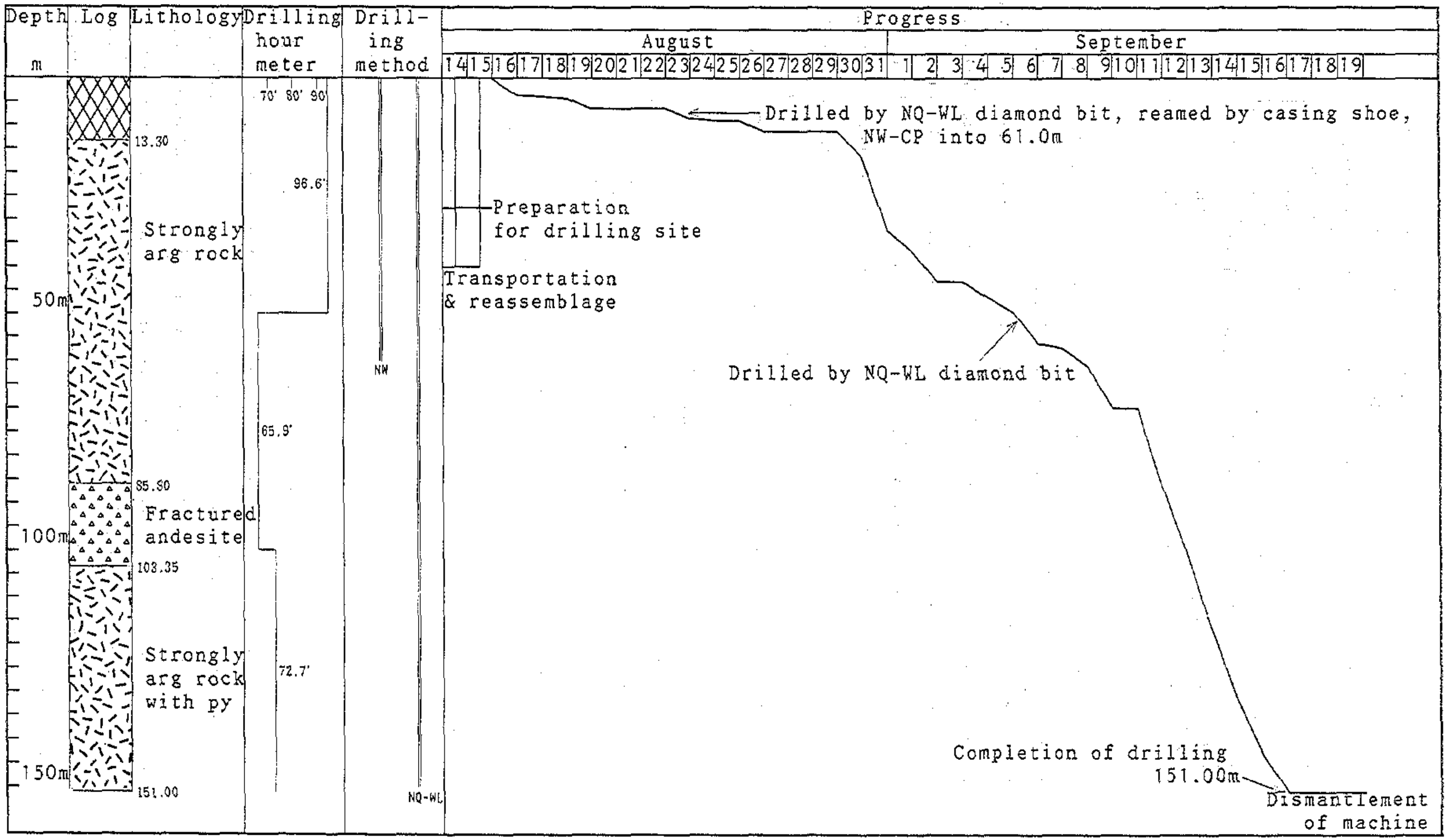


Fig. 5-6 Drilling Progress of MJTC-2

| Depth (m) | 0～9.10 | 9.10～151.00 |
|---|---|---|
| Mud Water | BMW | BMW |
| Bit Exchange(pcs) | NQWL bit(1) | NQWL bit(4) |
| Pump Pre. ($kg/cm^2$) | 1～5 | 5～10 |
| Pump Feed (ℓ/min) | 40 | 40 |
| Pump Deri (ℓ/min) | 40 | 40 |
| Bit Pre. ($kg/cm^2$) | 1,000～1,500 | 1,000～1,500 |
| Bit Rot. (rpm) | 200 | 200 |
| Core Recovery (%) | 98 | 96 |

5-3-2 MJTC-2

As a silicified zone of the Şapçı Volcanics was exposed at the surface of the site, this hole was drilled using NQ diamond bits with circulating dense bentonite mud water. After reaming with the NX casing shoe bits, NX casing pipes were inserted at 61.00m because of severe collapse of the hole wall. However, the lithology of silicified zones is hard, massive and fractured from surface to 13.30m, and unconsolidated limonitic argillized zones from 13.30m to 54.20m; therefore collapse of the wall causing loss of water circulation occurred, and the blend of cement and sand was repeatedly poured into the hole. Below 54.20m, an NQ wire line method, and bentonite mud water were used for the drilling operation. The drilling was completed at 151.00m.

| Depth (m) | 0～61.00 | 61.00～151.00 |
|---|---|---|
| Mud Water | BMW | BMW |
| Bit Exchange(pcs) | NQWL bit(6) | NQWL bit(3) |
| Pump Pre. ($kg/cm^2$) | 1～5 | 5～10 |
| Pump Feed (ℓ/min) | 40 | 40 |
| Pump Deri (ℓ/min) | 40 | 40 |
| Bit Pre. ($kg/cm^2$) | 1,000～2,000 | 1,000～1,500 |
| Bit Rot. (rpm) | 200 | 200 |
| Core Recovery (%) | 62 | 100 |

5-4 Alteration of Drill Holes

5-4-1 MJTC-1

An inclined hole (-50°) drilled through the silicified and argillized zones of Şapçı Volcanics. Silicified zones gradually decreased downward, and the argillized zone and unaltered fractured andesites increased in the subsurface. Advanced argillization took place between the silicified blocks. Altered minerals consist of montmorillonite and kaoline. Mineralization of fine-grained pyrite was observed from 26.00m to 106.00m. Below 106.00m, unaltered fractured andesites have undergone propylitization and are accompanied by chlorite and calcite.

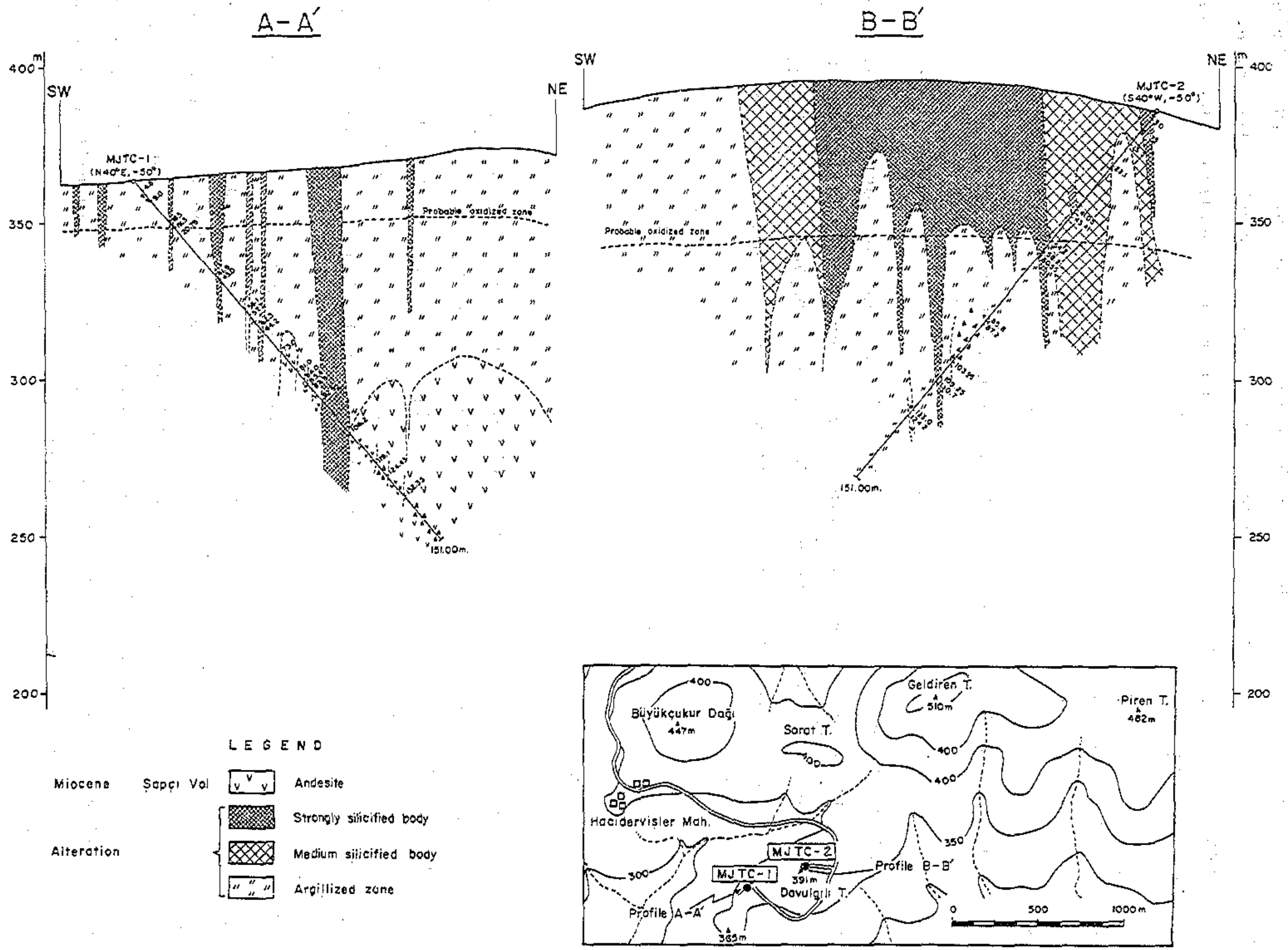


Fig. 5-7 Geologic Cross Section of Drill Holes(MJTC-1 & 2)

#### 5-4-2 MJTC-2

Silicified zones decreased downward, and argillized zones increased in the subsurface. Alteration zones accompanied by limonite exist until 54.00m, Below 54.00m, mineralization of fine-grained pyrite were observed. The altered minerals consist of kaoline until 60.00m, and mainly montmorillonite and kaoline below 90.00m.

### 5-5 Assay Results of Core

#### 5-5-1 MJTC-1

Gold mineralization was not detected by drill hole MJTC-1.

#### 5-5-2 MJTC-2

Mineralization containing gold in excess of 100 ppb was detected in the limonitic argillized zones accompanying silicified blocks from 18.00m to 54.20m. The average grade of gold is 0.7g/T for 36.20m in width. In the zones, silver, antimony and mercury content is higher than in other mineralization zones.

## CHAPTER 6 DISCUSSION

### 6-1 Alteration Zones

The alteration zones of the Piren Hill area distributed at Piren Hill, Büyükçukur Mountain, and Davulgılı Hill. Piren alteration zones are the largest scale in the vicinity; its scale is 2km long east-west and 1km wide north-south. Gold was detected from chip samples collected during two years. The auriferous samples were significant at Davulgılı Hill and southeast of Piren Hill.

The silicified zones consist of massive, brecciated and porous parts, which gradually change into each other. Generally, the massive part is in the center of the silicified zones, and the porous and brecciated parts occur in the margin. The silicified zones often result in protruding topography and they can be identified by air photographs. The silicified zones accompanied by limonite and hematite due to oxidation, the quantity of limonite is low in the massive part, and high in the porous part.

### 6-2 Alteration of the Deeper Zone

Two drill holes, MJTC-1 and 2, were inclined -50°. The lithology of two drill holes were mainly argillized rocks. The thickness of silicified zones became thin in the subsurface. However, the auriferous limonitic argillized zones continued from surface to the lower section in hole MJTC-2. Argillized zones accompanied by pyrite dissemination occur surrounding the silicified zone excepting the oxidation zones accompanied by limonite. Native sulfur locally occurs in the upper part of MJTC-1.

### 6-3 Gold and Silicified Zone

It is significant that gold was detected in the chip samples collected from the Davulgılı and Piren alteration zones, as well as drill hole MJTC-2. The results of the second phase indicate the possibility of medium-scale low-grade gold deposits in the alteration zones.

## CHAPTER 7 CONCLUSIONS AND RECOMMENDATIONS

### 7-1 Conclusions

The geology consists of Şapçı Volcanics in this vicinity. The original rocks cannot be distinguished in the altered zones. The volcanic rocks become thick with distance from the geologic basement. Altered zones with limonite and hematite are predominant on the outcrops, and pyrites are not observed because of oxidation.

Gold anomalies were detected in the silicified zones located in the southern part of the large alteration zone. The zones extend in an E-W direction in the vicinity of Piren Hill. The auriferous zones, which occur in limonitic clay such as those in fault zones, were detected by drill hole MJTC-2. Silicified zones are considered to be "jellyfish-shaped" in geologic section.

### 7-2 Recommendations for the Third Phase

Gold anomalies were detected in the silicified zones which are located in the southern part of the large alteration zone. Also, the zone extends in an E-W direction in the vicinity of the Piren Tepe. The auriferous zone was found by drill hole MJTC-2 in the Davulgılı silicified zones belonging to the concession of MTA. During the third phase, drilling survey should be carried out in the southeastern part of the Piren silicified zones

# PART VI DIKMEN AREA

# PART VI DİKMEN AREA

## CHAPTER 1 GEOLOGICAL SURVEY OF THE DIKMEN AREA

### 1-1 Outline

The Dikmen area locates in the southwestern part of Zone C. The basement rocks of this zone are the Emeşe Formation composed of green schist, pelitic schist and crystalline limestone and Ovacık Granite(Triassic). The Emeşe Formation occurs widely in the southern part of the zone, and it is overlain unconformably by the Sarısuvat Formation in the northern part. The Sarısuvat Formation comprises sandy limestone, and the age is Late Jurassic.

Cretaceous sediments are lacking here, and the Karanlık Formation was deposited in the Tertiary. The lower part of this formation is the Kızılcık Member, which is believed to be the basal conglomerate, and the upper part consists of the Kirazlıgeçit Member composed of alternating siltstone and sandstone. These are considered to be flysch-type sediments.

Eocene and Miocene volcanics are lacking, and Akkayrak Volcanics consisting of post-Late Tertiary dacite overlie the Karanlık Formation unconformably.

As for intrusive rocks, Late Cretaceous to Eocene granodiorite(Dikmen granite) and porphyry are distributed in the area. The porphyry molybdenum (copper) deposit associated with these intrusive rocks was discovered, and it is considered that epithermal mineralization occurred after the porphyry molybdenum mineralization.

### 1-2 Objective of the Survey

A significant result of the survey during the first phase is that the auriferous rocks were found from chip samples collected in the upstream section of Sığırirek Stream, and that the mineralization zones bearing molybdenum were detected in downstream of Sığırirek Stream. Geological and geochemical surveys were conducted in the Dikmen Area, and geophysical surveys of IP and SIP methods were carried out to clarify the downward extension of mineralization zones

### 1-3 Contents of the Survey

The contents of the survey are shown in the following table:

| Survey | Laboratory Studies | Quantity | Components for Analysis |
| --- | --- | --- | --- |
| Geol. S. Geoch. S ($12km^2$) | Chip Samples | 112pcs | Cu, Pb, Zn, Au, Ag, Mo, Hg, As, F, Ba, Tl, Se |
| | Ore Analysis | 10pcs | Au, Ag, Cu, Pb, Zn, Sb, Hg, Mo |
| | Total Rock | 2pcs | $SiO_2$, $TiO_2$, $Al_2O_3$, $Fe_2O_3$, MnO, MgO<br>CaO, $Na_2O$, $K_2O$, $P_2O_3$, LOI, FeO |
| | Thin Section | 2pcs | |
| | Polished Section | 10pcs | |
| | X-ray Diffractive M. | 3pcs | |
| | Isotopic Age | 2pcs | K-Ar Method |
| Geophysical Prospecting | IP Method (2 line) | 4km | 160 point |
| | SIP Method(2 line) | 4km | 160 point |
| | SIP Test | 34pcs | |

# Chapter 2 GEOLOGY OF DIKMEN AREA

## 2-1 General Geology

The Dikmen area locates in the southwestern part of Zone C. The geology of this area consists mainly of the Late Triassic Emeşe Formation, Eocene Karanlık Formation, and Pleistocene Akkayrak Volcanics. The stratigraphic column, geologic map, cross sections, and mineralization and alteration map are shown in Figures 1-5, 6-1 and 6-2.

## 2-2 Stratigraphy

### 2-2-1 Emeşe Formation

Distribution: This formation is widespread in this area.

Lithology and occurrence: This formation is composed mainly of green schist which was derived from basic volcanic rock, metagabbro, black pelitic schist, metasediments derived from sandstone, conglomerate and crystalline limestone (marble). Green schist becomes more abundant downward and pelitic schist upward. Green schists are usually greyish green, sometimes light brown, greyish brown and reddish brown in colour, and are of different softnesses to break down. Fine-grained metamorphosed sandstones are characteristic of this formation. Bedding of the sandstones is not very good and show thin to medium thickness. Schistosity is parallel to the bedding. Silicification and limonitization are the alteration types observed on the rocks which are also cut by dense quartz veinlets.

Crystalline limestones are usually greyish in colour, highly fractured and bear vugs. Silicification and limonitization are the alteration types observed in these rocks although they are not common. Saccharoidal texture showing marbles are also locally observed. It is believed that this texture was formed by the temperature effect related to a granite intrusion.

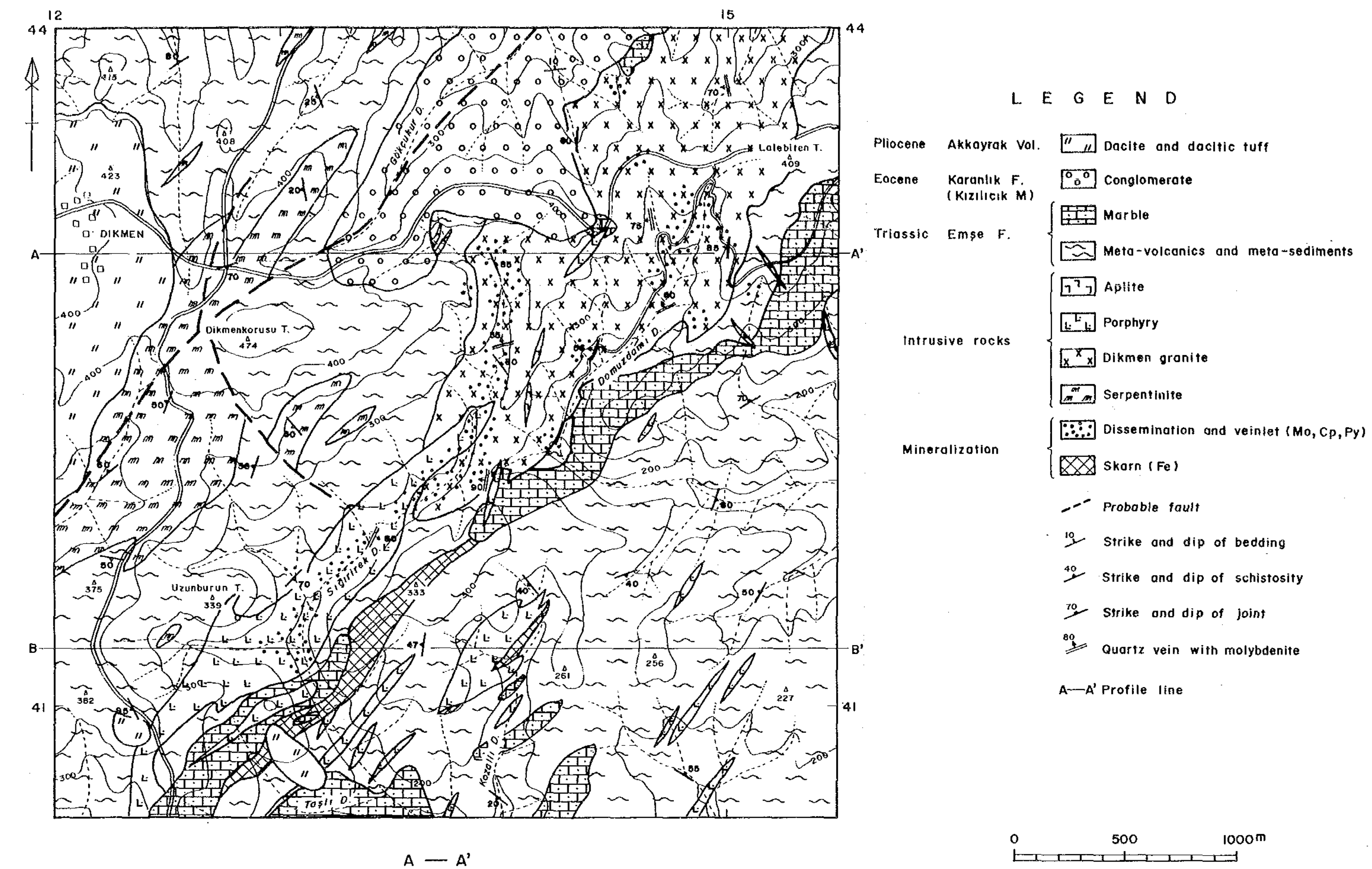


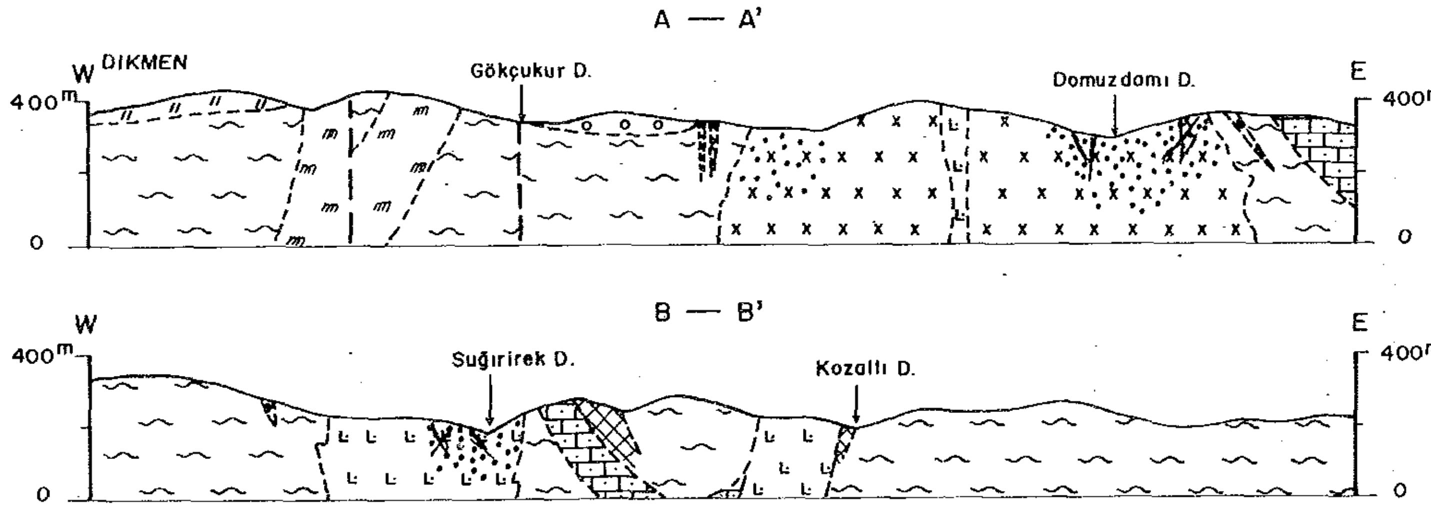


Fig. 6-1 Geologic Map and Cross Sections of the Dikmen Area

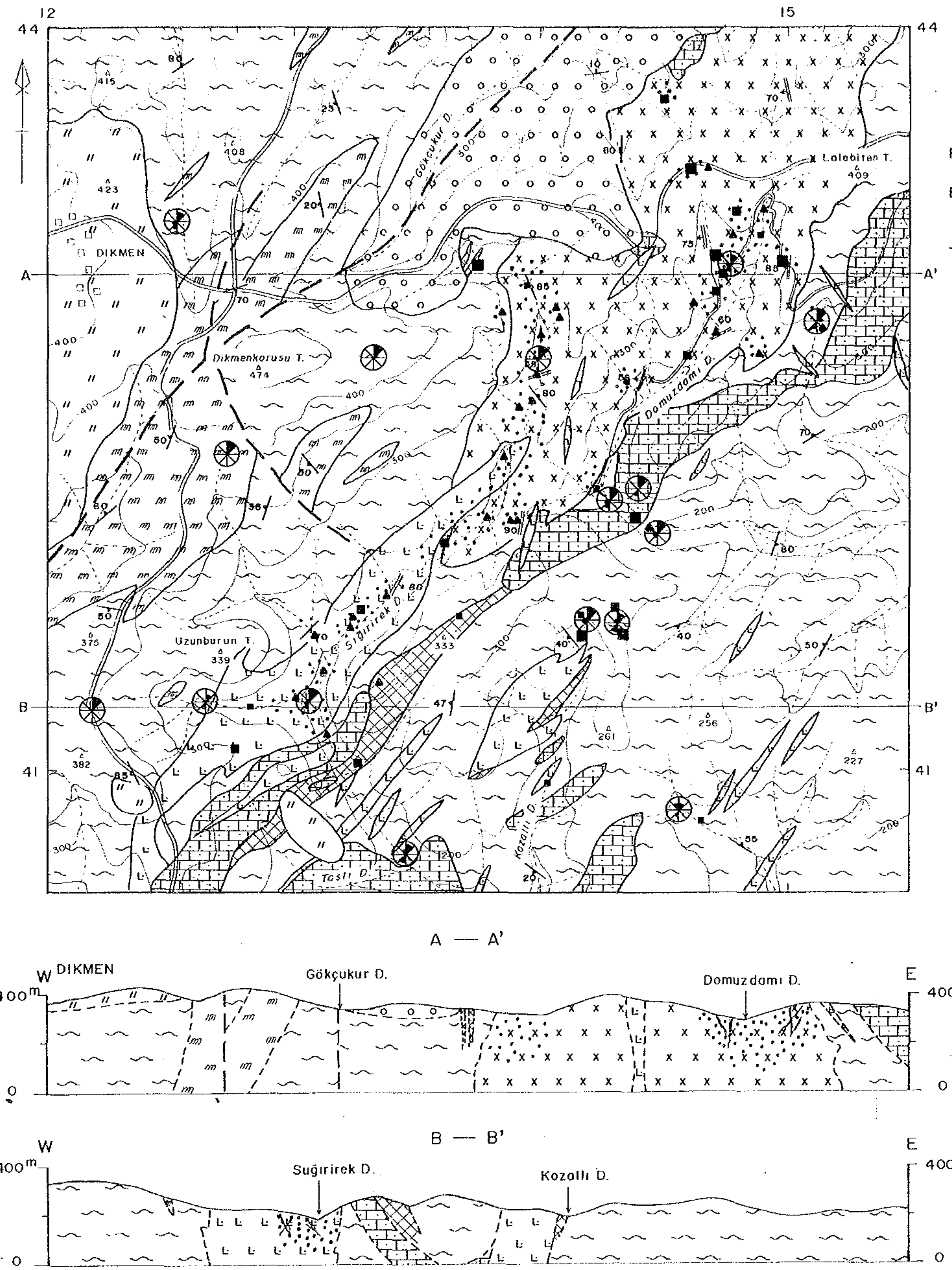


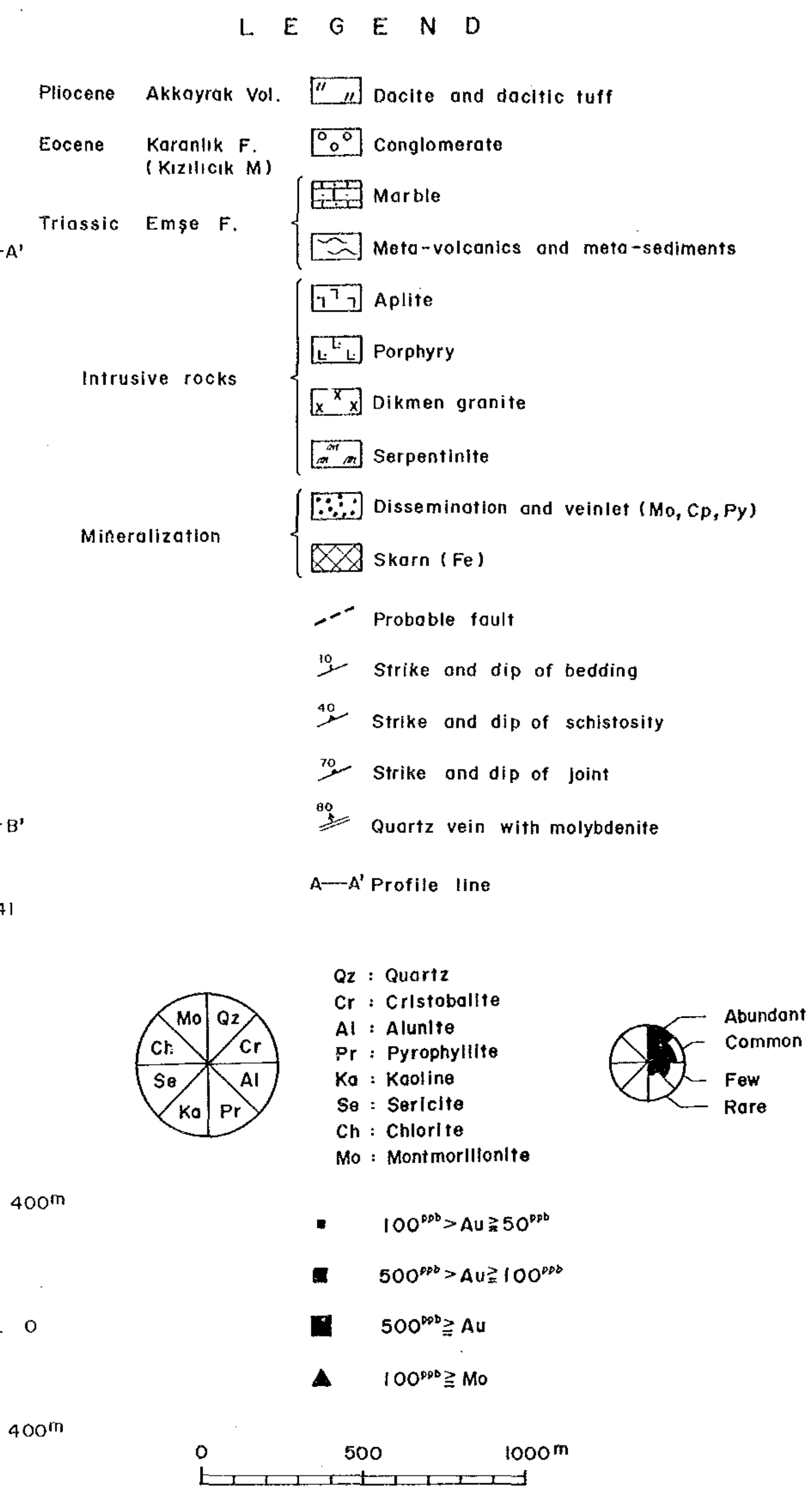


Fig. 6-2 Mineralization and Alteration Map of the Dikmen Area

This formation has been weakly metamorphosed, and a series of fold structures are revealed. The crystalline limestone of the southern part can be correlated by considering the schistosity of the pelitic schists as bedding and thus interpreting the geology. All of the above are in the same horizon including massive olistoliths.

### 2-2-2 Karanlık Formation (Kızılcık Member)

Distribution: This member occurs in the midstream section of Gökçukur Stream.

Lithology and occurrence: The formation is pale gray in colour and consists of poorly consolidated porous conglomerate with pebbles of 5~6cm size. The pebbles are not well rounded and show subrounded to plate forms. The bedding and sorting of the conglomerate are poor. The rocks are oxidized by weathering and are discoloured. The pebbles are green schist, metavolcanics, marble and metasediments. The matrix is predominantly quartz and micas.

### 2-2-3 Akkayrak Volcanics

Distribution: The rocks are distributed in the vicinity of Dikmen Village, and two localities in the south of Uzunburu Hill.

Lithology and occurrence: The major components of this unit are greyish-white to pale yellow dacite lava with flow structure and dacitic pyroclastic rocks. The lower beds of this unit are exposed in the southern part and most of them are greyish-white to pale yellow tuff. These volcanics are generally argillized by weathering and diagenesis. X-ray diffraction showed the constituent to be montmorillonite, kaoline and other clay minerals. Bedding is not observed and the, structure of the unit is difficult to clarify, but the general layout indicates a synclinal structure with a depression along the Biga River.

## 2-3 Intrusive Bodies

### 2-3-1 Serpentinite

This unit has intruded into the Emeşe Formation mainly along the Dikmen Fault. It is approximately 500m wide and over 3km long. Serpentinite also occurs in small scale in the northeastern part of Dikmen Village. Similar rock is distributed outside of the survey area, and is considered to be latest Triassic (SIYAKO 1987).

### 2-3-2 Dikmen Granite

This granite occurs at two localities along Sıgırirek Stream and the upstream section of Domuzdamı Stream.

At the Sığırirek Stream upstream portion, it is 500m wide and 3km long in the same direction as the Dikmen Fault. Dikmen Granite has coarse-grained crystals and is greyish white in colour. It is generally formed by coarse plagioclase, quartz potassium feldspars and biotite crystals. Plagioclases were locally argillized while biotites are partially altered, giving yellowish colour to the rock. The rocks were usually cut by quartz veinlets which have up to 50cm thickness. The number of quartz veins and veinlets together with pyritization and molybdenite increase from north to south along the Sığırirek Stream. Molybdenite-bearing quartz veins generally trend between N60°E and N60°W with northward dip.

The same rocks also crop out at the northern part of Domuzudamı Stream with the same texture, minerals and colours. Plagioclase and biotite are also altered in a similar way in the Domuzdamı Stream. The granite, which is cut by quartz veins and aplite dykes bearing partially pyrite, chalcopyrite and molybdenite, was observed to consist of coarse crystals of plagioclase, quartz, biotite and hornblende.

Regarding the age of intrusion, similar rock intruded into the latest Cretaceous melange, and is overlain by Neogene sediments. Thus the intrusion is inferred to have taken place between the end of the Cretaceous and the Miocene (SIYAKO 1987). This evidence coincide with the isotopic age (Table 1-12). Although the rock appears unaltered to the unaided eye, alteration of potash feldspars to chlorite and epidote is observed microscopically.

2-3-3 Porphyry

Porphyries with light brownish colour and porphyritic texture are distributed in the east and southeast of Uzunburun Hill. Quartz crystals are observed as phenocryst. Argillization and silicification are locally traced. These rocks were also cut in different directions by quartz veins whose thicknesses range between a few mm to 30cm and which bear pyrite, sometimes molybdenite and rarely azurite-malachite. Outcrops of the rocks usually showing greyish white and grey colour are also observed at the west slope of Kozallı Stream, Ortaburun and Tepetarla district. Their texture is porphyritic bearing phenocryst of quartz. Plagioclases were mostly altered to sericite, biotites were usually altered, and the rock was also cut by many quartz veinlets. In addition, limonitization is sometimes traced along fractures and cracks.

The direction of intrusion is NE-SW east of the Dikmen Fault. The age of the intrusion is not clear, but is inferred to be latest Cretaceous, the same time as the Dikmen Granite intrusion.

## 2-4 Geologic Structure

The Emeşe Formation, which is widely distributed in the area, dips westward and eastward to the Dikmen Fault. The fault trends NE-SW in the eastern part of Dikmen Village. The Emeşe Formation is a folded zone with a N-S fold axis in the eastern part. The Karanlık Formation also is gently folded to the west of the Dikmen Fault. The existence of the Dikmen Fault is inferred also from Landsat image analysis, and geological survey revealed the intrusion of serpentinites, Dikmen Granite and porphyries parallel to this fault. It is inferred that unobserved fractures are developed in a NE-SW direction.

# CHAPTER 3 MINERALIZATION AND ALTERATION

Molybdenite and pyrite are traced in the Sığırirek Stream in eastern Dikmenkorsu Hill, within the granodiorite as disseminations, as strains along fractures and cracks, and quartz veins as grains or groups of grains and veinlets. Quartz veins with various directions generally bear pyrite and sometimes molybdenite are also observed in the Yaylapınarı district. The porphyries, aplites and in particular, granodiorites in Domuzdamı Stream are cut by quartz veinlets (with thicknesses between 2mm and 30cm) bearing pyrite, molybdenite and chalcopyrite as disseminated and/or veinlets. Malachite, azurite, limonite and hematite are additionally traced as fracture fillings in silicified zones of the Emeşe Formation.

The silicified zones of NEN-SWS direction are partially observed in the northern part of Sığırirek Stream within the Emeşe Formation. Silicification especially are traced within metamorphosed volcanics and sedimentary rocks of the Emeşe Formation around Dikmenkorsu Hill and northwest of the survey area as blocks which are in different sizes. They are highly limonitized and hematitized. Copper hydroxides are also associated with these silicified blocks around Karaleylek Hill and Uzunburun Hill. Advanced argillization are also always associated with the silicified blocks. Silicifications are abundant within the metamorphosed volcanic and sedimentary rocks at the southeastern part of the survey area, although advanced argillization are mainly limited to the porphyries.

CHAPTER 4 GEOCHEMICAL PROSPECTING OF CHIP SAMPLES

## 4-1 Sampling

Chip samples were collected from the $12km^2$ geological survey are in the southwestern part of Zone C. Sampling density was twenty-two samples per square kilometer. Mostly Dikmen Granite and porphyry were sampled in Zone C.

## 4-2 Analytical Methods

All the samples were analyzed by Chemex Labs Ltd., of Canada. Gold was analyzed by the wet method and atomic absorption, fluorine by SPECIFIC ION method, arsenic, selenium, mercury barium and thallium by atomic absorption spectrometry, and other elements by ICP-AES method. The limits of detection of the elements and results of chemical analysis are shown in Table 2-1 and Table 4 of the Appendix.

## 4-3 Statistical Analysis of the Chemical Results

### (1) Outline of Method

Basic statistical values and correlation matrix of the chemical values of the chip samples were calculated and principal component analysis was carried out in the same manner as in the first phase.

Table 6-1 Basic Statistical Values of Chip Samples

(Number of Samples:269)

| Element | Mean | Dispersion | S.D. | Min. | Max. |
|---|---|---|---|---|---|
| Au | 6.446 | 0.470 | 0.686 | 2.50 | 10000.0 |
| Cu | 37.369 | 0.416 | 0.645 | 1.00 | 10000.0 |
| Mo | 7.242 | 0.776 | 0.881 | 0.50 | 3550.0 |
| Pb | 19.939 | 0.791 | 0.889 | 1.00 | 10000.0 |
| Zn | 64.625 | 0.545 | 0.739 | 1.00 | 10000.0 |
| Ag | 0.297 | 0.434 | 0.659 | 0.10 | 153.5 |
| As | 34.606 | 0.582 | 0.763 | 1.00 | 8900.0 |
| Se | 0.171 | 0.052 | 0.228 | 0.10 | 2.0 |
| Hg | 609.591 | 0.615 | 0.784 | 10.00 | 100000.0 |
| F | 149.645 | 0.127 | 0.356 | 20.00 | 2120.0 |
| Ba | 179.243 | 0.296 | 0.544 | 20.00 | 10000.0 |
| Tl | 0.244 | 0.188 | 0.434 | 0.05 | 84.0 |

(2) Basic Statistical Values

Basic statistical values for the 12 components with the population of all 269* samples were calculated. Of the 12 components, gold content was at times below the detection limit and thus less than 2.5ppb was used for samples below 5ppb. Copper, molybdenum, lead, zinc, arsenic, mercury, and barium contents were high while those of silver, selenium, fluorine and thallium were low. The basic statistical values are shown in Table 6-1 (*: 157 samples from the first phase and 112 samples from the second phase).

(3) Principal Component Analysis

The values for gold, many of which were below the detection limit, were processed by the same method as for the basic statistical values. Also as in the case for first phase, principal component analysis was carried out with all samples as the population. The correlation matrix is shown in Table 6-2.

It can be seen that when the elements up to an accumulated proportion of 75% are taken, the eigenvalue will generally 0.79 and the proportion 6.6%. Thus, those up to the fifth principal component express the major variations of this area.

First principal components: The components with large absolute eigenvector are copper, lead, zinc, arsenic and mercury.

Second principal components: Gold, molybdenum, silver and barium show positive while zinc and arsenic negative values.

Third principal components: Fluorine, barium and thallium show positive values.

Fourth principal components: Copper, molybdenum and selenium show positive while barium and thallium show negative values.

Fifth principal components: Molybdenum and selenium show positive while gold, copper and zinc show negative values.

The above are the components with high absolute eigenvectors. The first principal components are metallic elements and they express the variation caused by epithermal mineralization. These are the elements with high content in the mineral showings in all five areas.

The proportion is somewhat low but the eigenvalues are high. The second principal components are believed to show the variation of the silicified and argillized zones. The third and forth principal components are mostly non-metallic with high scores in areas excepting alteration zones. Thus these are considered to express variations caused by igneous activity and other factors. The fifth principal components are believed to indicate a portion of the mineralization because they contain metals although the proportion and the eigenvalues are low. By showing the localities with the second principal component exceeding 1 on the map (Figure 6-3), they are shown to cover most of the localities where gold and molybdenum were detected.

Table 6-2 Coefficients and Covariance Matrix of Chip Samples

| | Au | Cu | Mo | Pb | Zn | Ag | As | Se | Hg | F | Ba | Tl |
|---|---|---|---|---|---|---|---|---|---|---|---|---|
| Au | 0.470 | 0.349 | 0.291 | 0.368 | 0.180 | 0.521 | 0.251 | 0.056 | 0.274 | 0.025 | 0.180 | 0.060 |
| Cu | 0.155 | 0.416 | 0.336 | 0.201 | 0.421 | 0.283 | 0.436 | 0.226 | 0.405 | 0.232 | 0.129 | 0.132 |
| Mo | 0.176 | 0.191 | 0.776 | 0.195 | -0.128 | 0.362 | 0.004 | 0.074 | 0.311 | 0.130 | 0.194 | 0.096 |
| Pb | 0.224 | 0.116 | 0.153 | 0.791 | 0.529 | 0.662 | 0.587 | 0.121 | 0.493 | -0.041 | 0.290 | 0.241 |
| Zn | 0.091 | 0.201 | -0.084 | 0.348 | 0.545 | 0.194 | 0.661 | 0.188 | 0.391 | 0.079 | 0.074 | 0.289 |
| Ag | 0.235 | 0.120 | 0.210 | 0.388 | 0.094 | 0.434 | 0.375 | -0.023 | 0.488 | 0.013 | 0.428 | 0.121 |
| As | 0.131 | 0.215 | 0.002 | 0.398 | 0.372 | 0.189 | 0.582 | 0.275 | 0.575 | 0.009 | 0.063 | 0.375 |
| Se | 0.009 | 0.033 | 0.015 | 0.024 | 0.032 | -0.003 | 0.048 | 0.052 | 0.169 | 0.162 | -0.090 | 0.100 |
| Hg | 0.147 | 0.205 | 0.215 | 0.344 | 0.227 | 0.252 | 0.344 | 0.030 | 0.615 | 0.108 | 0.196 | 0.293 |
| F | 0.006 | 0.053 | 0.041 | -0.013 | 0.021 | 0.003 | 0.003 | 0.013 | 0.030 | 0.127 | 0.338 | 0.355 |
| Ba | 0.067 | 0.045 | 0.093 | 0.140 | 0.030 | 0.154 | 0.026 | -0.011 | 0.084 | 0.066 | 0.296 | 0.262 |
| Tl | 0.018 | 0.037 | 0.037 | 0.093 | 0.093 | 0.034 | 0.124 | 0.010 | 0.099 | 0.055 | 0.062 | 0.188 |

Table 6-3 Eigenvectors and Eigenvalues of Chip Samples

| | Z( 1) | Z( 2) | Z( 3) | Z( 4) | Z( 5) | Z( 6) | Z( 7) | Z( 8) | Z( 9) | Z(10) | Z(11) | Z(12) |
|---|---|---|---|---|---|---|---|---|---|---|---|---|
| Au | 0.27450 | 0.28178 | -0.20152 | 0.18621 | -0.35323 | 0.28251 | 0.65288 | -0.15606 | 0.12261 | 0.29204 | 0.10861 | 0.05165 |
| Cu | 0.30700 | -0.04530 | 0.09519 | 0.45005 | -0.49816 | -0.24424 | -0.19821 | 0.26053 | 0.18672 | -0.30078 | -0.22551 | 0.31770 |
| Mo | 0.18687 | 0.45850 | 0.09821 | 0.42062 | 0.31729 | -0.33509 | -0.01587 | 0.30166 | -0.36709 | 0.18814 | 0.23419 | -0.19773 |
| Pb | 0.38790 | 0.00788 | -0.25288 | -0.25393 | 0.21421 | 0.20107 | -0.06096 | 0.09734 | -0.45990 | -0.03241 | -0.05148 | 0.63744 |
| Zn | 0.32147 | -0.43439 | -0.06761 | -0.13722 | -0.31935 | -0.00840 | -0.10312 | 0.19351 | -0.34301 | 0.41596 | -0.21422 | -0.44481 |
| Ag | 0.35857 | 0.36113 | -0.21774 | -0.13005 | 0.07936 | 0.16189 | -0.06497 | -0.13582 | 0.00700 | -0.53718 | -0.33041 | -0.47300 |
| As | 0.38369 | -0.36011 | -0.12751 | -0.05745 | 0.03918 | -0.09657 | 0.01777 | -0.01434 | 0.15272 | -0.29319 | 0.75313 | -0.12523 |
| Se | 0.13253 | -0.31401 | 0.17071 | 0.48955 | 0.42071 | 0.61190 | -0.03792 | 0.12413 | 0.16536 | 0.03792 | -0.12025 | -0.05949 |
| Hg | 0.37723 | -0.02265 | -0.03371 | 0.05812 | 0.25743 | -0.33336 | -0.23813 | -0.58793 | 0.30941 | 0.37446 | -0.16719 | 0.09493 |
| F | 0.11728 | 0.02999 | 0.69822 | 0.02072 | -0.20968 | 0.16176 | -0.03139 | -0.47353 | -0.40700 | -0.14196 | 0.12697 | 0.01165 |
| Ba | 0.20309 | 0.37204 | 0.31414 | -0.38909 | -0.10862 | 0.27355 | -0.35873 | 0.32360 | 0.38574 | 0.26262 | 0.17965 | 0.01409 |
| Tl | 0.22587 | -0.14507 | 0.43820 | -0.29578 | 0.26771 | -0.29271 | 0.57229 | 0.24736 | 0.15905 | -0.09734 | -0.25845 | 0.02861 |
| Eigenvalue | 3.94881 | 1.62137 | 1.43271 | 1.18923 | 0.78651 | 0.74798 | 0.62787 | 0.47918 | 0.43947 | 0.32078 | 0.23301 | 0.17310 |
| Proportion | 0.32907 | 0.13511 | 0.11939 | 0.09910 | 0.06554 | 0.06233 | 0.05232 | 0.03993 | 0.03662 | 0.02673 | 0.01942 | 0.01442 |
| Accum. Prop. | 0.32907 | 0.46418 | 0.58357 | 0.68268 | 0.74822 | 0.81055 | 0.86287 | 0.90280 | 0.93943 | 0.96616 | 0.98558 | 1.00000 |

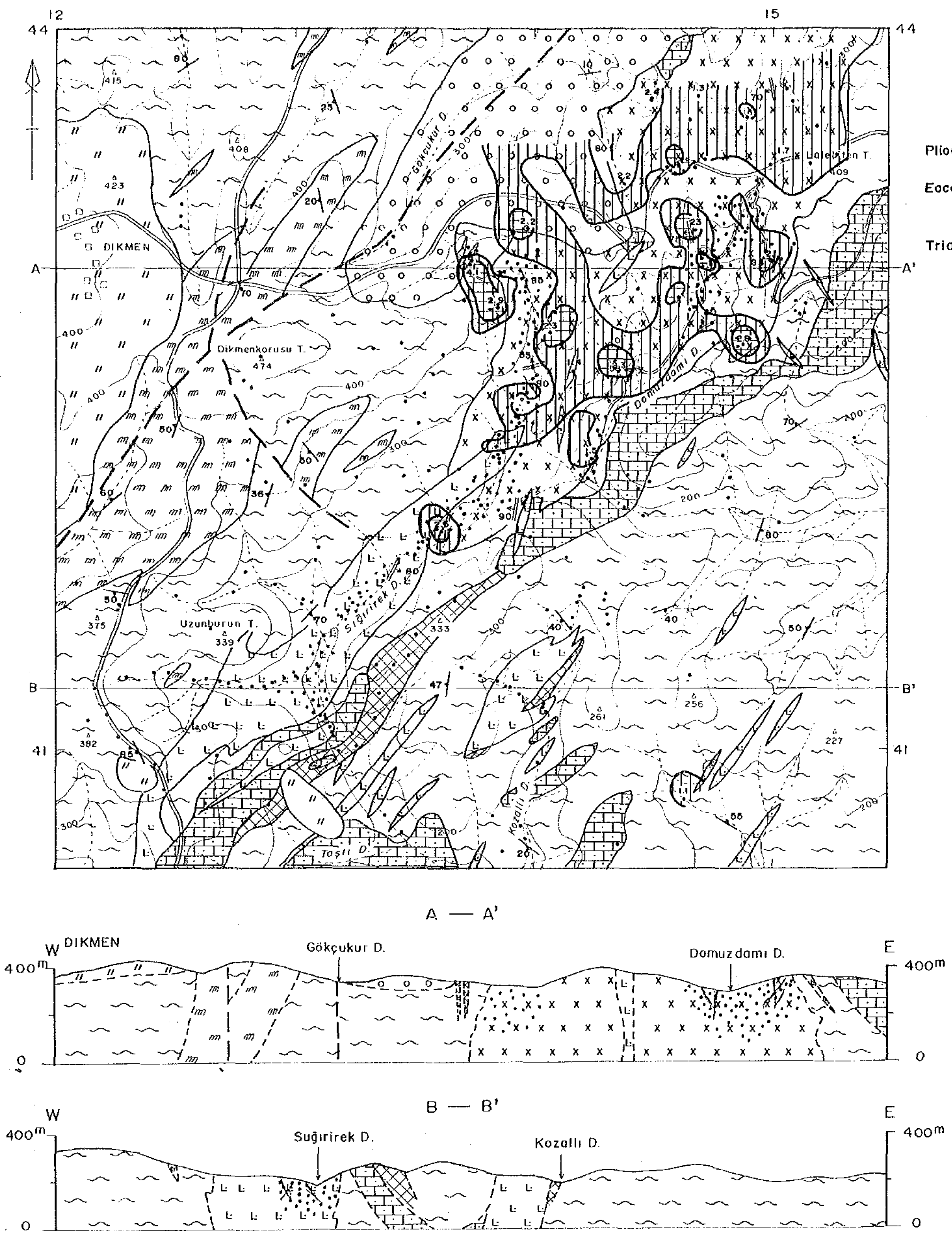


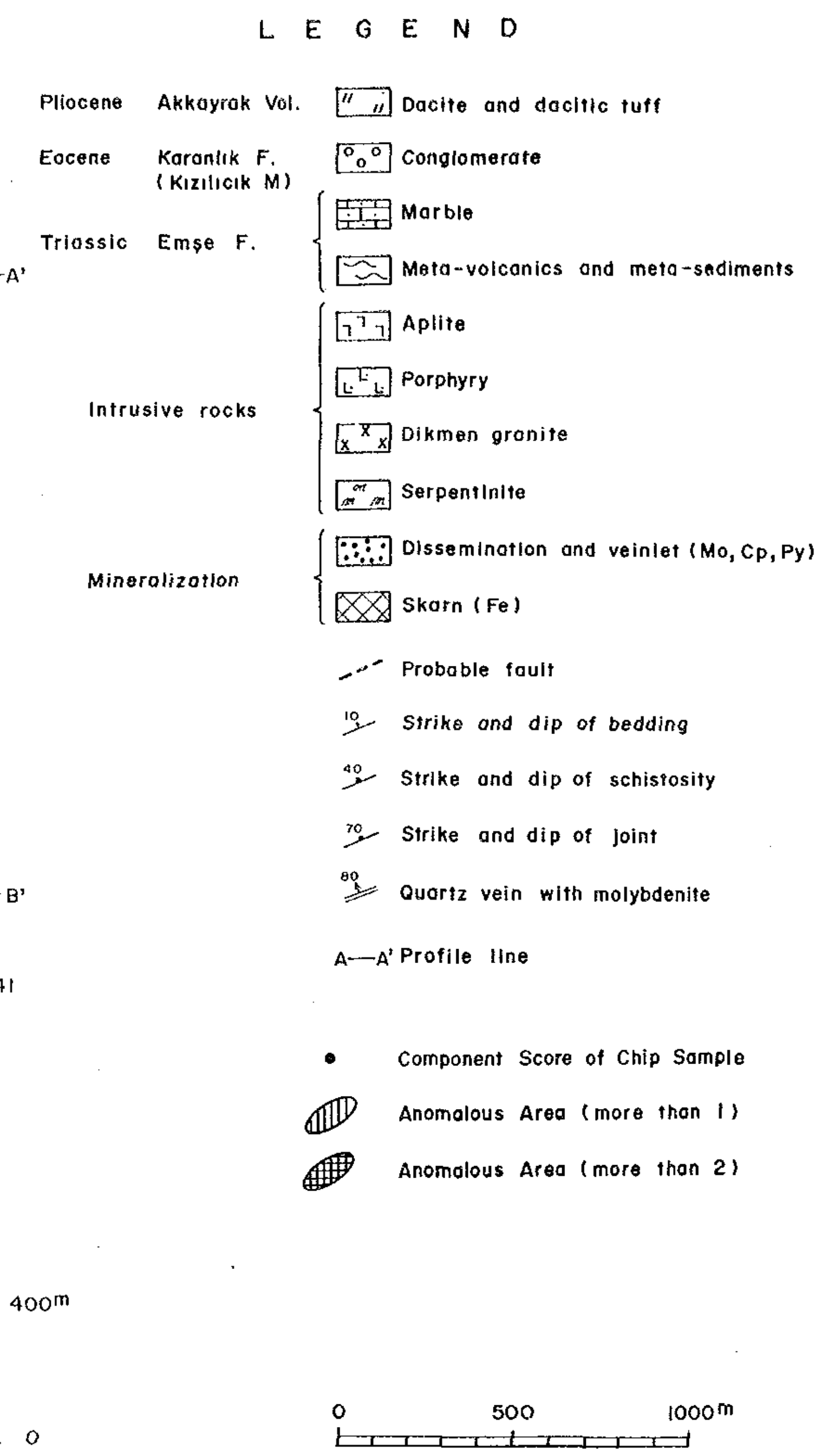


Fig. 6-3 Map of Component Scores of Chip Samples in the Dikmen Area

## CHAPTER 5 GEOPHYSICAL SURVEY (SIP AND IP METHODS)

### 5-1 Outline of the Survey

#### 5-1-1 Objectiveof the Survey

The survey refers to an area where a mineralized zone of porphyry copper type has been found through geological and geochemical surveys of the initial phase. This year, the geophysical methods of SIP and IP were used to elucidate the emplacement condition and continuity of the mineralized area.

#### 5-1-2 Area of the Survey

The area of the SIP & IP survey is situated around the confluence of Domuzudamı Stream and Sıgırirek Stream, some 2 km east of Dikmen Village. Four survey lines 1,000 m apart were laid parallel. The area and arrangement of the survey lines are illustrated in Figures 1-2 and 6-4.

#### 5-1-3 Survey Specifications

Fieldwork specifications were set as follows :

| | | |
|---|---|---|
| a. Electrode Configuration | | dipole-dipole array |
| b. Electrode Separation | | 100 m |
| c. Electrode Separation coefficient | | n = 1 ~ 5 |
| d. Measurement Method | | Frequency domain |
| e. Frequencies | SIP | 0.125 Hz~ 88 Hz(18 frequencies) |
| | IP | 0.3 Hz/ 3.0 Hz |
| f. Length of Survey Line | | 8.0 km in four lines |
| SIP: Line B,C | | 4.0 km in two lines 160 points |
| IP : Line A,D | | 4.0 km in two lines 160 points |

#### 5-1-4 Survey Methods

The SIP method is the abbreviated name of the Spectral Induced Polarization method and operates on the same principal as the conventional IP method. The SIP method measures apparent resistivity and phase difference over a frequency range of 0.01 Hz to 100 Hz, while the conventional IP method measures the difference in apparent resistivity expressed as a ratio of two frequencies. The measurement data are expressed in spectral diagrams of phase and magnitude and in Cole-Cole diagrams. Analysis of these responses allows discrimination of minerals or types of mineralization and eliminates electromagnetic coupling which occurs at low resistivity in the ground, at wide electrode separations, and with a large number of electrode coefficients.

In this survey, the Harmonic System of Zonge (USA) was applied. The IP responses over a range of 0.125 Hz to 88 Hz are measured through calculation and extraction of high frequency, using the fast Fourier transform of 3rd, 5th, 7th, 9th and 11th harmonics from three fundamental frequencies of 0.125 Hz, 1.0 Hz and 8.0 Hz.

Observation of a waveform is necessary for measurement of phase, and a communication cable which connects the transmitter with the receiver is laid parallel with the survey line separated by 25 m to 30 m. At the receiving station, response is amplified through three porous pot-electrodes in copper-saturated solution with a copper rod. Amplified responses are transmitted through the communication cable to the receiver(GDP-12/2GB). Data is processed and printed out.

5-1-5 Measuring Equipment

The equipment used in this survey are listed in Table 6-4. The illustrated diagrams of the equipment for SIP measurements as shown in Figure 6-6.

5-2 Data Processing and Rock Sample Measurement

5-2-1 IP Data Processing

Sections of percent frequency effect (PFE) and apparent resistivity (AR) were provided from pseudosections of each line. Five plan maps were prepared on each electrode separation coefficient of n = 1~ 5.

(1) PFE

The PFE value is calculated by magnitudes (M) at 0.3 Hz and 3.0 Hz as follows:

$$PFE = \frac{M(0.3\ Hz) - M(3.0\ Hz)}{M(3.0\ Hz)} \times 100 \qquad (\%)$$

(2) AR

A value of AR is calculated by the following AR

The AR value is calculated by the following equation :

$$AR = \pi a \cdot n(n+1)(n+2) \cdot V/I\ , \qquad (ohm\text{-}m)$$

where a : electrode separation in meters
n : electrode separation coefficient
V : voltage received in volts
I : transmitted current in amperes

In the present survey, the apparent resistivity at 0.3 Hz was calculated, and topographic correction was made with the computer.

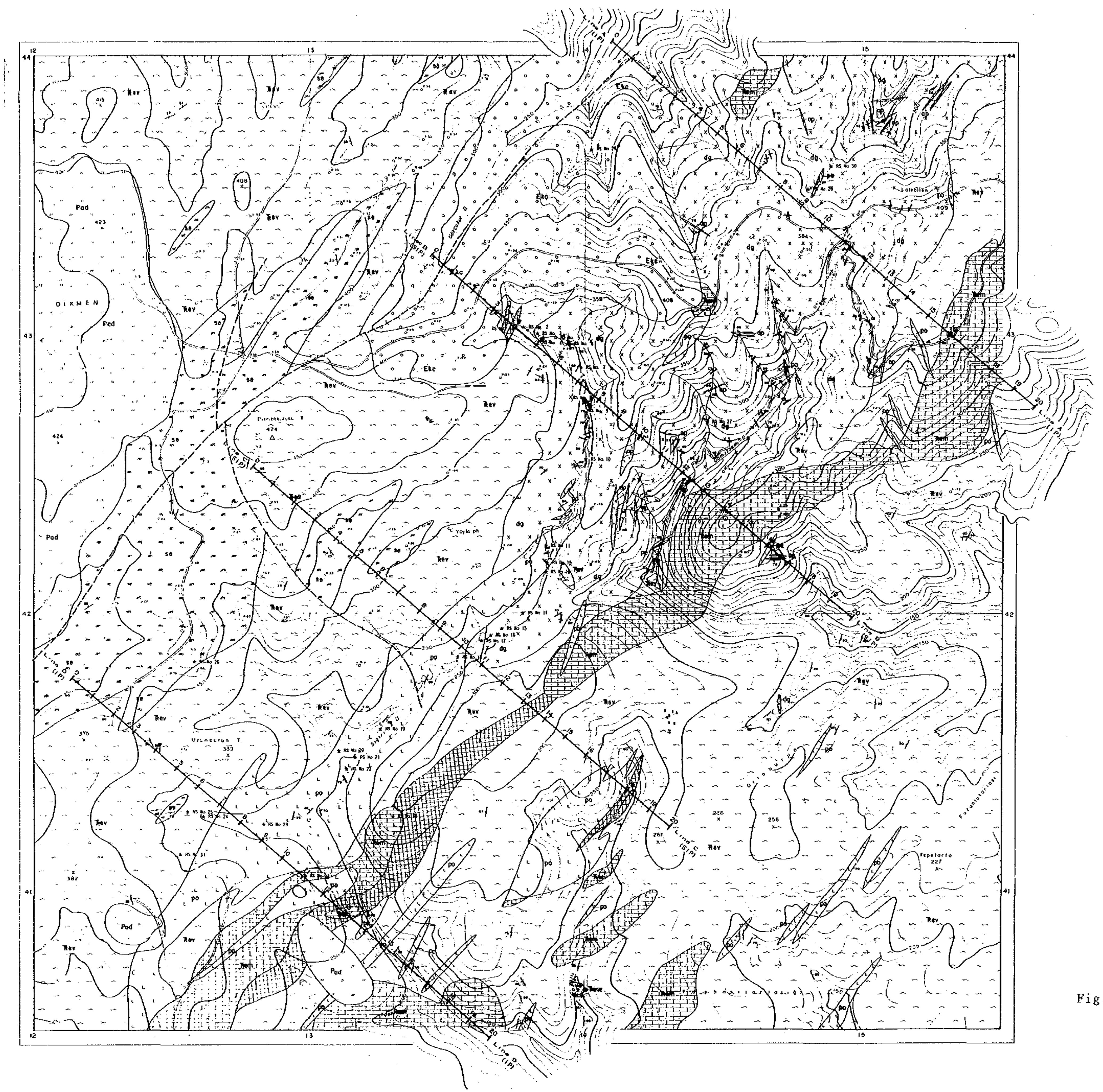


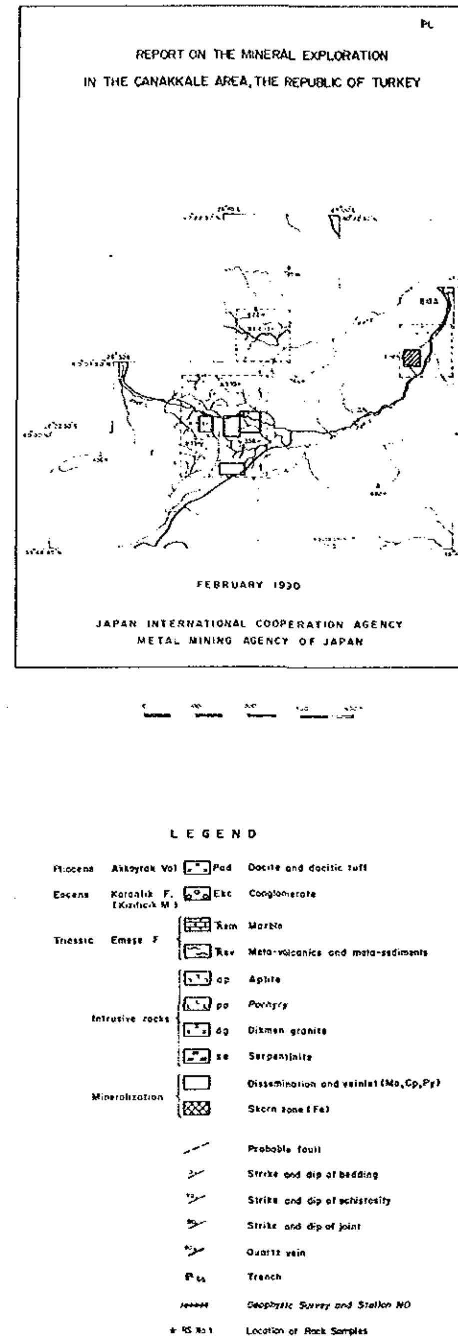


Fig. 6-4 Location Map of IP & SIP Survey Lines in the Dikmen Area

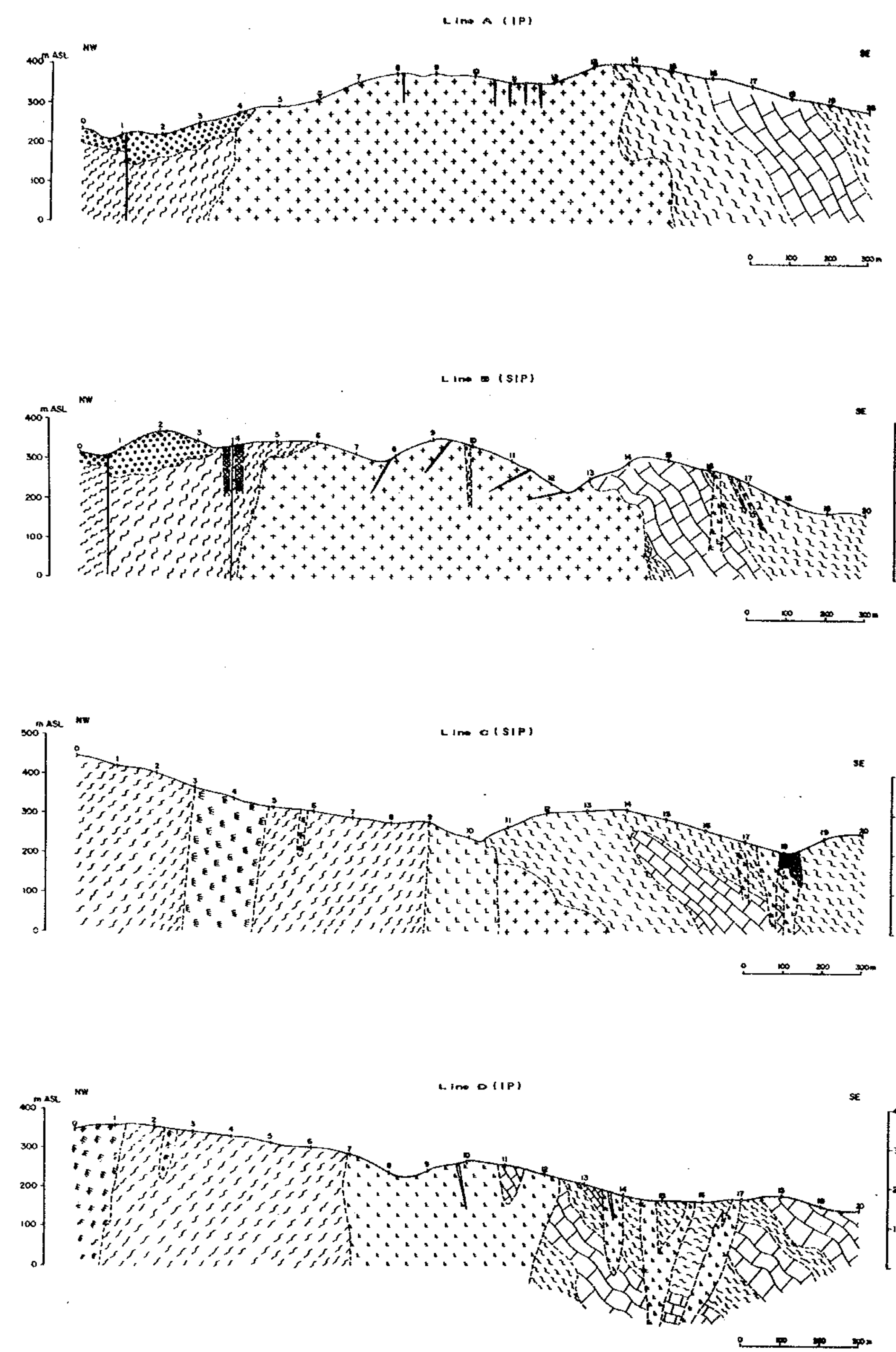


REPORT ON THE MINERAL EXPLORATION
IN THE CANAKKALE AREA, THE REPUBLIC OF TURKEY

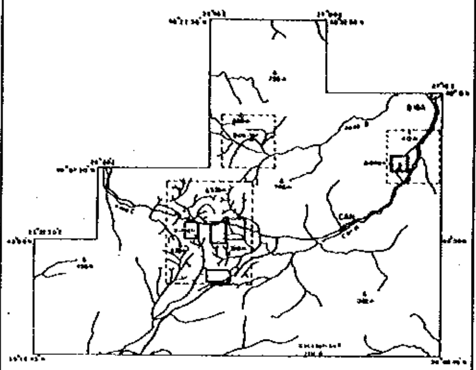


FEBRUARY 1990

JAPAN INTERNATIONAL COOPERATION AGENCY
METAL MINING AGENCY OF JAPAN

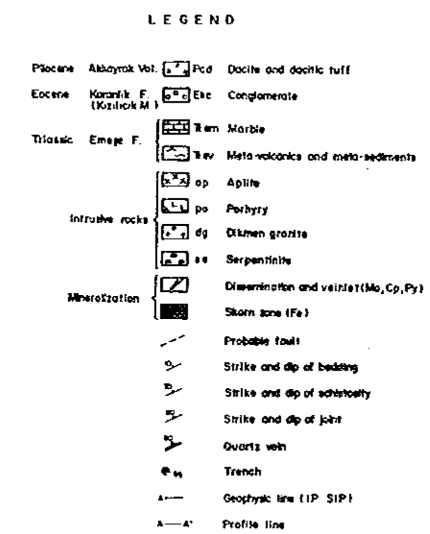


Fig. 6-5 Geological Sections of IP & SIp Survey Lines

Table 6-4 Measuring Equipment for SIP and IP Surveys

| ITEM | NAME | SPECIFICATION | QUANTITY |
|---|---|---|---|
| Transmitter System | Chiba Electric CH-86A SIP Transmitter | Output Voltage : 200, 400, 600, 800, 1000V<br>Output Current : 0.2~5.0 A<br>Wave Form : Square wave<br>Frequency : 0.125 Hz~8 Hz<br>Weight : 37 Kg | 1 |
| | Zonge XMT-1 Transmitter Controller | Frequency Range : 1/1,024 Hz~2,048 Hz<br>Weight : 5.8 Kg<br>Power : 12V Battery | 1 |
| | Chiba Electric Model 8104T IP Transmitter | Output Voltage : 200, 350, 500, 650, 800V<br>Output Current : 0.2~2.5 A<br>Wave Form : Square Wave<br>Frequency : 0.1 Hz~3 Hz<br>Weight : 14 Kg | 1 |
| Engine Generator | Zonge ZMG-5 SIP Engine Generator Honda G400 | Output Power : 5 KW<br>Frequency : 400 Hz<br>Output Voltage : 115V<br>Engine : 10 HP 4 Cycle | 1 |
| | McCulloch MK-II I P Engine Generator | Output : 2 KW<br>Frequency : 400 Hz<br>Output Voltage : 115V<br>Engine : 5 HP 4 Cycle | 1 |
| SIP Reciever System | Zonge GDP-12/2GB | Signal Input : 2 Channel<br>Frequency range : 1/8~88Hz (18 Freq.)<br>Senstivity : 0.2$\mu$V<br>Weight : 15 Kg<br>Power : 12V Battery | 2 |
| | Zonge CAP-12 Mini Cassette/ Tape Racoder | Weight : 6.2 Kg<br>Power : 12V Battery | 2 |
| | Laptop Computer NEC. PC-9800 LV21 | 16Bits : 1Mb x2 disket<br>memory : 640K byte | 1 |
| | Zonge ISO/ Isolation Amp | | 3 |
| | Zonge FP-1 Field Preamp. | | 5 |
| I P Reciever | Chiba Electric Model 8104R IP Reciever | Frequency Range : 0.1 Hz~3 Hz<br>Sensitivity : 10$\mu$V (1, 10, 100, 1000mV)<br>Weight : 3 Kg<br>Power : 006P Battery 4 pcs | 1 |
| Electrode | Currrent | Stainless $\phi$0.6cm, Length 61cm | 200 |
| | Potensial | Non Polarizable CuSO4 Porous Pot | 5 |

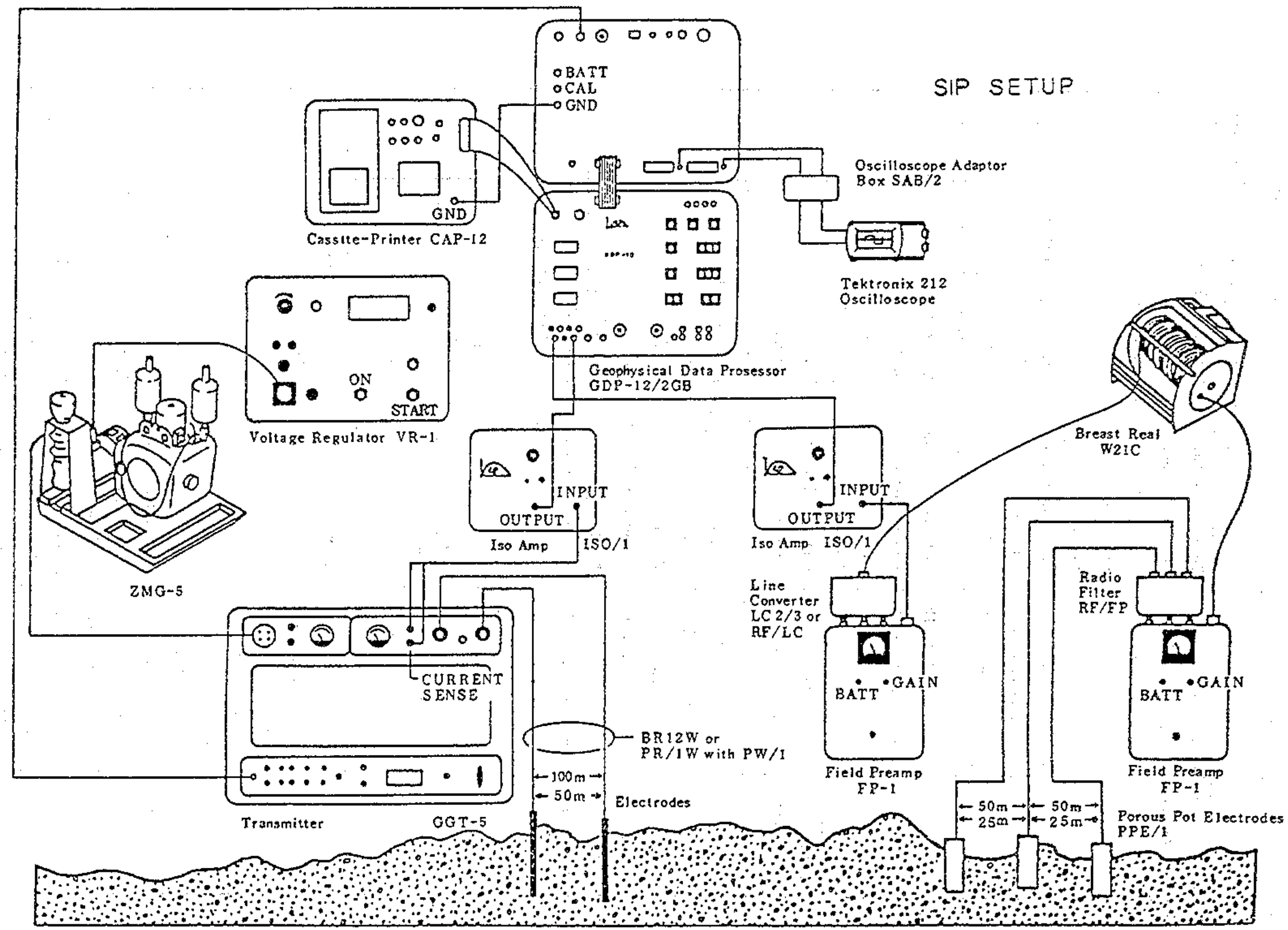


Fig. 6-6 Illustrated Diagram for SIP Equipment

5-2-2 SIP Data Processing

Data obtained in the field consist of real and imaginary parts of complex resistivity response at each frequency, apparent resistivity, phase and magnitude of received basic frequency, and so on. The following figures are determined using these data :

① Cole-Cole Diagram
② Magnitude Spectrum
③ Phase Spectrum
④ Raw Phase at five frequencies
⑤ PFE Pseudosection
⑥ Apparent Resistivity Pseudosection

Data processing and method of analysis are given as follows.

(1) Cole-Cole Diagram

In a Cole-Cole diagram, print-out data for each frequency are plotted on a coordinate by setting the negative imaginary part on the vertical axis and the positive real part on the horizontal axis. An example is shown in Figure 6-7. $\theta i$ and Mi in the figure are, respectively, phase angle and magnitude. The Cole-Cole diagram is known to display a special spectrum depending on the kind of mineral or rock.

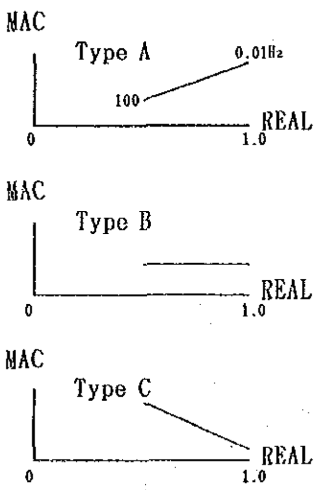


According to Zonge et al, there are three types of spectra as illustrated in the left-hand figure. Type A, showing a pattern of ascent to the right, indicates existence of sulphide minerals, graphite or strong alteration. The flat-line pattern of Type B indicates moderate alteration, and the Type C pattern of descent to the right indicates weak alteration, alluvium sediment, fresh igneous rock or limestone. Discrimination of Cole-Cole diagrams in this survey was based on this classification of the three types.

(2) Magnitude Spectrum

The magnitude refers to Mi and Mj of Figure 6-7 and is easily obtained from positive real and negative imaginary components of field data. The values are normalized by dividing by magnitude $M_0$ of minimum frequency ( 0.125 Hz). A magnitude spectrum figure is plotted by setting the magnitude value on the vertical axis and frequency on the horizontal axis (Figure 6-8). In the

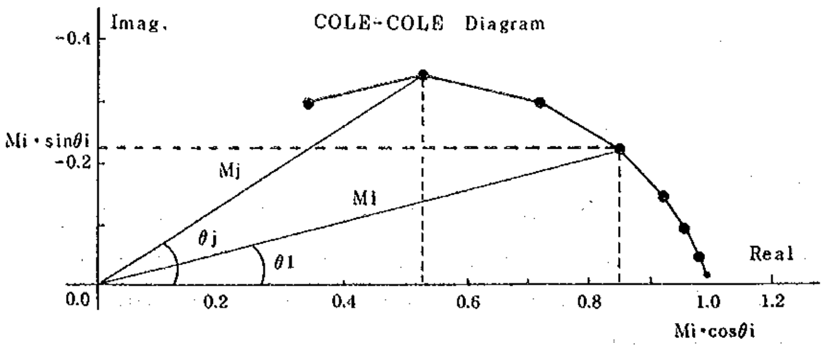


Fig. 6-7 Cole-Cole Diagram

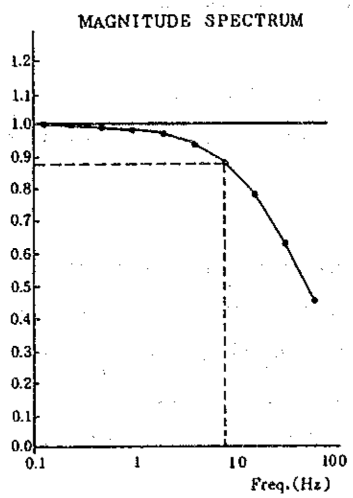


Fig. 6-8 Magnitude Spectrum

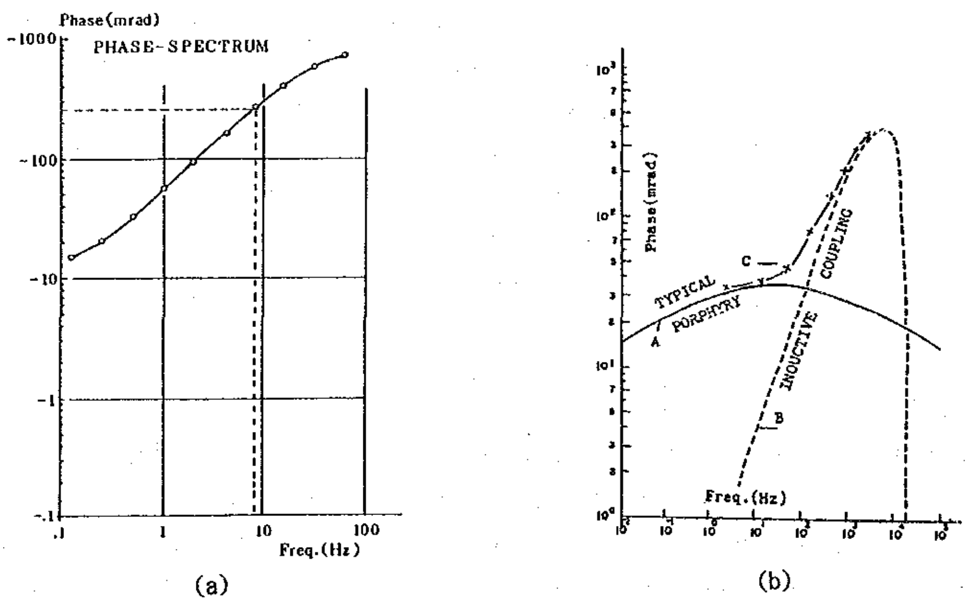


Fig. 6-9 Phase Spectrum

figure, a flat line indicates fresh rock without mineralization or alteration, whereas the spectrum line descending to high frequency indicates strong alteration, sulphide minerals and graphite.

(3) Phse Spectrum

In a phase spectrum, the vertical axis is the phase angle $\theta$ of Figure 6-7, and the horizontal axis is frequency (Figure 6-9a). Data obtained in the field survey are a combination of original IP responses (solid line A in Figure 6-9b) and pseudo-IP responses (dotted line B in Figure 6-9b ) derived from electro-magnetic coupling. Line C (-x---x-) in Figure 6-9b shows the combined IP responses. The phase spectrum indicated in Figure 6-9a was obtained through measurement.

5-2-3 Decoupling Manipulation

Decoupling denotes the removal of a false component in IP responses originating from electromagnetic coupling. The decoupling process was conducted on data over the entire lines of A and B. The decoupling procedure on the SIP measurement in this area was based on the method provided by P.G.Hallof and W.H.Pelton. The analytical method is summarized below. A complex impedance ZA(f) obtained from the SIP survey is approximated by the following equation.

$$ZA(f) = Ro[1 - m_1\{1 - \frac{1}{1+(i2\pi f\tau_1)c_1}\} - m_2\{1 - \frac{1}{1+(i2\pi f\tau_2)c_2}\} + m_3\{1 - \frac{1}{1+(i2\pi f\tau_3)c_3}\}]$$

where $m$ : chargeability
$\tau$ : time-constant
$c$ : frequency dependence
$f$ : frequency

The equation can be separated into three parts as follows :

$$1 - m_1\{1 - \frac{1}{1+(i2\pi f\tau_1)c_1}\} \qquad (i)$$

$$- m_2\{1 - \frac{1}{1+(i2\pi f\tau_2)c_2}\} \qquad (ii)$$

$$+ m_3\{1 - \frac{1}{1+(i2\pi f\tau_3)c_3}\} \qquad (iii)$$

The first nominal refers to an IP response, the second indicates electromagnetic coupling derived from a homogeneous earth and the third represents the value of electromagnetic coupling in a conductor. Ten parameters ( Ro, $m_1$, $\tau_1$, $c_1$, $m_2$, $\tau_2$, $c_2$, $m_3$, $\tau_3$, $c_3$ ) of the equation above are determined from the SIP measurement using the least squares method of a nonlinear type. Mominals (ii) and (iii), being the values of electromagnetic coupling, are removed from the equation, and only the complex impedance Zco(f) of the IP response is obtained.

$$Zco(f) = [1-m_1\{1-\frac{1}{1+(i2\pi f\tau_1)c_1}\}]$$

5-2-4 Rock Sample Measurements

In the analysis and interpretation of the survey results, it is essential to understand the SIP features of main rocks and ores distributed in the surveyed area. The measurement of SIP was conducted over samples totaling 34 pieces to investigate spectra of phase and magnitude, Cole-Cole property, percent frequency effects and resistivities. The procedure of measurement is as follows:

① Sample preparation : A cube of 3 cm is prepared.

② Saturation with water: The samples are soaked in distilled water for 24 hours.

③ Measurement : The instruments used are illustrated in Figure 6-10. Except for the laboratory transmitter, all instru ments and measuring methods are the same as those used in the field. Standard value of current was set at 50 $\mu$A.

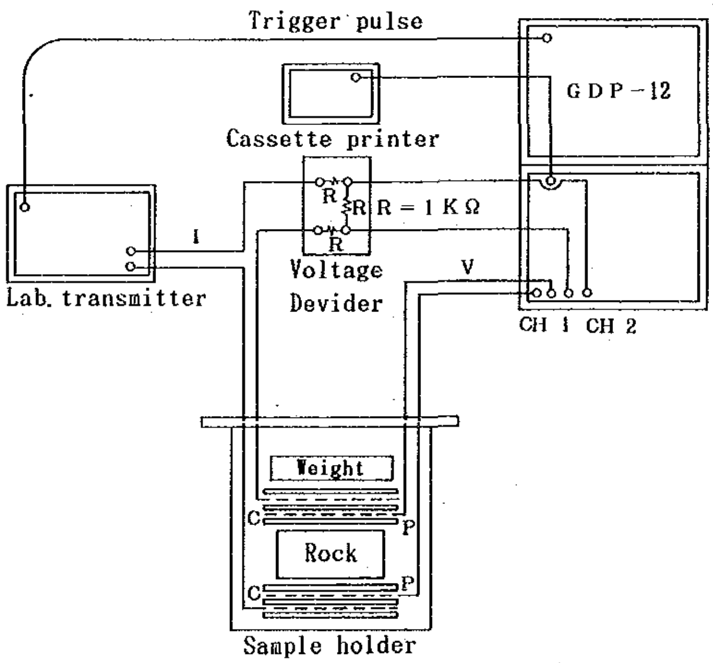


Fig.6-10 Laboratory Equipment for Rock Samples

Results of SIP Measurement of Rock Samples

The measurement results are summarized by rock type in Table 6-5. The phase spectra after plotting the rock's SIP response can be classified into seven kinds, A, B, C, D, E, F and G, as shown in Figure 6-11.

From these results the following are pointed out.

(1) By PFE value, serpentinite ranks at the top, showing 5.3%, followed by marble, silicified rock and the quartz vein, all attaining over 4%. They belong to a group of high PFE values among the rocks distributed in the present area. On the other hand, porphyry and granodiorite have a low PFE value, each being 2.2%. Green schist, widely distributed in this area, has an intermediate value of 3.3%.

(2) Many of the rock samples are generally high in resistivity. Very high values, over 10,000 ohm-m, are exhibited by the quartz vein, silicified rock, porphyry and marble. Lower resistivity is found in serpentinite and green schist, with the values of 20～270 ohm-m or so.

(3) The phase variation is within the range of 3～30 mrad values; next are granodiorite and green schist with values around 16 mrad, and the lowest value is 2.7 mrad for the quartz vein. In general, the phase variation is proportionately correlated with PFE, but no such correlation is noticed in the samples from this area. This may be explained by the fact that many samples have very high resistivity. Meanwhile, the phase variation is inversely proportionate to resistivity, and so there is a trend of increasing resistivity with decreasing towards larger resistivity value with smaller phase variation.

(4) The phase spectrum is exemplified by the mountain-shape spectrum (Type A) of Sample 32. Nearly flat-lying spectra are predominant except for some samples, and when these are excluded the spectra can be classified into six kinds (Types B～G). Little correlation is recognized between the spectral type and the rock type.

5-3 Results of Interpretation

The results of the investigation are summarized as follows. The plan maps of apparent resistivity and PFE were compiled by setting planes of n=1～5 for the electrode coefficient. The pseudosection for each survey line is represented on the panel diagram. As the apparent resistivity is found to be affected by topographic undulations, a terrain correction was applied. As for

Table 6-5 Results of Rock Sample Measurement (Dikmen Area)

| Sample No. | Rock | Resistivity (ohm-m) | PFE (%) | Phase (-m rad) | Spectrum type | Mineralization |
|---|---|---|---|---|---|---|
| 1 | Silicified Rock | 26,650 | 1.9 | 11.7 | A | |
| 13 | Silicified Rock | 208,100 | 6.7 | 6.4 | D | |
| | Average | 117,400 | 4.3 | 9.1 | | |
| 2 | Porphyry | 5,370 | 2.7 | 18.1 | B | |
| 11 | Porphyry | 5,206 | 2.3 | 19.7 | B | Py diss |
| 12 | Porphyry | 5,928 | 2.1 | 16.5 | B | |
| 18 | Porphyry | 25,200 | 3.4 | 16.8 | C | |
| 19 | Porphyry | 62,320 | -0.2 | 13.3 | D | Py diss |
| 20 | Porphyry | 5,645 | 2.7 | 16.5 | D | Py diss |
| 21 | Porphyry | 1,273 | 1.7 | 9.3 | A | Py diss |
| 22 | Porphyry | 311 | 2.8 | 14.8 | A | Py diss |
| 23 | Porphyry | 3,310 | 2.7 | 19.2 | D | |
| | Average | 12,730 | 2.2 | 20.6 | | |
| 3 | granodiorite | 2,897 | 2.4 | 15.3 | A | |
| 4 | granodiorite | 3,350 | 1.6 | 12.7 | E | Py |
| 5 | granodiorite | 9,192 | 1.3 | 15.2 | E | |
| 6 | granodiorite | 3,223 | 1.5 | 14.0 | E | |
| 10 | granodiorite | 8,055 | 4.1 | 23.3 | D | Py diss |
| 14 | granodiorite | 5,026 | 2.7 | 18.8 | D | |
| 16 | granodiorite | 14,020 | 3.0 | 17.5 | B | |
| 27 | granodiorite | 20,590 | 2.5 | 16.9 | D | |
| 29 | granodiorite | 15,070 | 1.4 | 15.9 | A | |
| 30 | granodiorite | 2,878 | 1.1 | 10.0 | A | |
| | Average | 8,140 | 2.2 | 16.0 | | |
| 7 | Quartz Vein | 249,500 | 4.3 | 3.3 | F | |
| 8 | Quartz Vein | 449,300 | 8.8 | 5.1 | F | Mo diss |
| 9 | Quartz Vein | 935,900 | -0.7 | 2.0 | E | Mo(few) |
| 15 | Quartz Vein | 67,260 | 3.5 | 1.1 | D | Py, Mo diss |
| | Average | 425,490 | 4.0 | 2.9 | | |
| 17 | green schist | 3,292 | 3.2 | 15.9 | D | |
| 24 | green schist | 922 | 1.8 | 14.0 | A | |
| 25 | green schist | 85 | 2.7 | 17.5 | A | |
| 31 | green schist | 265 | 3.1 | 14.2 | G | |
| 32 | green schist | 20.9 | 5.9 | 15.7 | A | |
| | Average | 917 | 3.3 | 15.5 | | |
| 26 | Serpentinite | 24.4 | 5.3 | 33.2 | A | |
| 28 | Sandstone | 2,100 | 0.3 | 17.2 | C | |
| 33 | Marble | 123,200 | 7.4 | 21.3 | C | |
| 34 | Marble | 44,230 | 1.4 | 37.5 | A | |
| | Average | 83,710 | 4.4 | 29.4 | | |

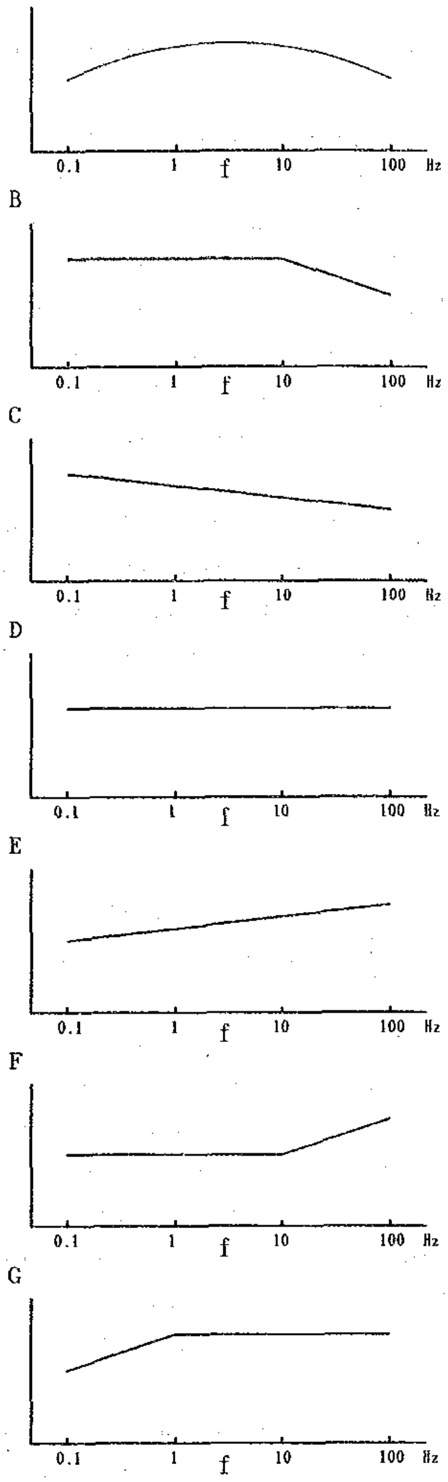


| Phase spectrum | Sample Nos. |
| --- | --- |
| Type A | 1 3, 21, 22, 24, 25, 26, 29, 30, 32, 34 |
| Type B | 2, 11, 12, 16 |
| Type C | 18, 28, 33 |
| Type D | 10, 13, 14, 15, 17, 19, 20, 23, 27 |
| Type E | 4, 5, 6, 9 |
| Type F | 7, 8 |
| Type G | 31 |

Figure 6-11 Phase Spectrum Types of Rock Samples

the SIP response, the phase variation (5 frequencies), phase spectrum, magnitude spectrum and Cole-Cole diagram are graphically represented on the pseudo section of each survey line. The post-decoupling data are presented alongside the pre-decoupling data.

The results of measurements based on these diagrams are described below.

5-3-1 Plans Map and Pseudosections of Apparent Resistivity

The apparent resistivity of the present area is in the range of 2~2,757 ohm-m. The arithmetic mean (M) is 17 ohm-m, and the standard deviation ($\sigma$) after taking common logarithms is 0.381. The values of M + $\sigma$ and M - $\sigma$ are 171 ohm-m and 80 ohm-m, respectively. The contour values, 300 ohm-m and 30 ohm-m, close to the above values, were taken as the standard values of high resistivity and low resistivity. Since the range of the apparent resistivity is wide, the contour intervals were drawn with logarithms, e.g., 10, 30, 100, 300 .....

The line space for the present investigation is 1,000 m, which is rather wide and causes difficulties in defining such features as the expanse of resistivity and the plane distribution of continuity, etc., so the investigation was performed mainly on the basis of sections of the respective lines.

Apparent Resistivity (refer to Figures 6-12~17)

As for the apparent resistivity of this area, high values are generally dominant. High values are rather widely distributed in the southeastern parts of Lines B, C and D. The zone of high resistivity is harmonious with the area of limestone distribution.

On the other hand, low values of resistivity are distributed on a small scale in the southeastern parts of Lines A and C. The sphere of their distribution is very limited, especially on the plan map, but the section (Figure 6-17), a remarkably low resistivity occurs in the distribution area of metavolcanics and metasediments in the southeastern part of Line A. Low resistivities of smaller scale are found in the central-southeastern part of Line C. Metavolcanics and metasediments are distributed also in the northeastern part of each line but not to such an extent as to constitute a low resistivity zone.

When the distribution of apparent resistivity is compared with the geology, the major rocks distributed in the present area come to show the following values of apparent resistivity:

Metavolcanics and metasediments 40~ 70 ohm-m

| | |
|---|---|
| Dikmen Granite | 50~ 200 ohm-m |
| Limestone | 200~ 3000 ohm-m |
| Serpentinite | 100~ 200 ohm-m |
| Porphyry | 40~ 200 ohm-m |

The metavolcanics and metasediments are distributed in the southeastern part and the northwestern part of all lines. In the former, they constitute a zone of low resistivity while in the latter, they show only intermediate values.

Thus, judging from the plans and sections of the apparent resistivity, the resistivity characteristic of the present area is lower than the result of the rock sample test, and the values are often intermediate, being 50~ 150 ohm-m, but in view of the distribution of the apparent resistivity, limestone in particular forms the zone of high apparent resistivity. The low apparent resistivity zone may be related either to the distribution of metavolcanics and metasediments or to the mineralized zone and groundwater.

5-3-2 Plans Map and Pseudosections of Percent Frequency Effect

The PFE values of the present area are in the range of 0.2~ 5.3%. The arithmetic mean (M) is 1.51%, the standard deviation ($\sigma$) is 0.799, and M + $\sigma$ and M + 2$\sigma$ are 1.85% and 3.11%, respectively. Accordingly, as the standard of judgment of the anomalous PFE in the present investigation, the values over 2% were assigned as weak anomalies and those over 3% to anomalies. The histogram with 0.5% divisions shows a roughly logarithmic normal distribution. The contour intervals were drawn every 0.5%. On the other hand, the results of the rock sample measurements revealed that PFE anomalies of more than 3% were found in 12 samples, accounting for 35% of the sample total.

Plans of PFE (Figures 6-18~ 22)

By isolating the weak anomaly zone (over 2% PFE) and the anomaly zone (over 3% PFE), the following are indicated.

On the N=1 plan, PFE anomalies over 2% are distributed from the southeastern part of Line B to the central-southeastern part of Line C; the former part corresponds to the distribution area of limestone and meta-volcanics and metasediments, and the latter to the porphyry distribution area.

On the N=2 plan, a weak anomaly zone, in addition to the above-mentioned anomaly zone, is found in the central part of Line D (porphyry distribution area).

On the N=3～N=5 plans, the anomaly zones show a tendency to expand. In particular, the anomaly of Line B turns to a weak anomaly zone from the line's center to the southeastern half.

These PFE anomalies correspond to the NE-trending distribution of Dikmen Granite, porphyry and limestone, so that they can be ascribed to mineralization which resulted from the intrusion of Dikmen Granite and porphyry.

By examining the downward continuity of high PFE anomalies as obtained on the plan based on the PFE section (Figure 6-23), the following can be pointed out.

The PFE anomalies detected in the southeastern end of Line B and in the central part of Line C are due to the anomaly source at a shallow depth, and the weak anomaly in the central part of Line D shows a contour pattern attributable to a deep-seated anomaly source.

The PFE anomalies located at Nos. 11～19 of Line B and at Nos. 9～19 of Line C are inferred to have originated from plural sources of anomaly at medium to deep depths. The characteristics of PFE distribution in the present area indicate that PFE anomalies in the central part to the northeastern part of the area continue in a shape which spreads out like a fan, and their occurrences are concordant with the distribution areas of porphyry, granite and limestone.

5-3-3 Pseudosection of Phase

The phase was expressed by pseudosections for 0.125, 0.375, 0.625, 1 and 3 Hz, and the phase dependence on frequency was examined. The data after the decoupling process were graphically represented as well.

Line B (Figure 2-24): By a comparative examination of sections of 5 frequencies, it was found that the sections generally show an almost identical pattern. It is thus presumed that electromagnetic coupling would be, on the whole, very rare. With a rise in frequency, particularly over 1 Hz, the 15 mrad domain tends to expand at depth (N=4, 5) in all sections, and some phenomena of electromagnetic coupling appear. As seen from the distribution of apparent resistivity of this area (Figures 6-12～17), low values of apparent resistivity, as low as under 30 ohm-m, are quite scarce (less than 3% of the total), and the resistivity values of the rock samples are large, over

1,000 ohm-m, and such values constitute 82%. These facts suggest that the resistivity of this area is large and that electromagnetic coupling is rare.

On the other hand, the pseudosections of phase after the decoupling processing present similar contour patterns for all five frequencies. These patterns agree with the phase pattern of the fundamental frequency, 0.125 Hz. Thus, it would be safe to assume that the electromagnetic coupling recognized in the over-1-Hz-frequency domain can be almost entirely excluded.

Line C (Figure 6-25): Similar to the case of Line B, the sphere of 20 mrad expands with an increase of frequency at depth (N=4, 5), and some influence of electromagnetic coupling is recognized with a frequency over 1 Hz. The pseudosections of phase after the decoupling process are similar to the sections of the fundamental frequency (0.125 Hz) for all five frequencies in that they show a decoupling effect.

5-3-4 Phase, Magnitude and Cole-Cole Spectrum

The phase spectrum, magnitude spectrum and Cole-Cole diagram are represented by pseudosections. The spectral diagram of each after the decoupling process is also given. The characteristics of these spectral diagrams are described below.

Line B (Figure 6-26)

(1) Phase spectrum: The phase in the field data shows a spectrum that gently increases between 1 and 10 Hz in the shallow part under the surface, and over 10 Hz it has an abrupt upward gradient. This is probably due to the influence of the measurement system. After decoupling, however, the phase generally shows a flat-lying or upturn spectrum. A somewhat characteristic spectrum is the one in the lower part (N=3, 4) of Sta. Nos. 8～14, which monotonously increases upward (Type E). However, the PFE values are in the range of background values, 1.0%～1.5%, and are not especially higher than the others.

(2) Magnitude spectrum: The magnitude in the field data shows a spectrum which is roughly flat at 0.125～10 Hz and becomes downturned at frequencies higher than 10 Hz, though the gradient is gentle. The magnitude spectrum after decoupling is flat-lying, showing no remarkable features. But a spectrum with a somewhat downturn trend is recognized at Sta. Nos. 17～19.

(3) Cole-Cole diagram: The shape of the spectrum cannot be defined because of the short Cole-Cole arcs owing to the small variations of phase against the changes of frequency. In the field data, a downturn spectrum of Type C is recognized in the deep part of Sta. Nos. 2~10. The Cole-Cole diagram after decoupling shows little variation of phase throughout all frequencies, and the Cole-Cole arcs are virtually absent.

Summarizing the above, no particularly anomalous spectrum is found along Line B. The insufficient SIP response may be ascribed to the high resistivity of rocks in the present area and to the low content of sulfide minerals.

Line C (Figure 6-27)

(1) Phase spectrum: The spectrum is similar to that of Line B, but in the deep part of the line's west side it often shows a linearly increasing upturn trend. After the decoupling process, the spectrum is predominantly flat-lying. However, a downturn spectrum is found beneath Sta. Nos. 15~17, and the one in the shallow part of Sta. Nos. 11 and 12 is a linearly increasing upturn type (Type E).

Where high values were recorded on the PFE and phase sections (beneath Sta. Nos. 10~16), the spectra are flat-lying, same as in the other parts, but the spectral level is higher than the others.

(2) Magnitude spectrum: The spectrum, in general, is of the flat-lying type similar to that of Line B. After decoupling the spectrum is mostly flat-lying, and no particularly characteristic spectrum is recognized.

(3) Cole-Cole diagram: As in the case of Line B, the phase variations with the change in frequency are small, and consequently, the Cole-Cole arcs are extremely short. After decoupling the phase variations decrease further, resulting in even shorter Cole-Cole arcs.

From the above, it is concluded to that Line C has no points to represent any anomalous spectrum. The ones only weakly indicated are the mountain-shape spectrum deep below Sta. Nos. 13~16 and the upturn spectrum in the shallow part of No.11 and in the medium to deep parts of No.17. The PFE values are over 2% at all these points.

5-3-5 Decoupling Percent Frequency Effect

The decoupling process is an effective means of eliminations, the electromagnetic coupling effect which arises when the space between electrodes becomes overly wide during the measurement in the low resistivity area, or when the electrode coefficient grows too large. In the present investigation, however, no coupling phenomenon is recognized because the resistivity of rocks is high and the electrode coefficient is merely N=5 or so. Coupling is noticed only when the frequency is over 1 Hz.

Since the discussion of the phase, magnitude and Cole-Cole spectra after the decoupling process have been presented in the foregoing paragraphs, along with the pre-decoupling data, and their characteristics described, this section does not refer to those items.

5-3-6 Model Simulation for IP Anomaly

The anomalies so far mentioned were the ones qualitatively assessed and defined on the pasudosections. In order to obtain the location of the anomaly source and the PFE and resistivity values, a quantitative analysis was done by means of model simulation. The model simulation was employed for Lines B, C and D, where PFE anomalies were noticed.

Line B (Figure 6-28): Along Line B, a PFE anomaly was recognized in the deep parts of Sta. Nos. 10～16. In the line's southeastern end, a strong PFE anomaly, 4% or more, occurs in the shallow to deep parts. As for the geology, granite is widely distributed in the central part of the line, limestone, metavolcanics and metasediments are distributed in the eastern part, and metavolcanics, metasediments and conglomerate are distributed in the western part. The simulation model has correlated the granite to Code 4, the limestone to Code 2, the metavolcanics and metasediments to Code 1, a strongly mineralized part to Code 5, a weakly mineralized part to Code 8, and the conglomerate near the ground surface in the line's western part to Code 3. The values of resistivity and PFE corresponding to the respective code numbers are shown in Figure 6-28.

The apparent resistivity and PFE patterns obtained by simulation were in agreement with the results of measurement. Thus, the established model is supposedly an appropriate one. Probable sources of PFE anomalies along this line are the granite-limestone border area (Sta. Nos. 14～16), which was assigned to Code 5, and also the metavolcanics and metasediments (Sta. Nos. 16～19).

Line C (Figure 6-29): The strongest of all PFE anomalies detected in the present investigation was found beneath Sta. Nos. 12～16. Distribution of metavolcanics and metasediments (Code 1) stretches almost entirely over this line. Serpentinite (Code 1) is distributed at Sta. Nos. 3～5, and porphyry

(Code 7) at Nos. 9~11 and Nos. 17~18. Occurrence of concealed granite and limestone is inferred from the resistivity and surrounding geology. The sources of PFE anomalies seem to lie deep under the ground. They were correlated to Codes 5 and 8. The patterns of resistivity and PFE obtained by simulation were similar to the measurement results, although the PFE values were somewhat lower than the measured values.

Line D (Figure 6-30): Along this line, a mountain-shape weak PFE anomaly of over 2% was detected under Sta. Nos. 4~11. Metavolcanics and metasediments (Code 1) are distributed in the northwestern part and porphyry (Code 7) in the central part of the line. In the southeast part of the line is the distribution area of metavolcanics and metasediments, limestone (Code 2) and porphyry (Code 7) intruding into all these rocks. High PFE values occur mostly in the porphyry, partly in the area of metavolcanics and metasediments. The parts with weak PFE anomalies are correlated to Codes 5 and 6.

The simulation indicated that the values of both apparent resistivity and PFE are generally in agreement with the measurement results. The anomaly source is considered to be located 200~300 m under Sta. Nos. 4~11. The PFE values are low, being 3~6%, which is probably a consequence of disseminated mineralization.

Locations of PFE anomalies and values of resistivity and PFE for each survey line as obtained through simulation have been estimated. These anomaly sources show the following characteristics.

| Line | Location | Depth (m) (underground) | Resistivity (ohm-m) | PFE (%) | Rock |
|---|---|---|---|---|---|
| B | Nos.14~19 | 30~300 | 200 | 5 | limestone, metavolcanics and metasediments |
| C | Nos.10~16 | 60~300 | 200 | 5 | granite, metavolcanics and metasediments |
| C | Nos.16~18 | 100~300 | 800 | 8 | metavolcanics and metasediments |
| D | Nos. 4~11 | 160~500 | 200 | 6 | porphyry |

5-3-7 Discussion and Interpretation

In the present examination, the SIP measurement (2 survey lines, 4 km) and IP measurement (2 survey lines, 4 km) were carried out. The survey lines were arranged at intervals of 1,000 m so as to seize the downward extension of the mineralized zone. The results and the items for further examination are given in the following.

(1) Distribution of apparent resistivity

The apparent resistivity of the present area showed dominant values of 100～150 ohm-m. Zones of low apparent resistivity (lower than 30 ohm-m) were found mostly in the southeastern part of Line A and in the central-eastern part of Line C. These zones were ascertained in the border area between metavolcanics and metasediments and limestone; they are attributable mainly to mineralization and groundwater.

Zones of high apparent resistivity occurred in the southeastern parts of Lines B, C and D, over a relatively wide sphere. These high resistivities are attributed mainly to limestone, partly to porphyry and skarn zone.

(2) Distribution of PFE

As for PFE, the values less than 1.5% account for 62% or more of all measurements. By setting 2% as a weak anomaly zone and over 3% as an anomaly zone, high PFE anomalies of 4.3% and 5.5% were found in the central-southeastern parts of Lines B and C, respectively. These high values occurred in the area of porphyry, metavolcanics and metasediments.

(3) SIP measurements were conducted on 34 rock samples. In addition, their phase spectra, resistivities and PFE were measured. The result revealed that many samples had high resistivity. Marble, silicified rock and the quartz vein showed very high values, over 10,000 ohm-m. On the other hand, low resistivity is represented by the 20～270 ohm-m range of serpentinite, metavolcanics and metasediments (green schist).

The PFE values ranged from the maximum of 8.8% (quartz vein) to the minimum of 0.3% (sandstone). Porphyry and granodiorite showed 2.2%, and the values over 4% were shown by silicified rock, the quartz vein and limestone (marble).

As for the phase spectrum, the mountain-shape type (Type A) was characteristic; the flat-lying type was also seen. The flat-lying spectra can be classified into seven kinds, but these are not necessarily correlative to rock types. No correlation was noticed either with the PFE values or phase values. This may be because the rocks distributed in this area have very high resistivity and low sulfide mineral content.

(4) The results of SIP measurements made for Lines B and C showed that the phase spectrum is dominantly the flat-lying type, and the magnitude spectrum is also, for the most of the part flat-lying. The Cole-Cole arcs are short,

and the phase variations with frequency are not so notable as to constitute a spectrum. This is because the resistivity of rocks is very high. Therefore, application of the spectral IP method for exploration of a high resistivity zone such as the porphyry-copper zone would call for careful consideration.

(5) By the simulation analysis of PFE anomalies detected along Lines B, C and D, the locations of the sources of PFE anomalies were inferred, and the depth of their occurrences and the values of PFE and resistivity were estimated. Consequently, it is concluded to that the anomaly sources occur in the Dikmen Granite and porphyry distributed in the NE direction from the southwestern part of the survey area, and also in the surrounding area where metavolcanics and metasediments and limestone are distributed. Their depth of occurrence becomes shallower from the southwestern part to the northeastern part. The low values of PFE, 5～8%, suggest the occurrence of low-grade iron sulfide.

(6) The results of the investigation were integrated into the interpretation map (Figure 6-31). Represented on the map are the zones of weak anomaly (over 2%) and the zones of anomaly (over 3%) based on the PFE plan maps of N=2 and N=5. The locations of PFE anomaly sources estimated from the simulation analysis are shown also. In the present investigation, the line spacing, 1 km, was too wide, but the continuity of the anomaly sources could be inferred from the geological distribution and geological structures, and so we dared to express the sphere of anomaly zones on the map. From the result of geochemical prospecting, anomaly zones of score 1 or over are also indicated. But the geochemically defined anomaly zones are located mostly in the northwestern part of the PFE anomaly zone, partly overlapping the PFE anomaly zone in the central part of Line B.

As mentioned in (1)～(5), the high PFE anomaly zones defined by the present investigation are located at and around the boundary between the distribution area of limestone, metavolcanics and metasediments and that of Dikmen Granite and porphyry intruding the former. It can be inferred, therefore, that porphyry-copper-type mineralization accompanying these intrusive rocks is responsible for the PFE anomalies.

Based on the above-described circumstances, an important sphere for prospecting would be the area around the granite, porphyry and limestone in the central and northeastern parts of the survey area.

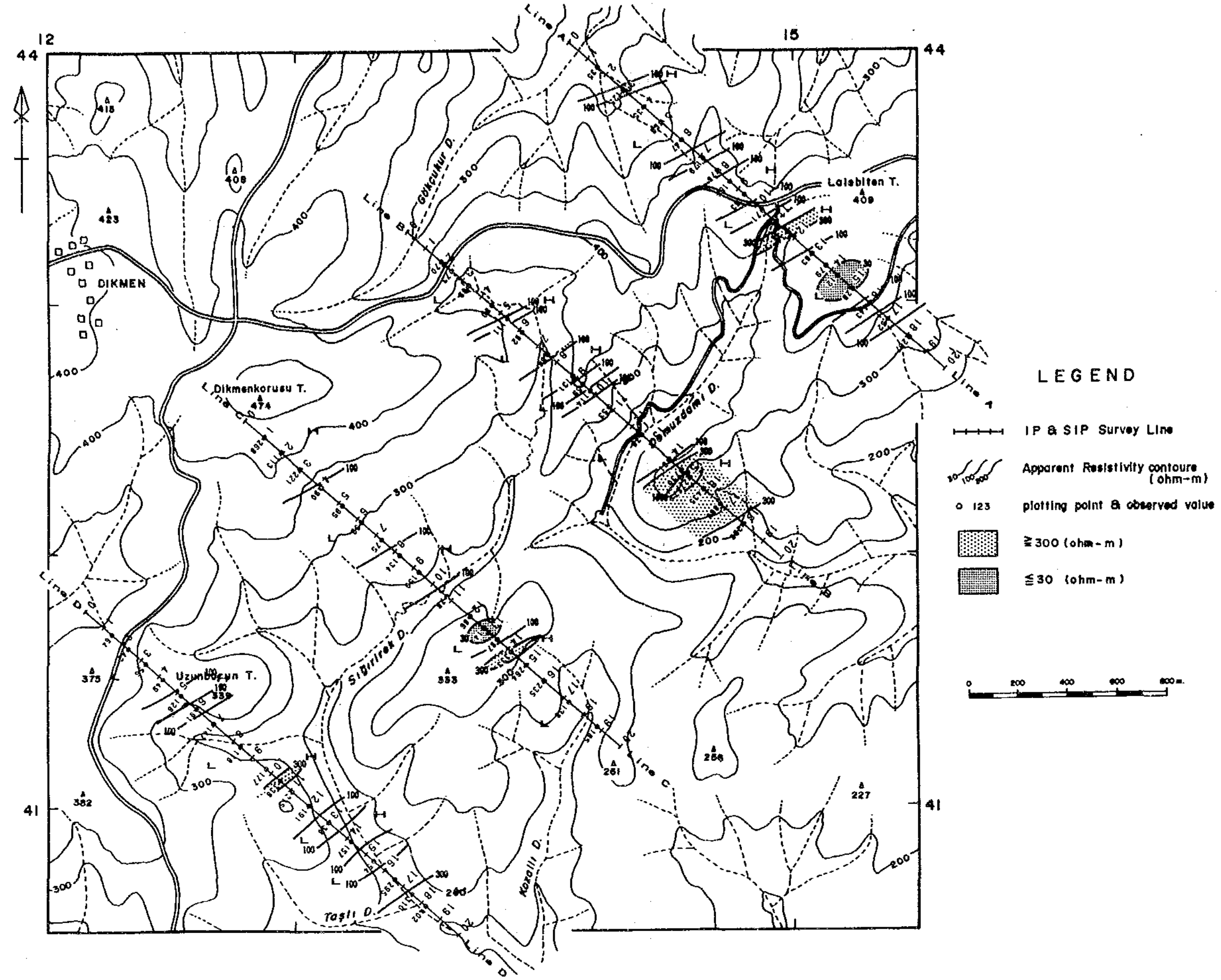


Fig. 6-12 Plan Map of Apparent Resistivity
[0.3/0.375 Hz] (n=1)

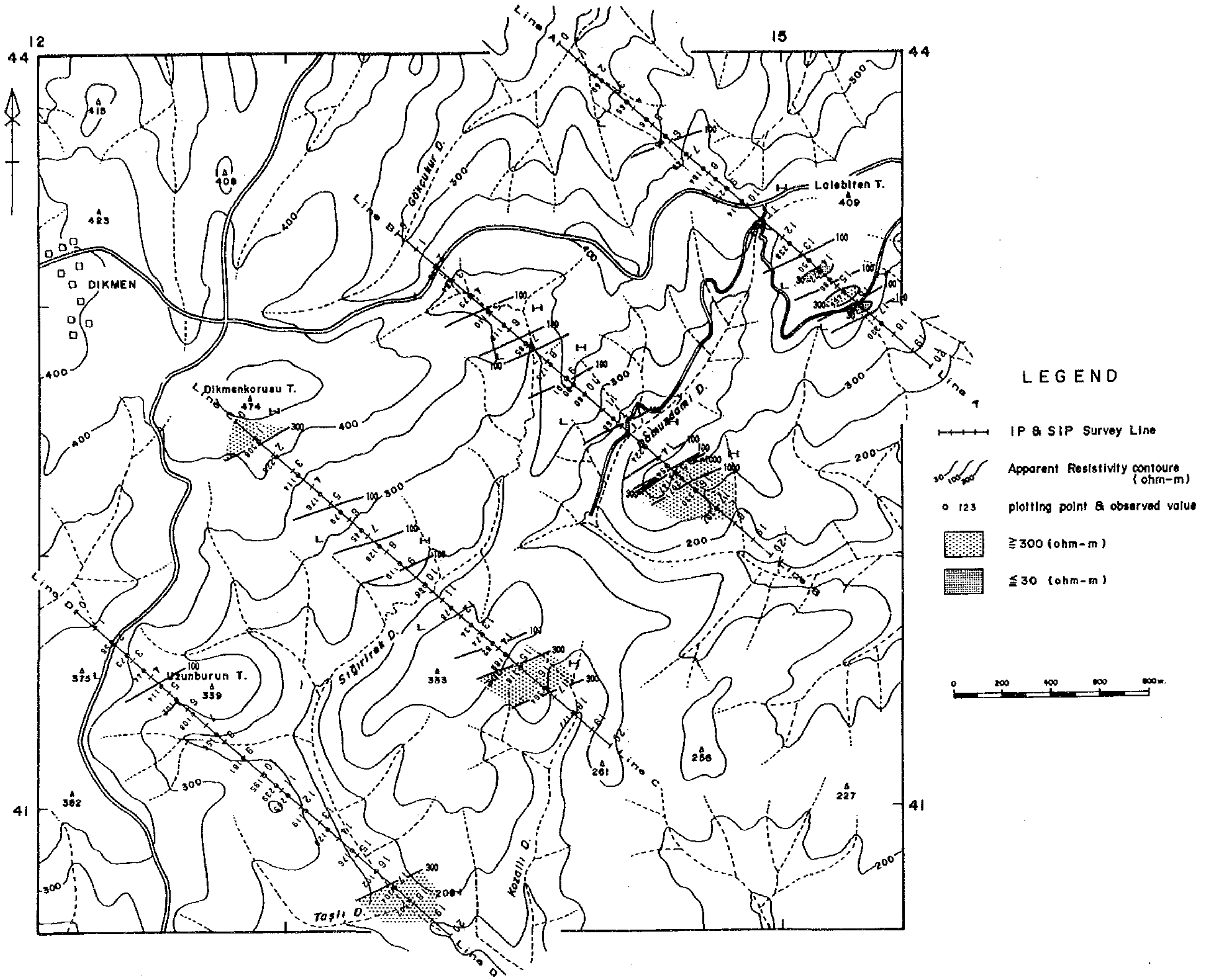


Fig. 6-13 Plan Map of Apparent Resistivity
[0.3/0.375 Hz] (n=2)

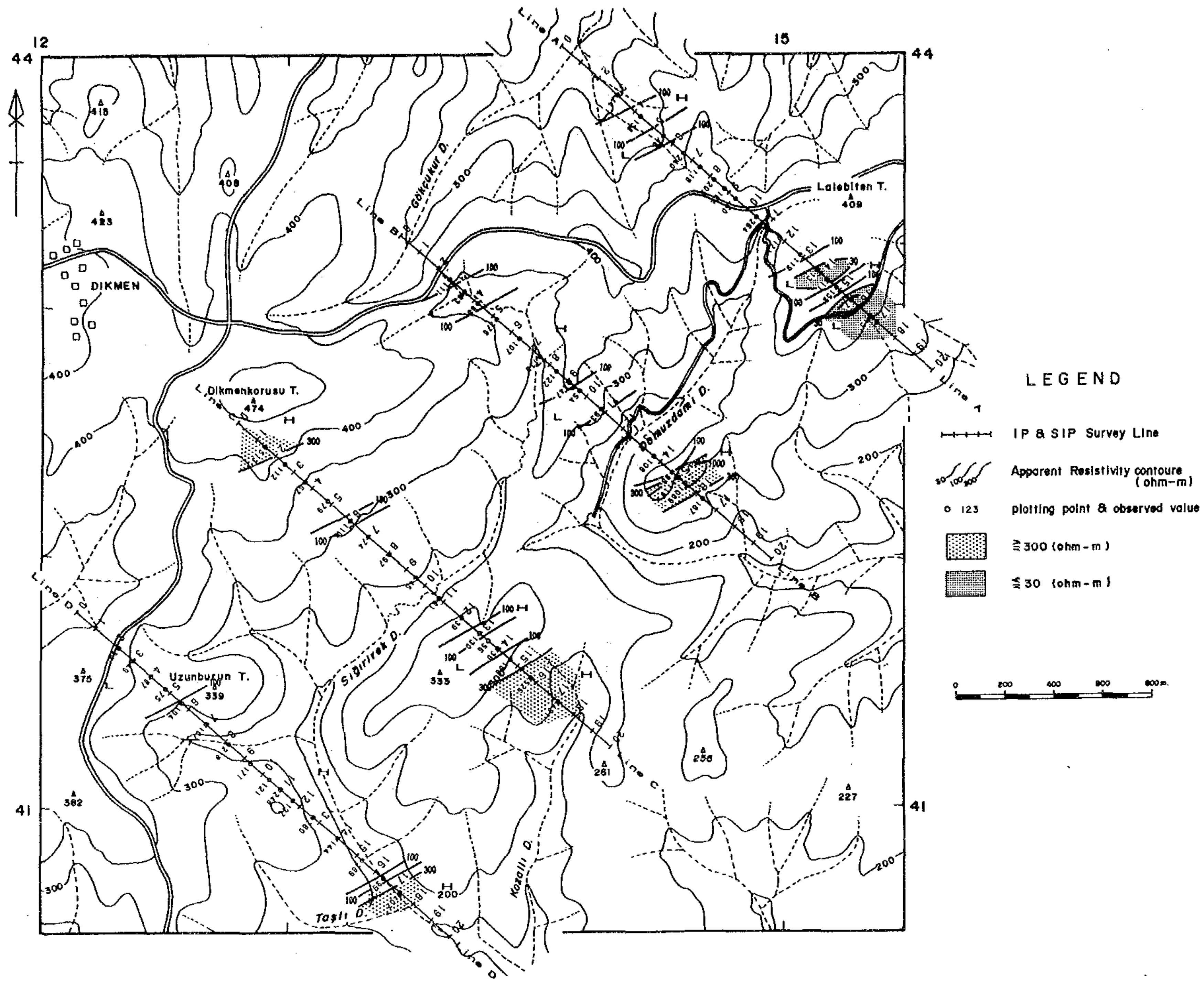


Fig. 6-14 Plan Map of Apparent Resistivity [0.3/0.375 Hz] (n=3)

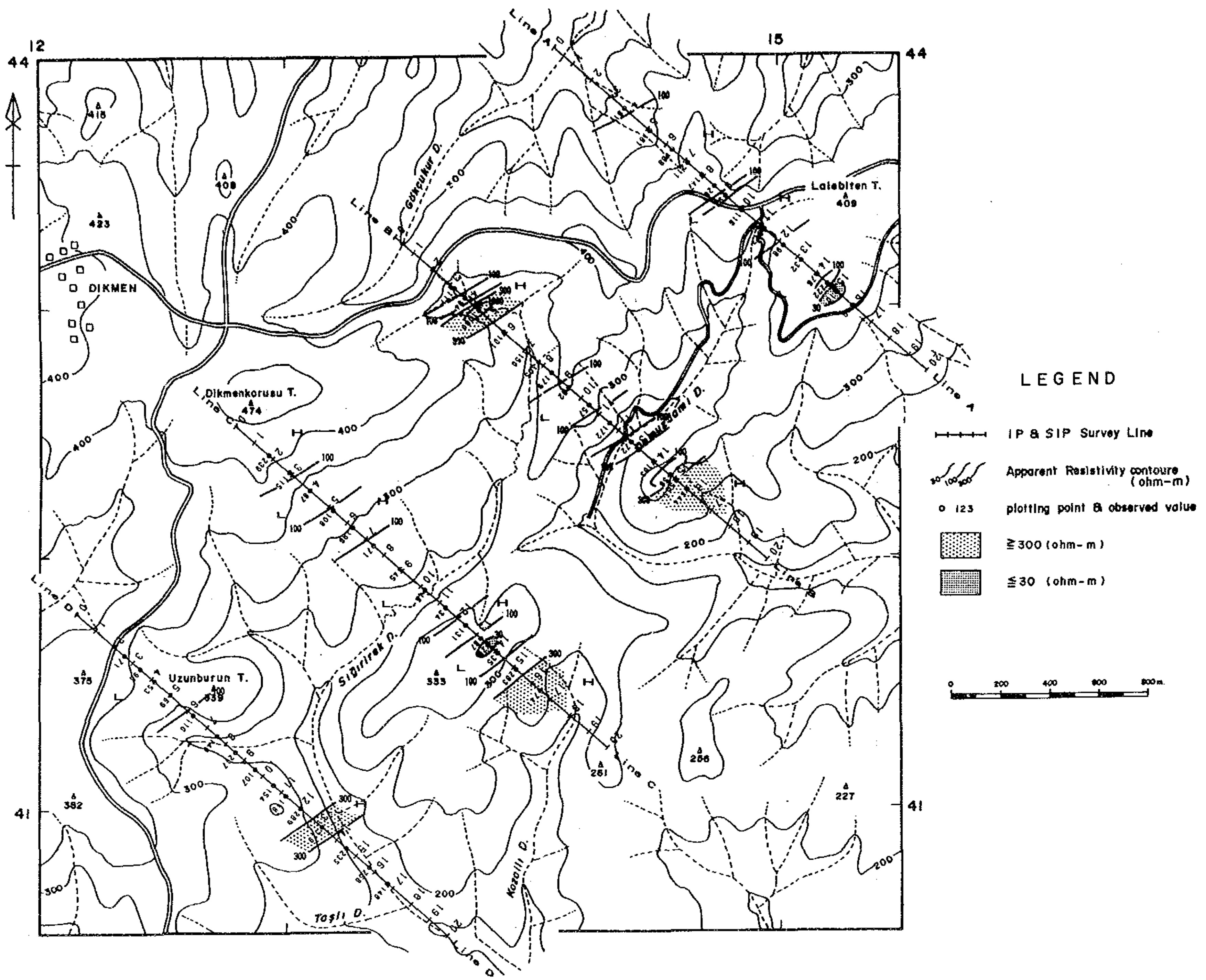


Fig. 6-15 Plan Map of Apparent Resistivity [0.3/0.375 Hz] (n=4)

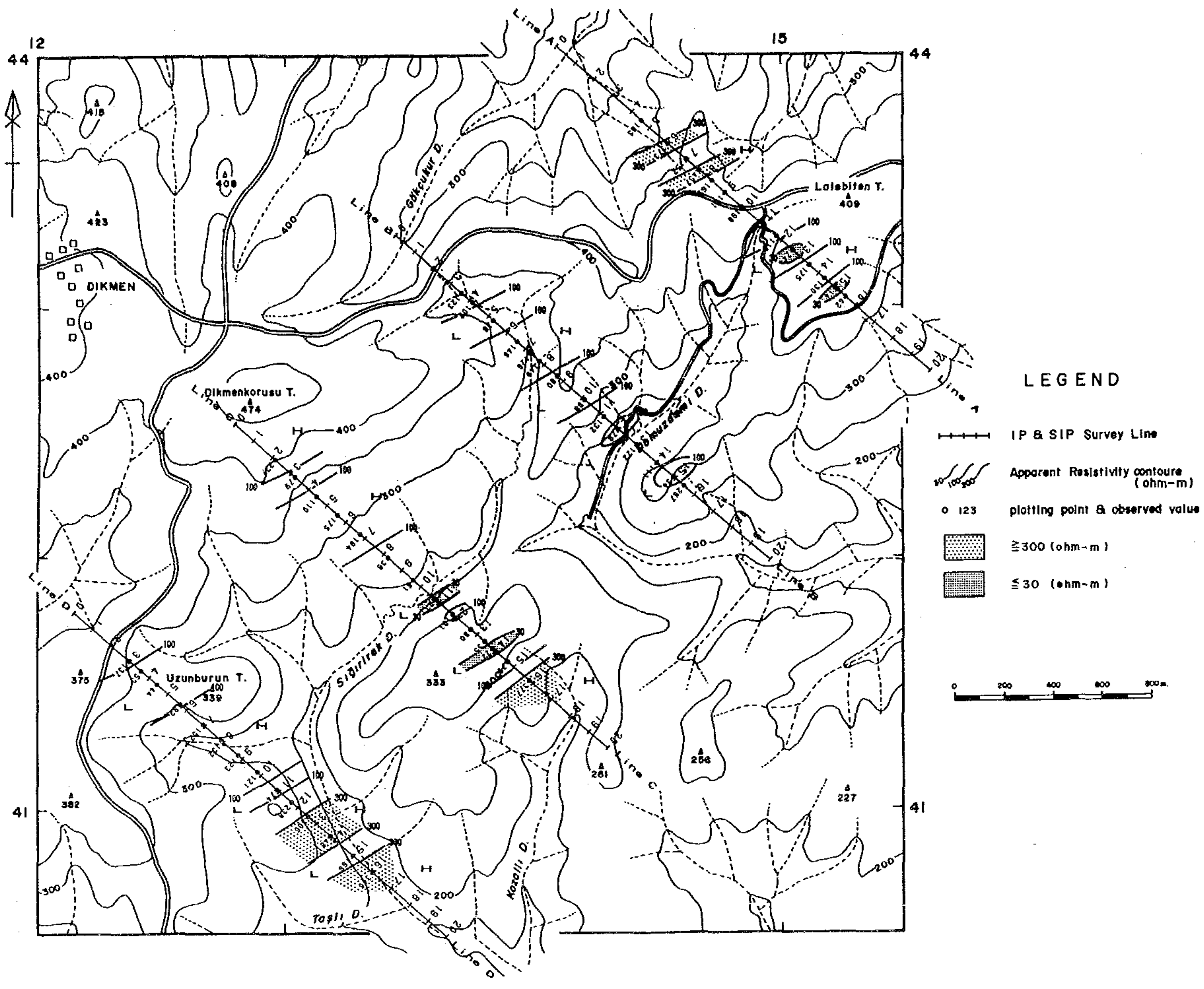


Fig. 6-16 Plan Map of Apparent Resistivity [0.3/0.375 Hz] (n=5)

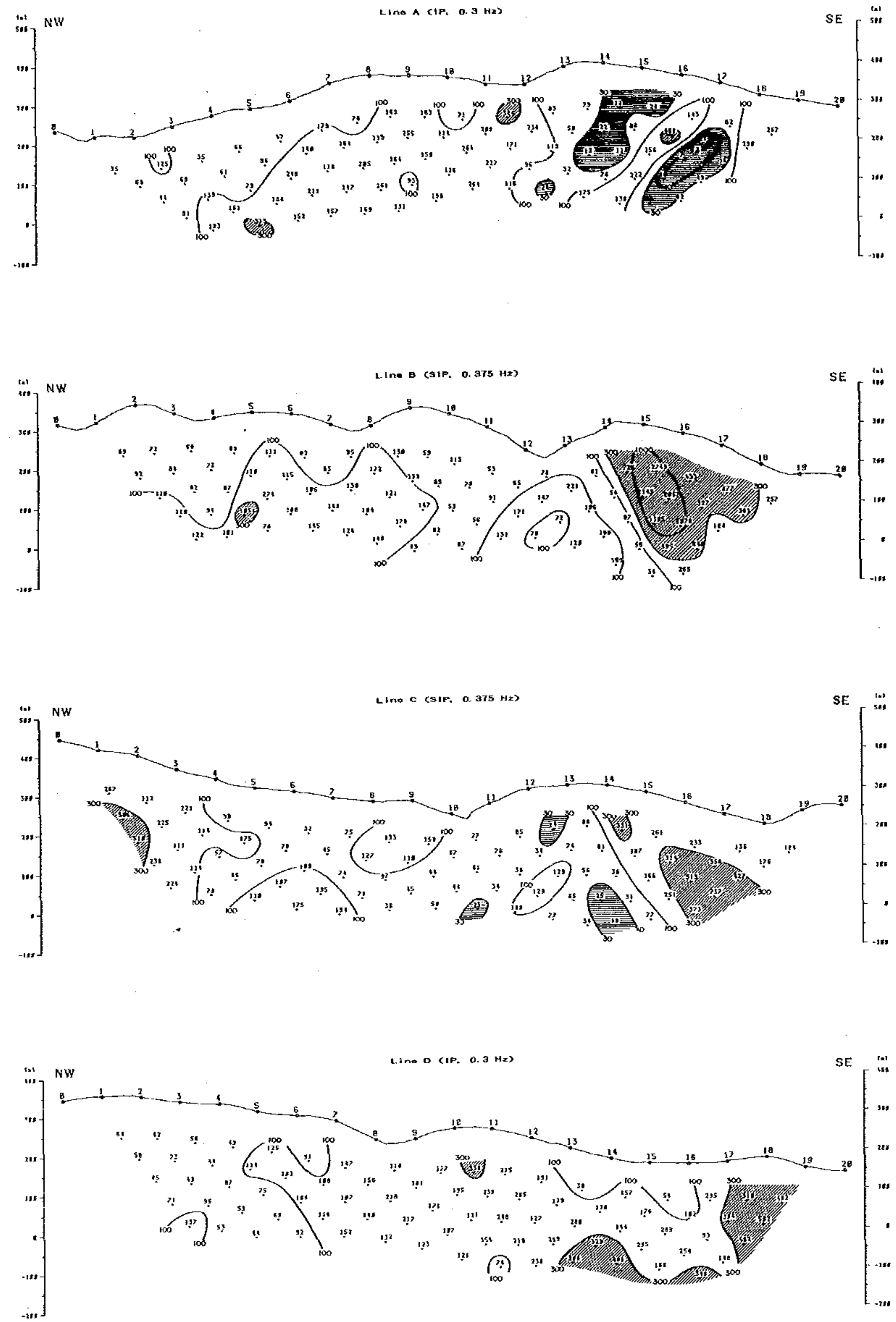


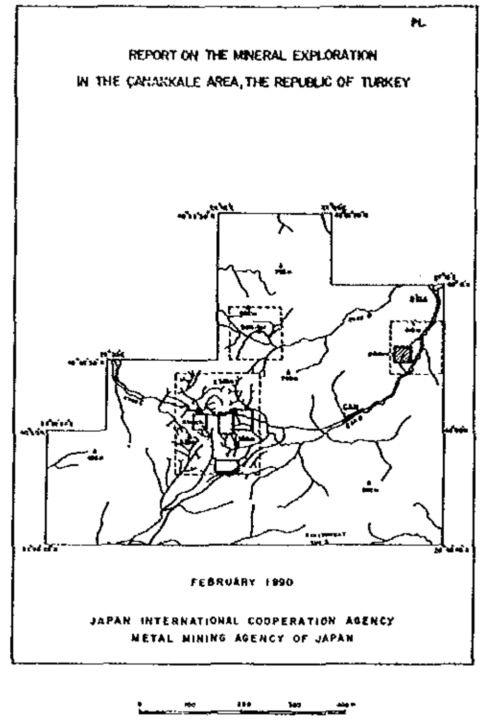


Legend

≥ 300(ohm-m)

≤ 30 (ohm-m)

Fig. 6-17 Sections of Apparent Resistivity (Line A-D)

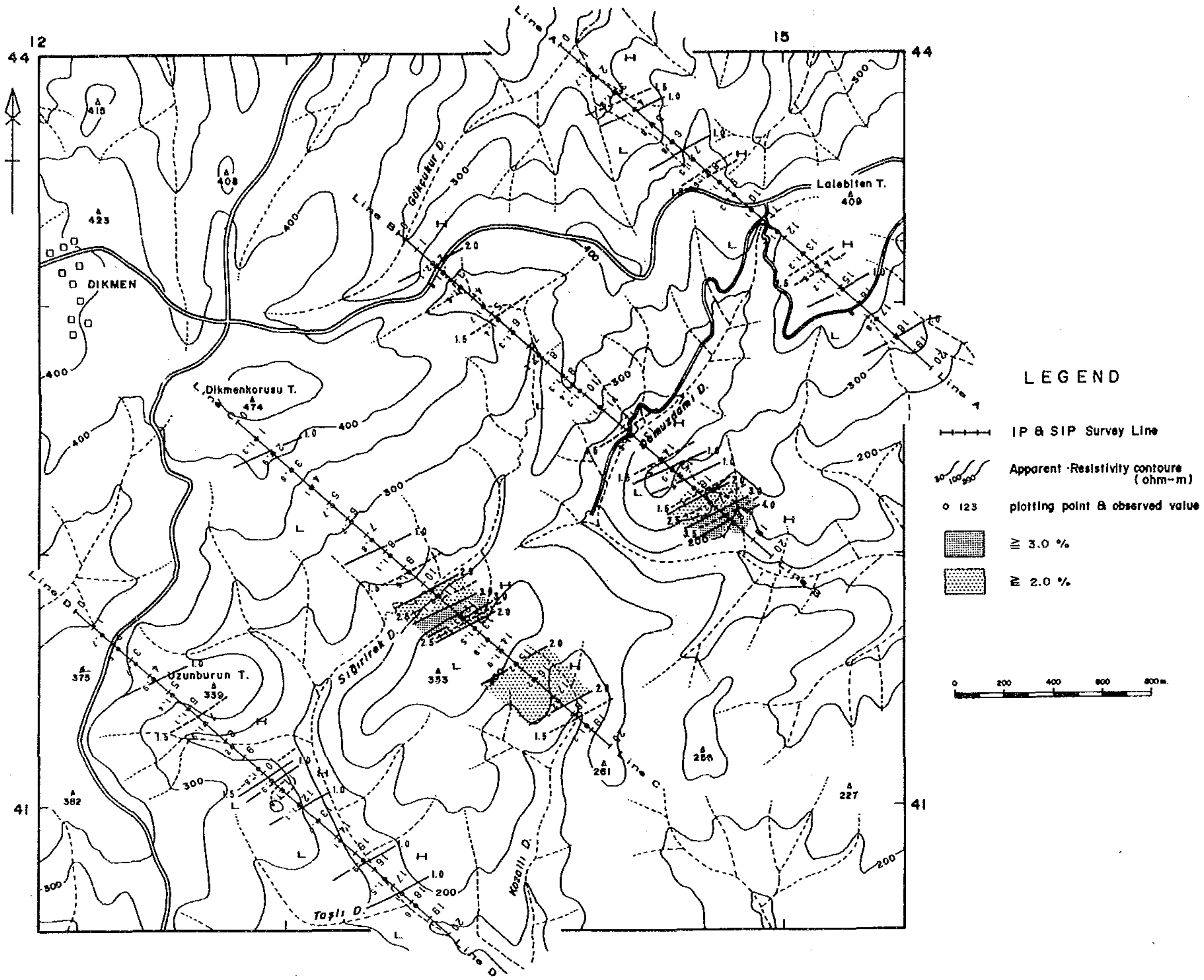


Fig. 6-18 Plan Map of PFE

[0.3-3.0, 0.375-3.0 Hz] (n=1)

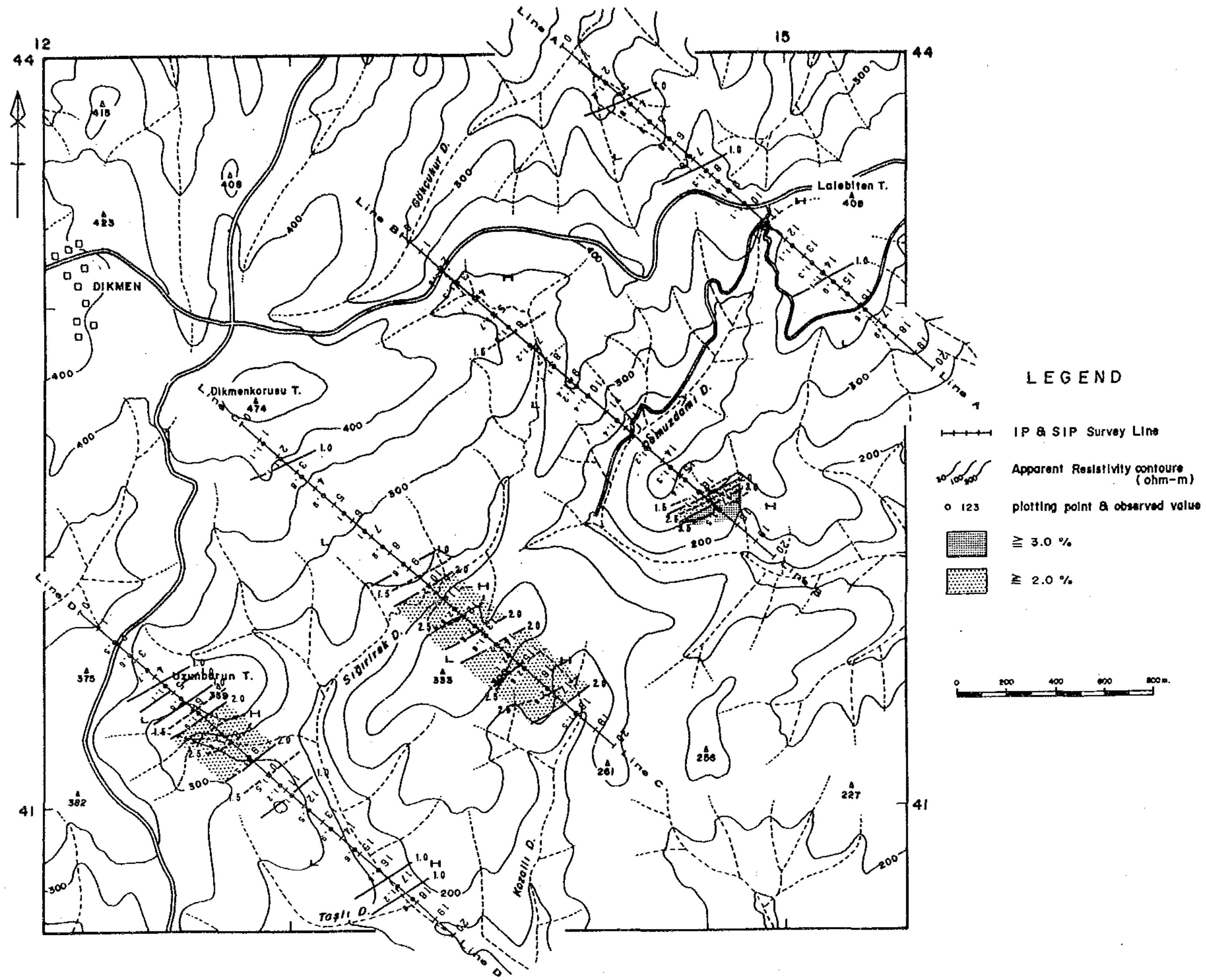


Fig. 6-19 Plan Map of PFE
[0.3-3.0, 0.375-3.0 Hz] (n=2)

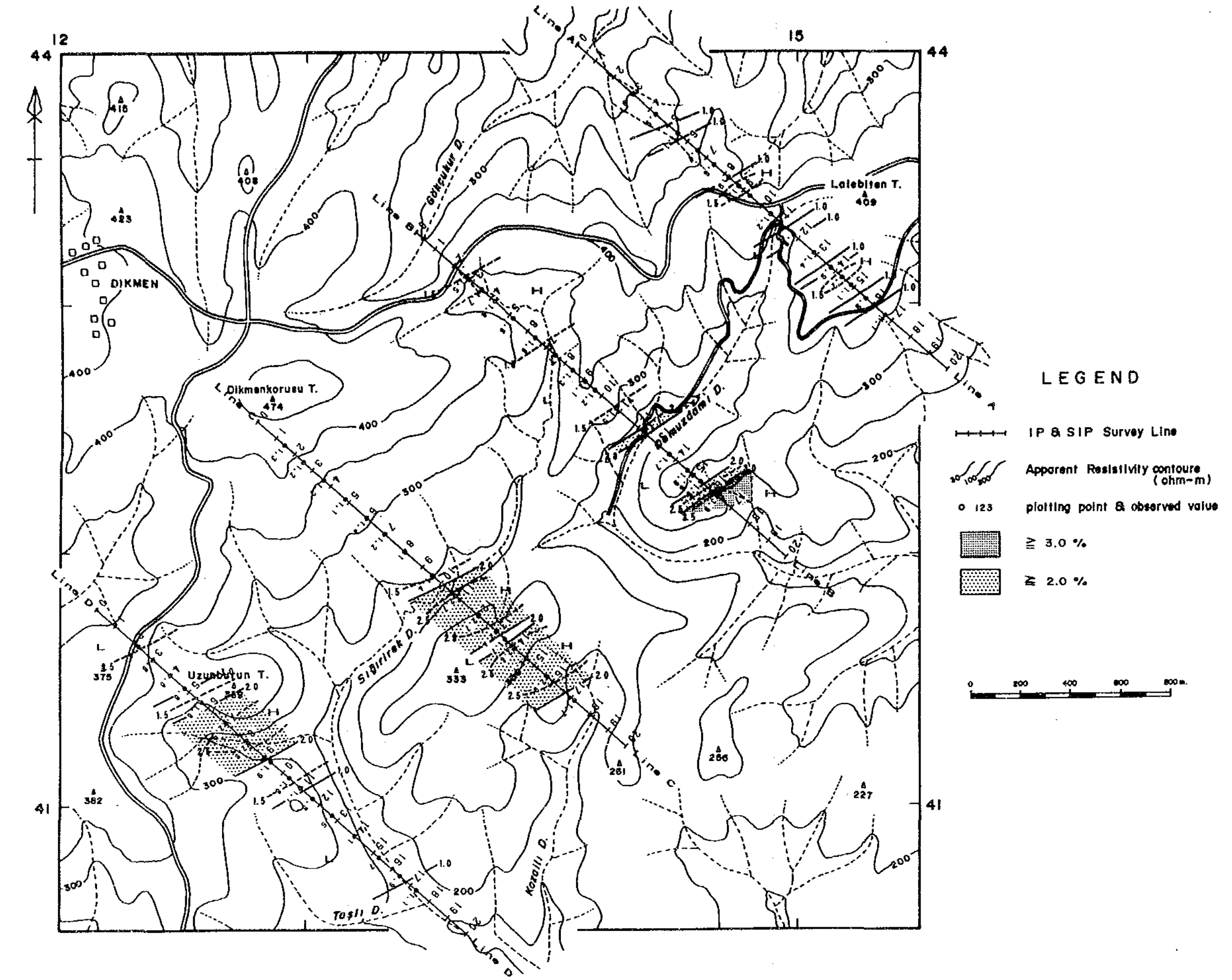


Fig. 6-20 Plan Map of PFE
[0.3-3.0, 0.375-3.0 Hz] (n=3)

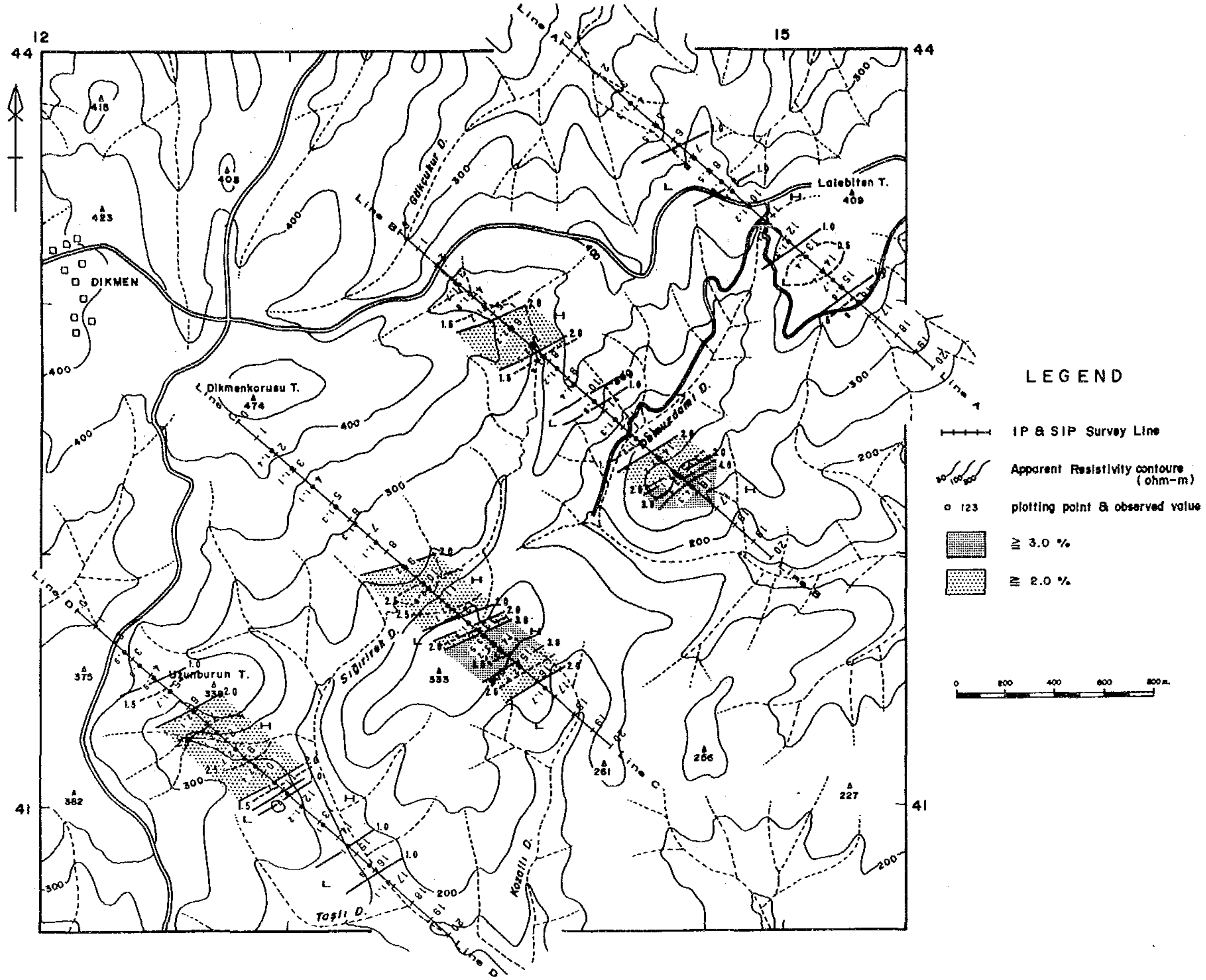


Fig. 6-21 Plan Map of PFE

[0.3-3.0, 0.375-3.0 Hz] (n=4)

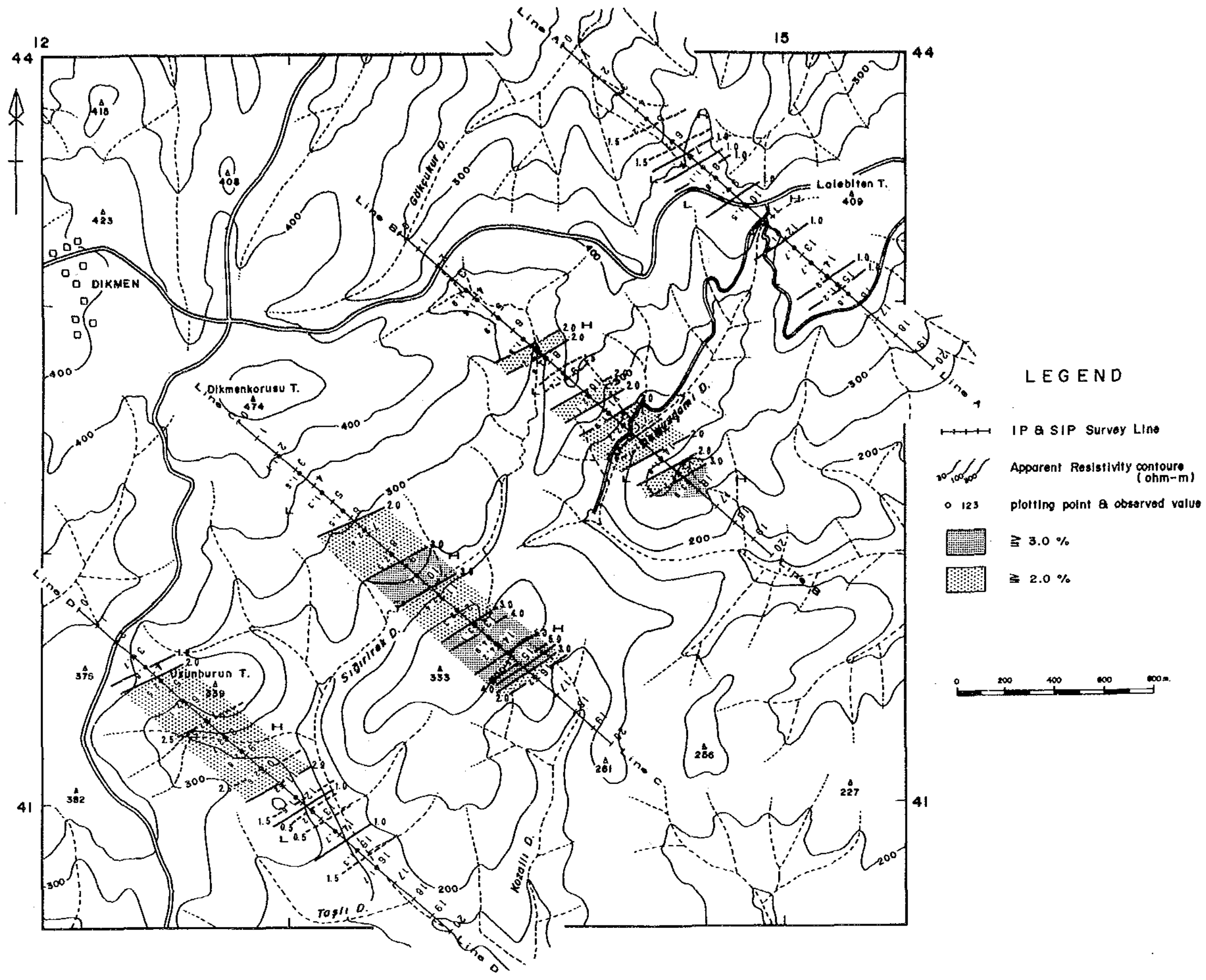


Fig. 6-22 Plan Map of PFE
[0.3-3.0, 0.375-3.0 Hz] (n=5)

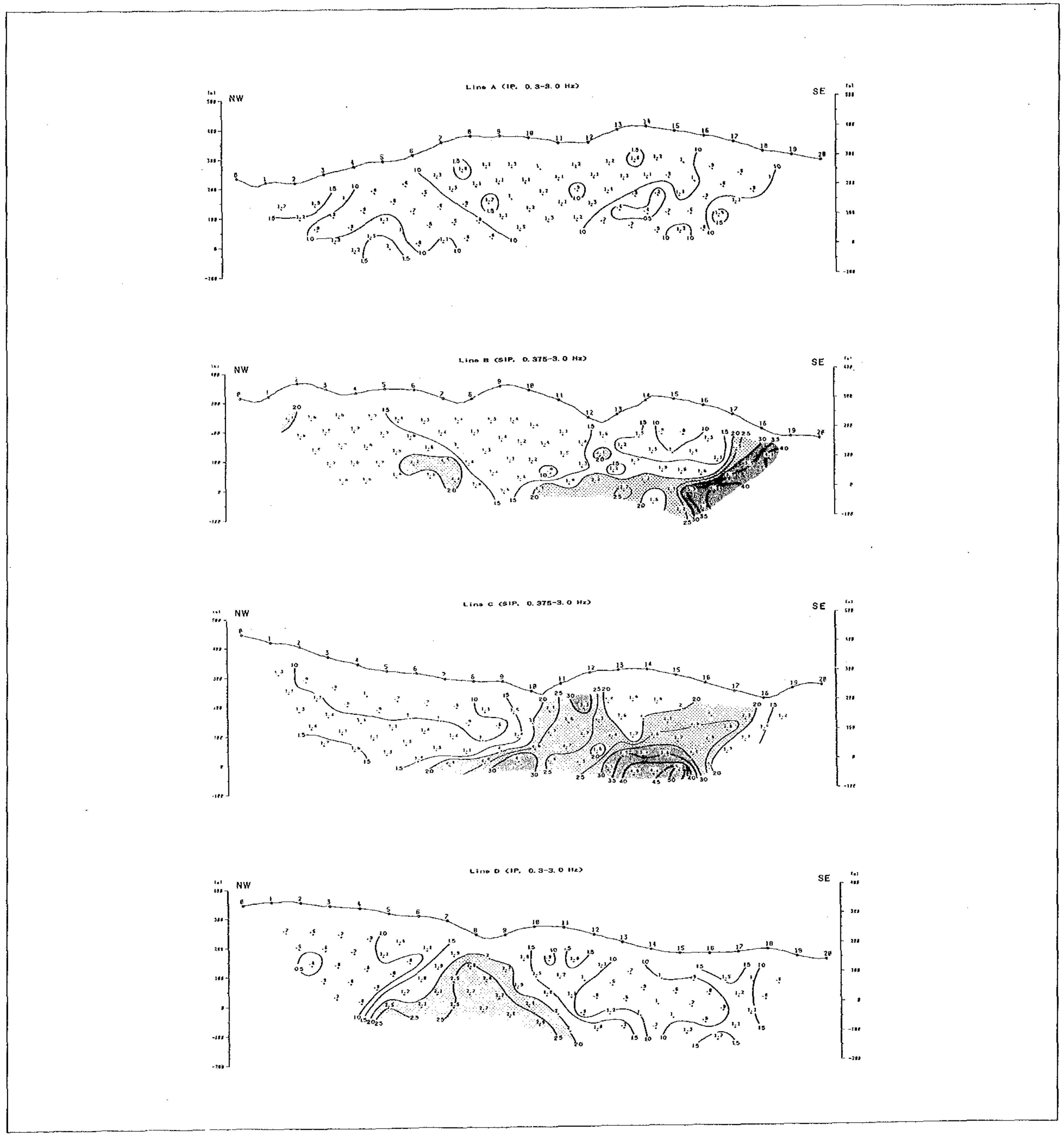


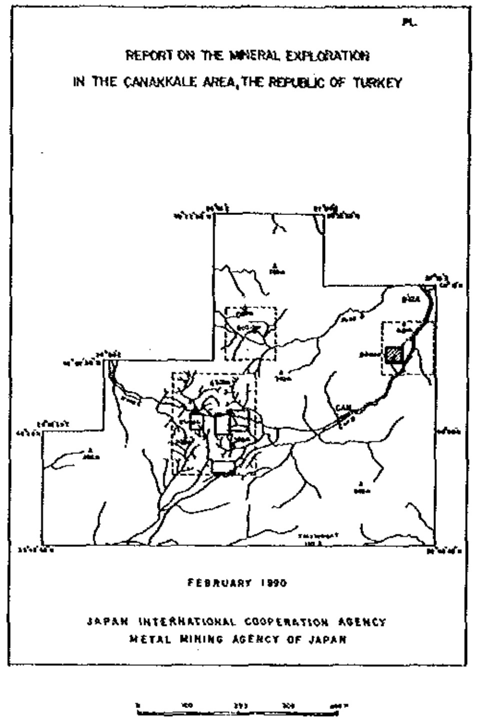


Legend

≥ 3.0%

≥ 2.0%

Fig. 6-23 Sections of PFE (Line A-D)

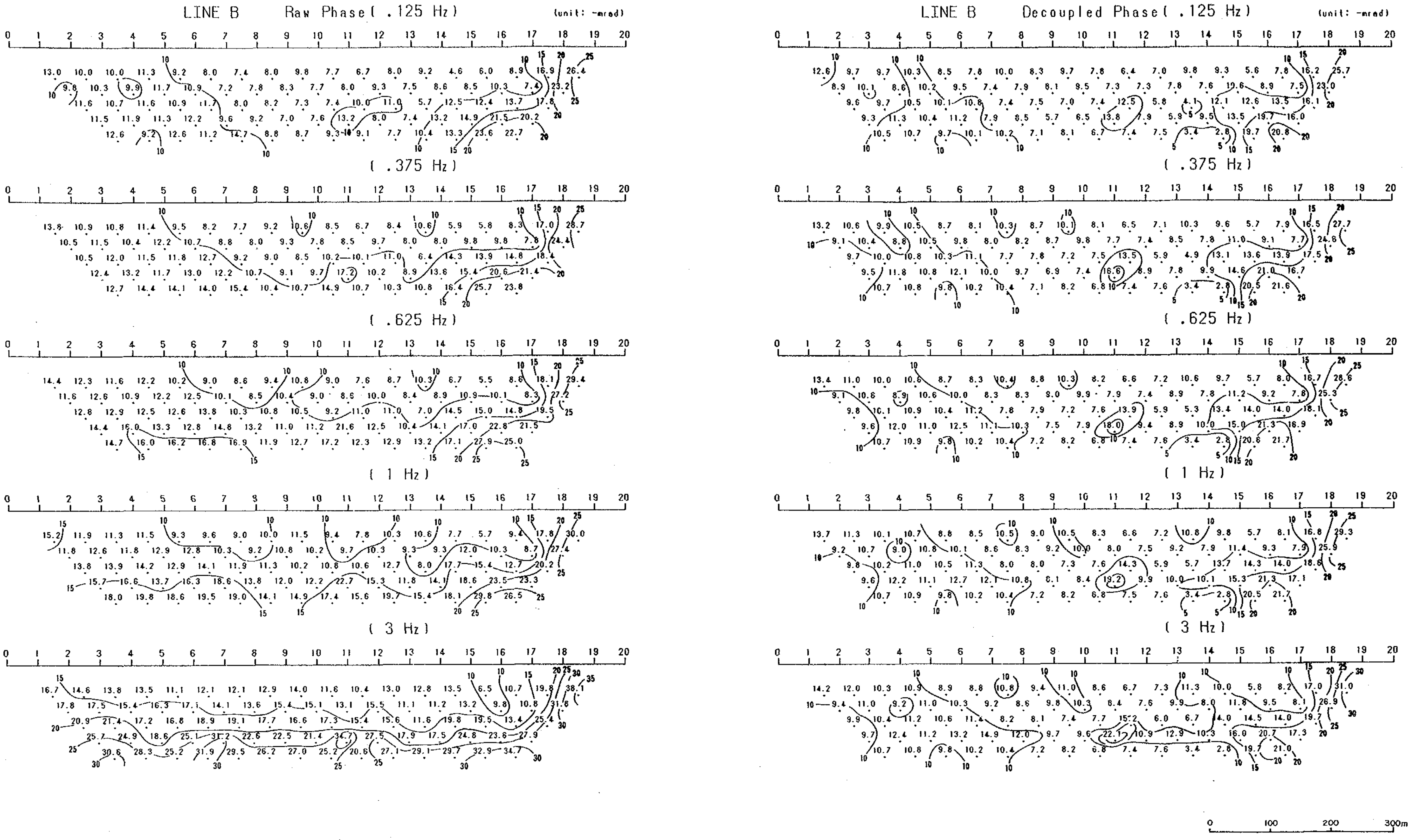


Fig. 6-24 Phase Difference at Five Frequencies (Line B)

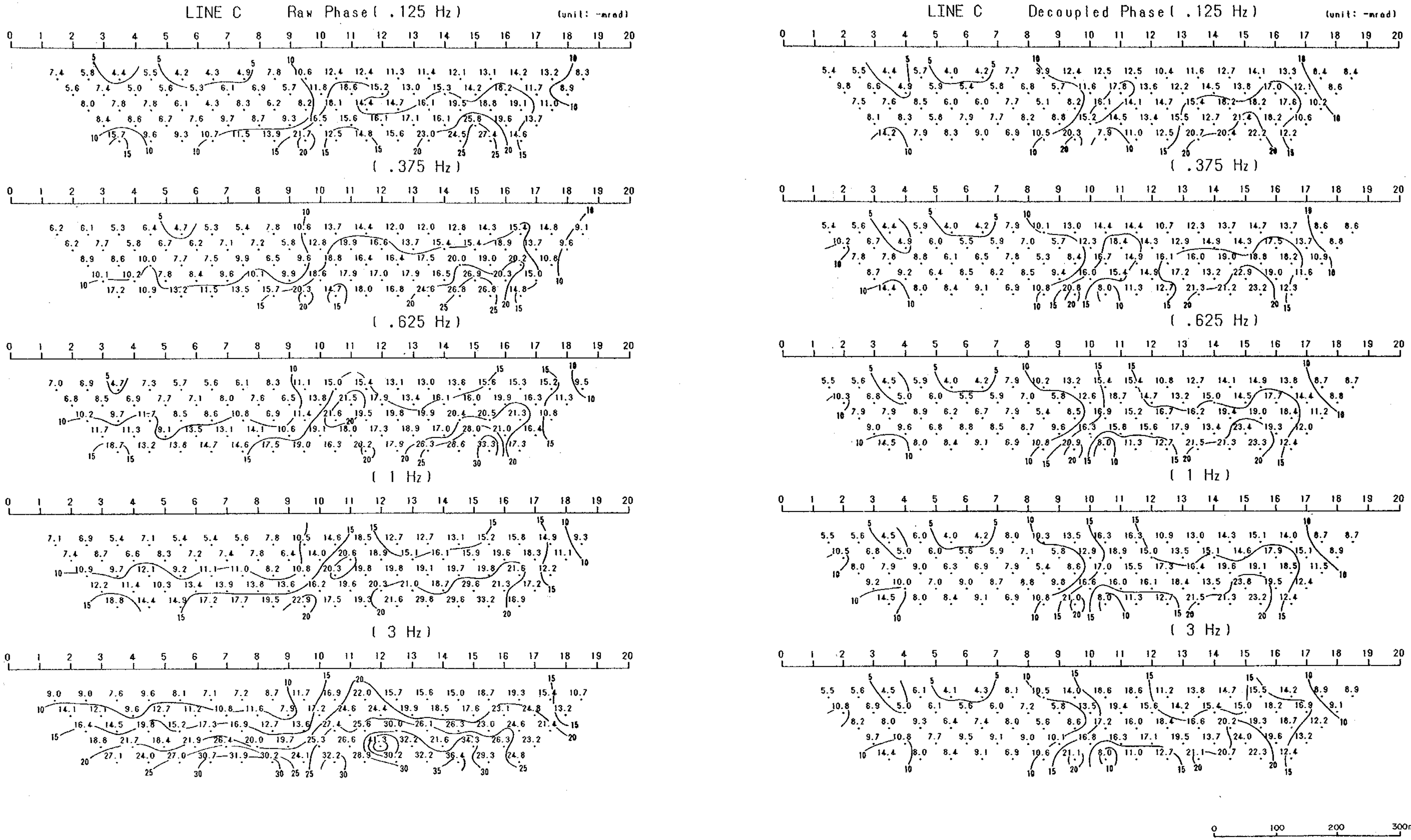


Fig. 6-25 Phase Difference at Five Frequencies (Line C)

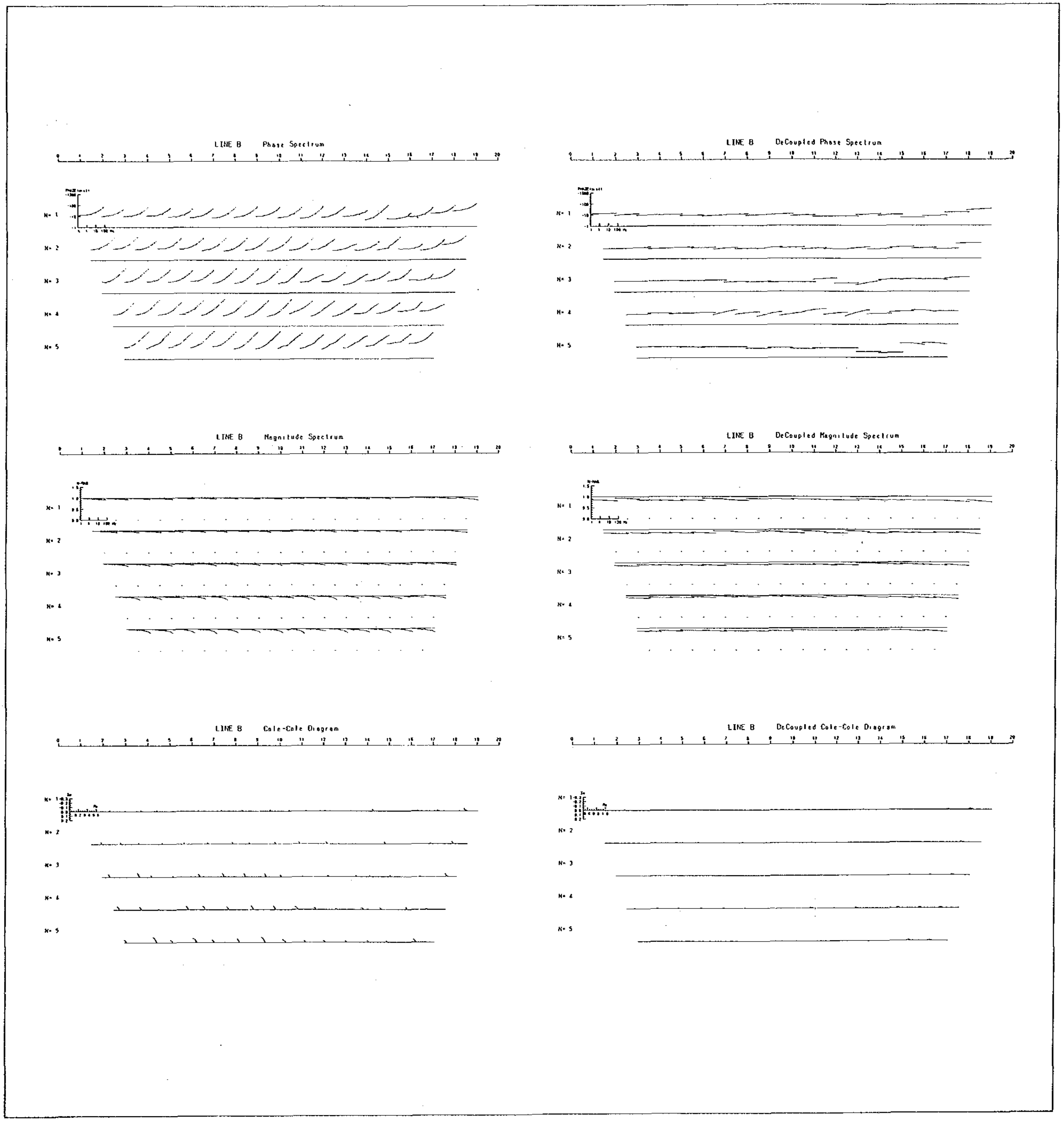


PL.

REPORT ON THE MINERAL EXPLORATION
IN THE CANAKKALE AREA, THE REPUBLIC OF TURKEY

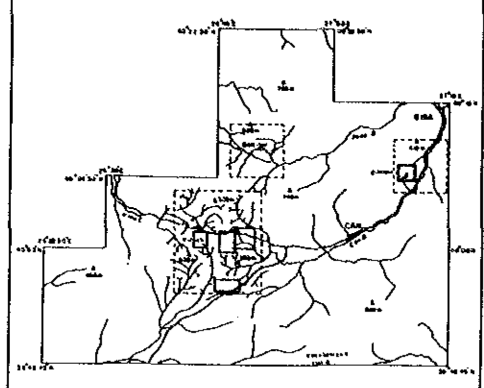

FEBRUARY 1990

JAPAN INTERNATIONAL COOPERATION AGENCY
METAL MINING AGENCY OF JAPAN

0 100 200 300m

Fig. 6-26 Phase, Magnitude and Cole-Cole Spectrums (Line B)

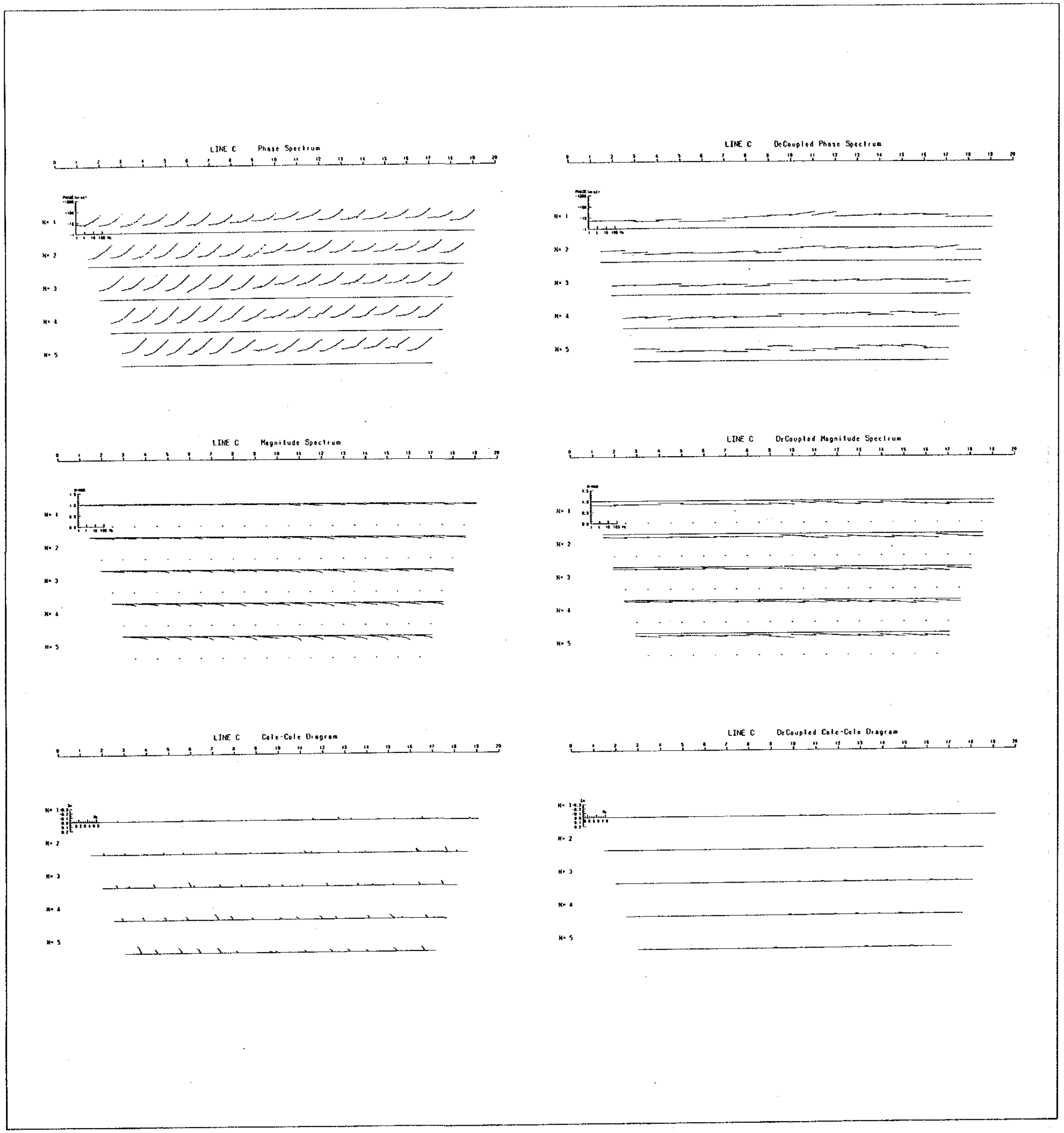


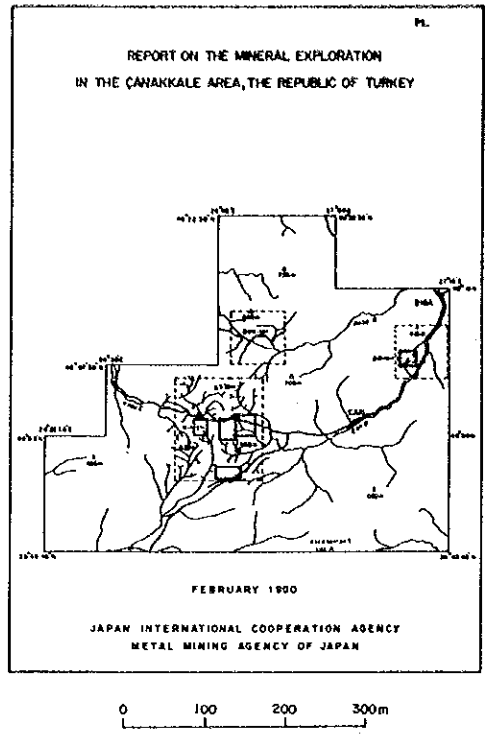


Fig. 6-27 Phase, Magnitude and Cole-Cole Spectrums (Line C)

## Simulation model

| | 1 | 2 | 3 | 4 | 5 | 6 | 7 | 8 | 9 | 10 | 11 | 12 | 13 | 14 | 15 | 16 | 17 | 18 | 19 | 20 |
|---|---|---|---|---|---|---|---|---|---|---|---|---|---|---|---|---|---|---|---|---|
| 1 | 000 | 333 | 333 | 301 | 111 | 114 | 440 | 000 | 444 | 444 | 400 | 000 | 000 | 000 | 000 | 000 | 000 | 000 | 000 | 000 |
| 2 | 333 | 333 | 333 | 318 | 884 | 444 | 444 | 444 | 444 | 446 | 444 | 400 | 000 | 002 | 222 | 222 | 000 | 000 | 000 | 000 |
| 3 | 111 | 333 | 111 | 118 | 884 | 444 | 444 | 444 | 444 | 446 | 444 | 440 | 000 | 222 | 222 | 222 | 761 | 000 | 000 | 000 |
| 4 | 111 | 111 | 111 | 118 | 884 | 444 | 444 | 444 | 444 | 446 | 444 | 444 | 444 | 888 | 822 | 222 | 716 | 110 | 000 | 000 |
| 5 | 111 | 111 | 111 | 118 | 884 | 444 | 444 | 444 | 444 | 446 | 444 | 444 | 888 | 888 | 822 | 222 | 716 | 111 | 111 | 111 |
| 6 | 111 | 111 | 111 | 111 | 884 | 444 | 444 | 444 | 444 | 446 | 444 | 444 | 444 | 448 | 822 | 222 | 711 | 611 | 111 | 551 |
| 7 | 111 | 111 | 111 | 111 | 884 | 444 | 444 | 444 | 444 | 446 | 444 | 444 | 444 | 448 | 822 | 222 | 721 | 161 | 115 | 551 |
| 8 | 111 | 111 | 111 | 118 | 844 | 444 | 444 | 444 | 444 | 444 | 444 | 444 | 444 | 444 | 552 | 222 | 722 | 116 | 115 | 551 |
| 9 | 111 | 111 | 111 | 118 | 844 | 444 | 444 | 444 | 444 | 444 | 444 | 444 | 444 | 444 | 555 | 222 | 722 | 111 | 115 | 551 |
| 10 | 111 | 111 | 111 | 118 | 844 | 444 | 444 | 444 | 444 | 444 | 444 | 444 | 444 | 444 | 455 | 522 | 722 | 211 | 155 | 511 |
| 11 | 111 | 111 | 111 | 114 | 444 | 444 | 444 | 444 | 444 | 444 | 444 | 444 | 444 | 444 | 445 | 552 | 722 | 222 | 555 | 111 |
| 12 | 111 | 111 | 111 | 114 | 444 | 444 | 444 | 444 | 444 | 444 | 444 | 444 | 444 | 444 | 445 | 555 | 555 | 552 | 555 | 111 |
| 13 | 111 | 111 | 111 | 114 | 444 | 444 | 444 | 444 | 444 | 444 | 444 | 444 | 444 | 444 | 445 | 555 | 555 | 555 | 551 | 111 |
| 14 | 111 | 111 | 111 | 114 | 444 | 444 | 444 | 444 | 444 | 444 | 444 | 444 | 444 | 444 | 445 | 555 | 555 | 555 | 111 | 111 |
| 15 | 111 | 111 | 111 | 114 | 444 | 444 | 444 | 444 | 444 | 444 | 444 | 444 | 444 | 444 | 444 | 111 | 722 | 225 | 211 | 111 |
| 16 | 111 | 111 | 111 | 114 | 444 | 444 | 444 | 444 | 444 | 444 | 444 | 444 | 444 | 444 | 444 | 111 | 722 | 225 | 211 | 111 |

| CODE | RESISTIVITY OHM-M | F.E. % |
|---|---|---|
| 1 | 100. | 1.5 |
| 2 | 5000. | 1.7 |
| 3 | 500. | 1.5 |
| 4 | 150. | 1.1 |
| 5 | 500. | 7.0 |
| 6 | 500. | 2.0 |
| 7 | 500. | 1.0 |
| 8 | 1500. | 3.0 |
| 9 | 20. | 5.3 |

DIPOLE-DIPOLE APPARENT RESISTIVITY PROFILE

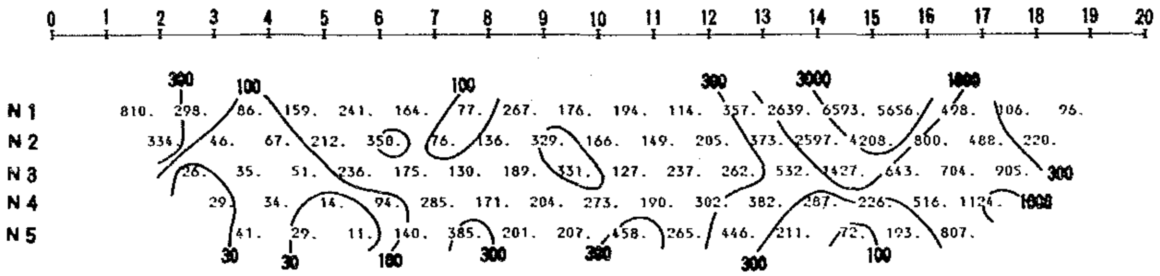

DIPOLE-DIPOLE APPARENT PERCENT FREQ. EFFECT

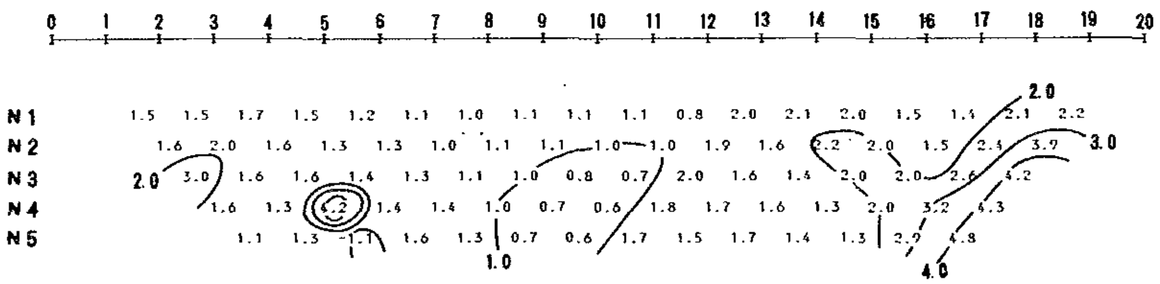

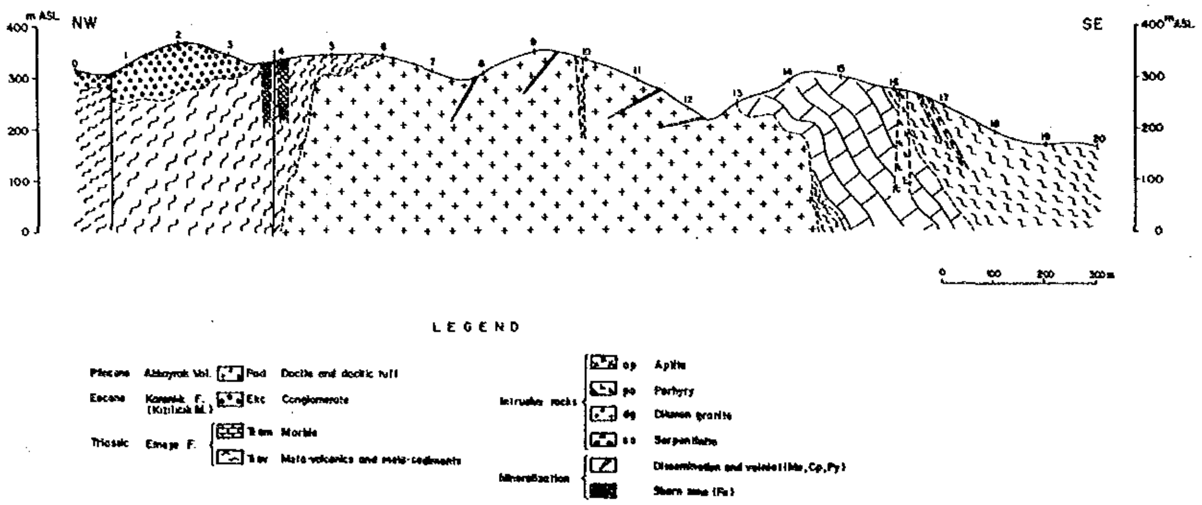

observed Apparent Resistivity

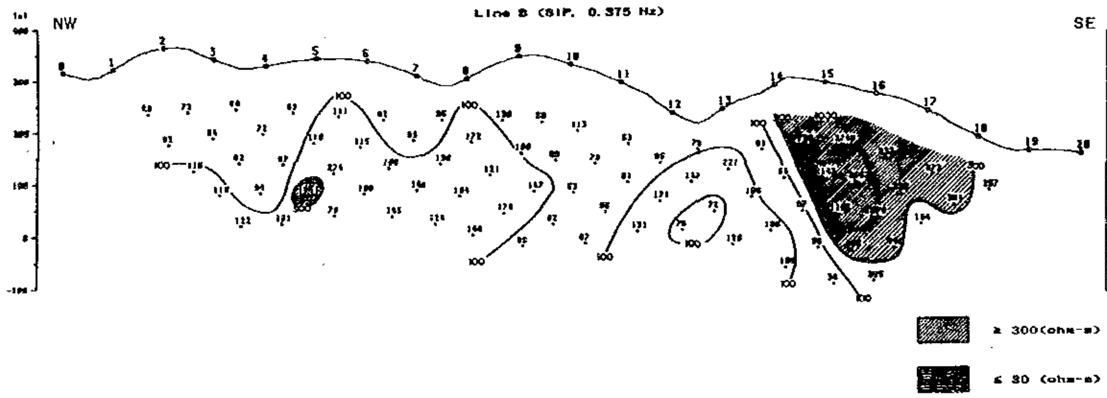

observed PFE

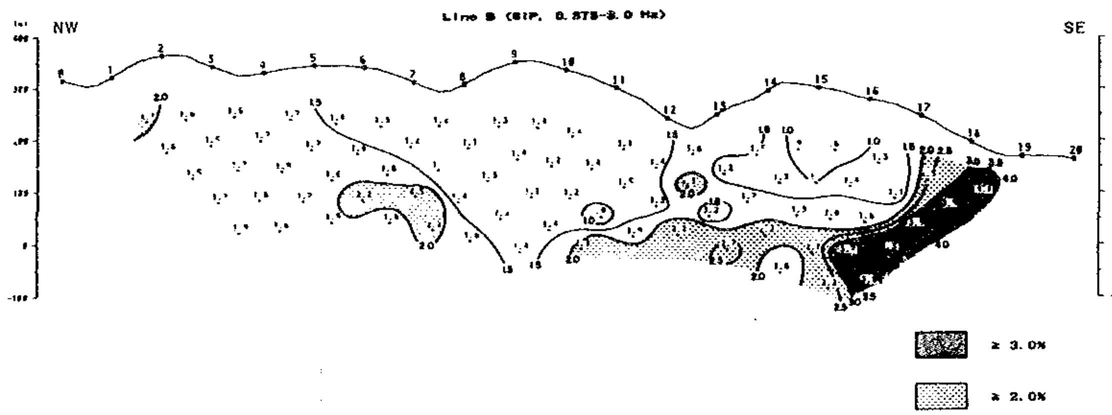

Fig. 6-28 Result of Model Simulation (Line B)

Simulation model

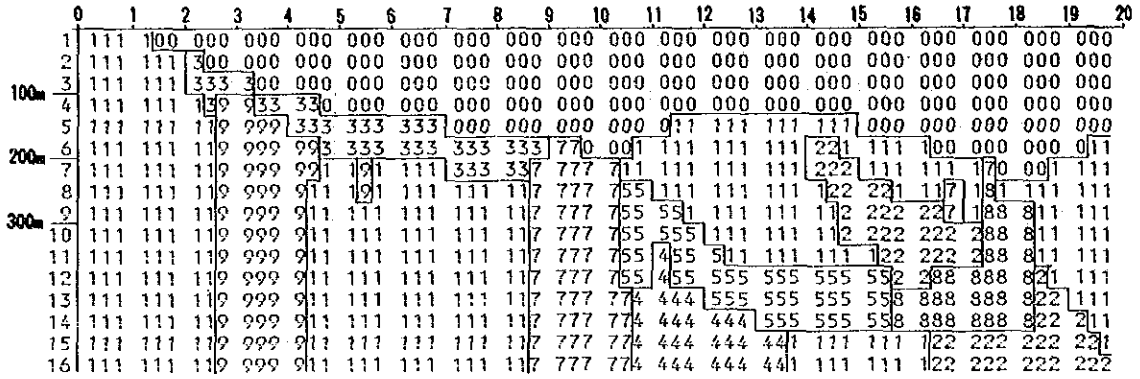

| CODE | RESISTIVITY OHM-M | F.E. % |
|---|---|---|
| 1 | 100. | 1.5 |
| 2 | 5000. | 2.0 |
| 3 | 50. | 0.7 |
| 4 | 500. | 4.0 |
| 5 | 200. | 5.0 |
| 6 | 1000. | 2.2 |
| 7 | 500. | 1.0 |
| 8 | 800. | 8.0 |
| 9 | 300. | 1.5 |

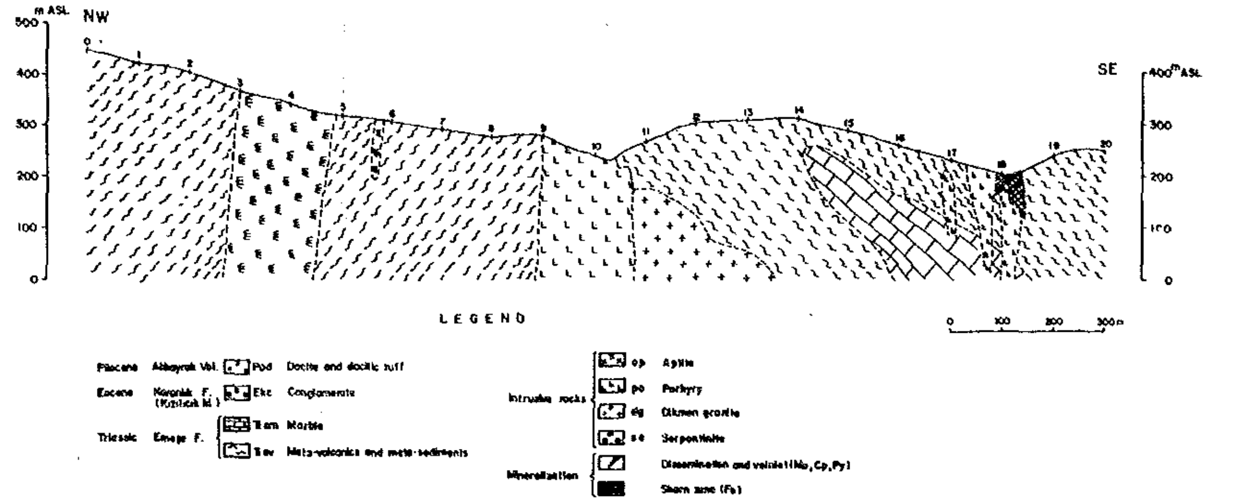


DIPOLE-DIPOLE APPARENT RESISTIVITY PROFILE

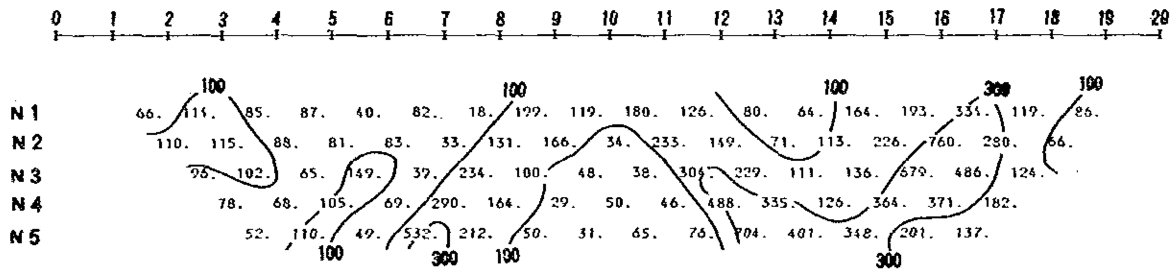


observed Apparent Resistivity

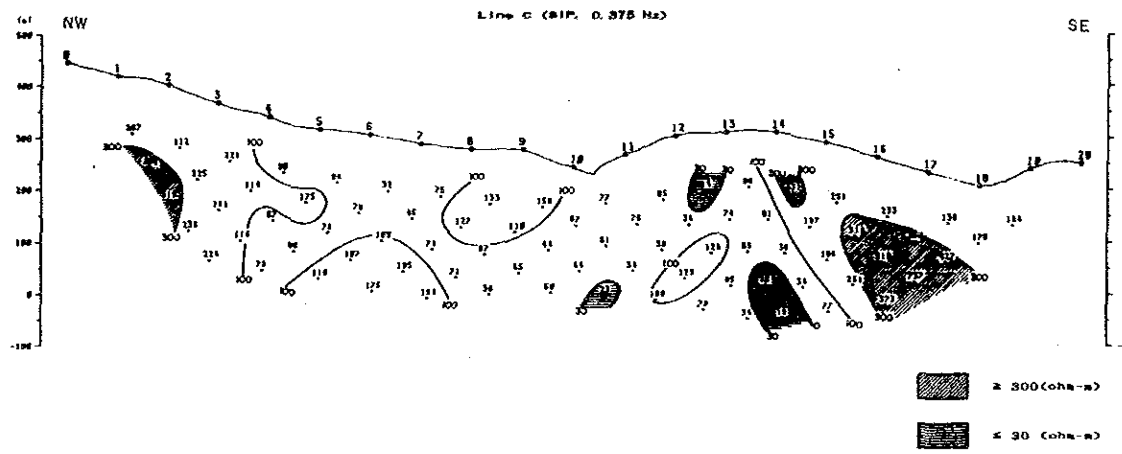


DIPOLE-DIPOLE APPARENT PERCENT FREQ. EFFECT

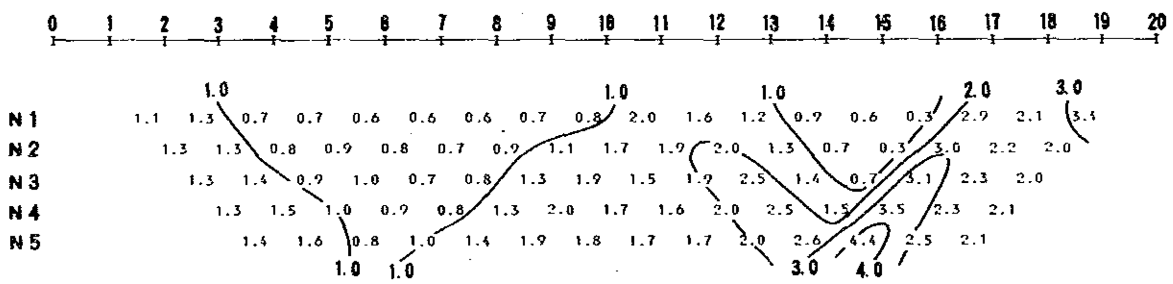


observed PFE

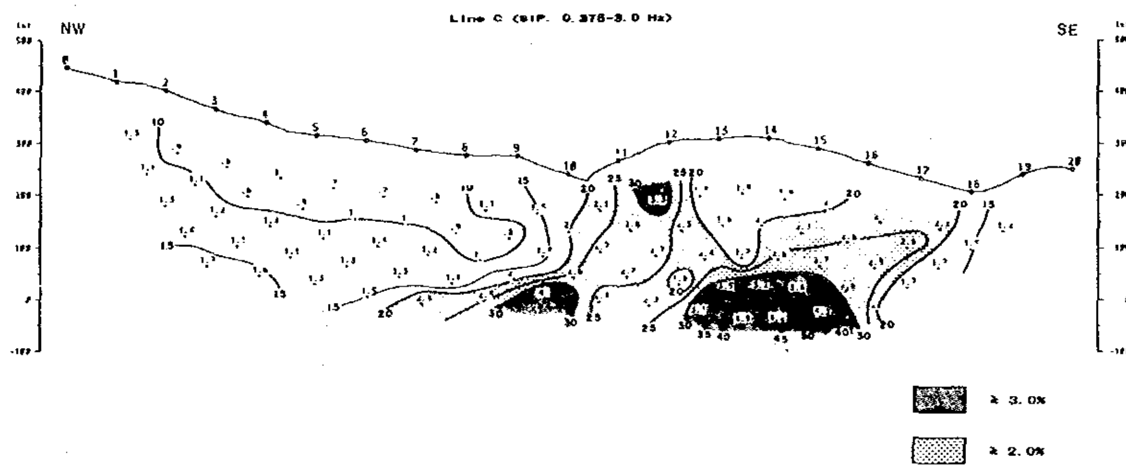


Fig. 6-29 Result of Model Simulation (Line C)

Simulation model

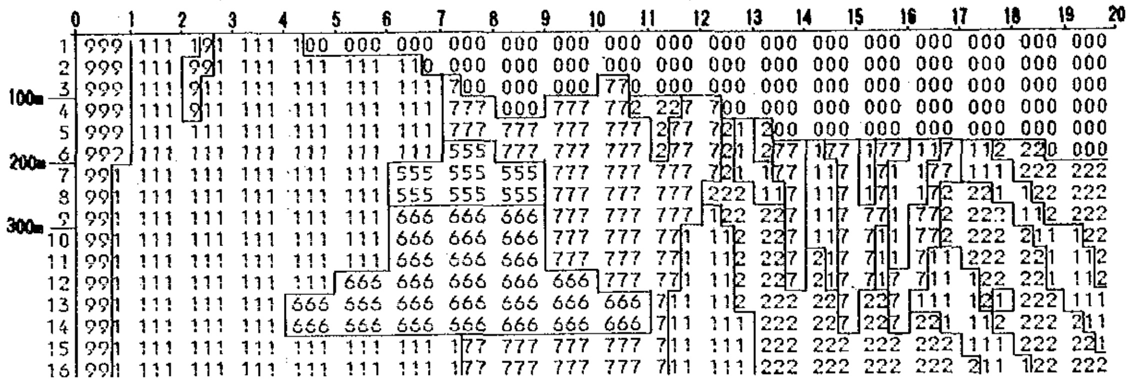

| CODE | RESISTIVITY OHM-M | F.E. % |
|---|---|---|
| 1 | 100. | 1.0 |
| 2 | 5000. | 1.7 |
| 3 | 0. | 0. |
| 4 | 0. | 0. |
| 5 | 150. | 3.0 |
| 6 | 200. | 6.0 |
| 7 | 500. | 1.5 |
| 8 | 0. | 0. |
| 9 | 80. | 0.5 |

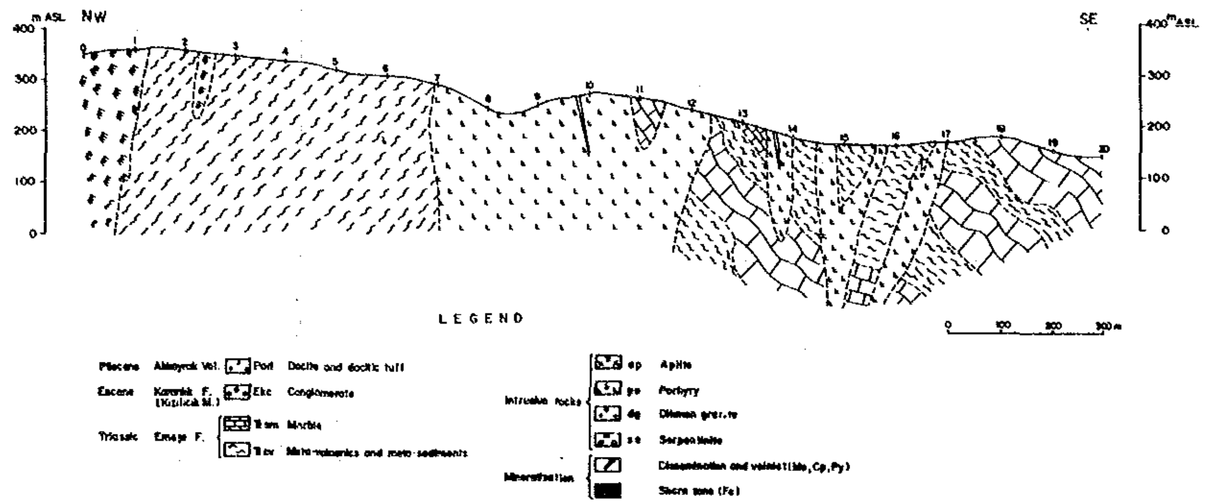

DIPOLE-DIPOLE APPARENT RESISTIVITY PROFILE

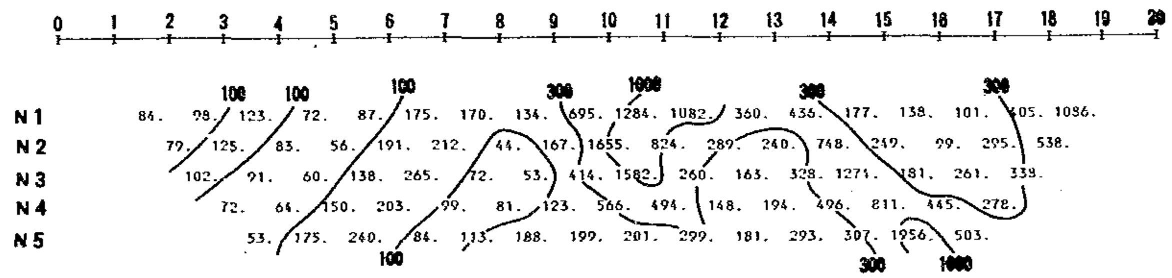

observed Apparent Resistivity

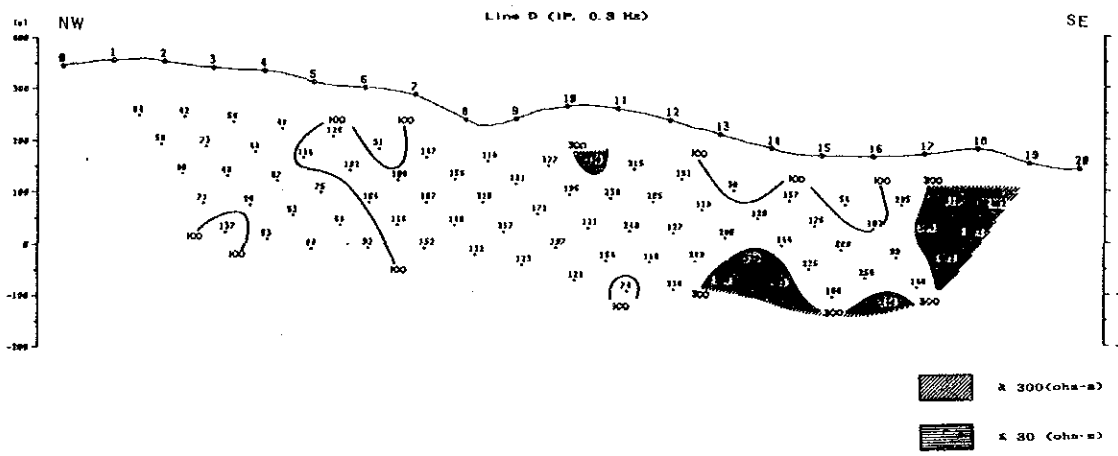

DIPOLE-DIPOLE APPARENT PERCENT FREQ. EFFECT

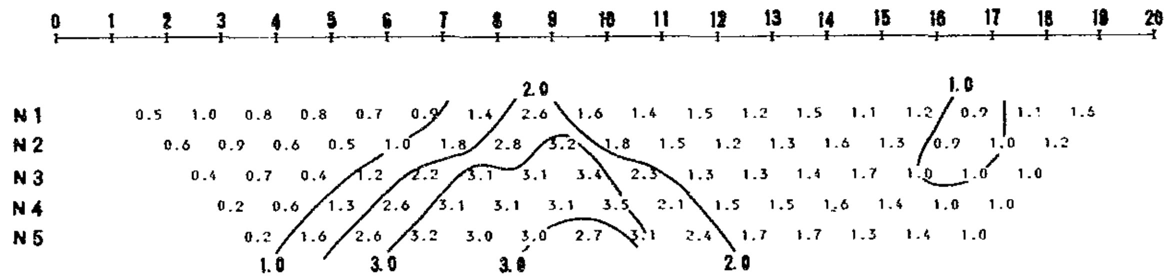

observed PFE

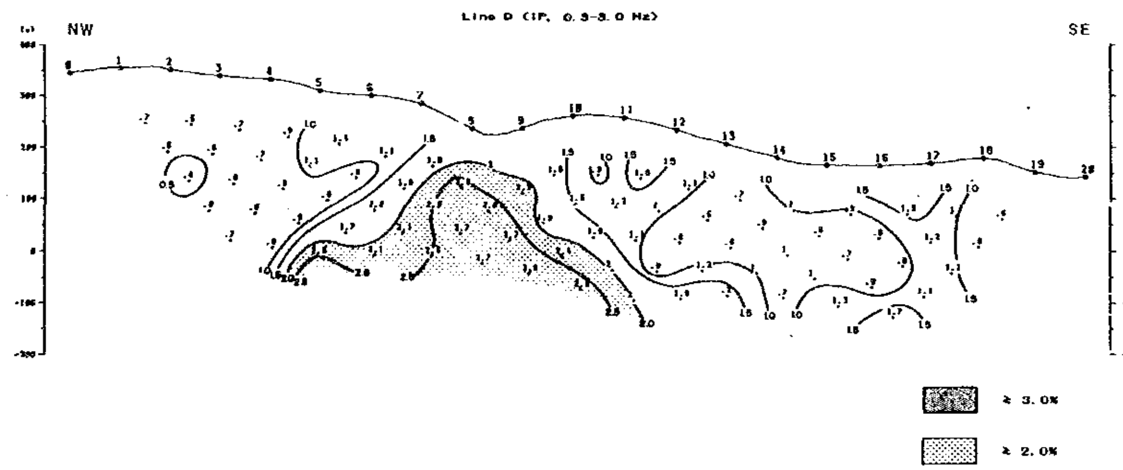

Fig. 6-30 Result of Model Simulation (Line D)

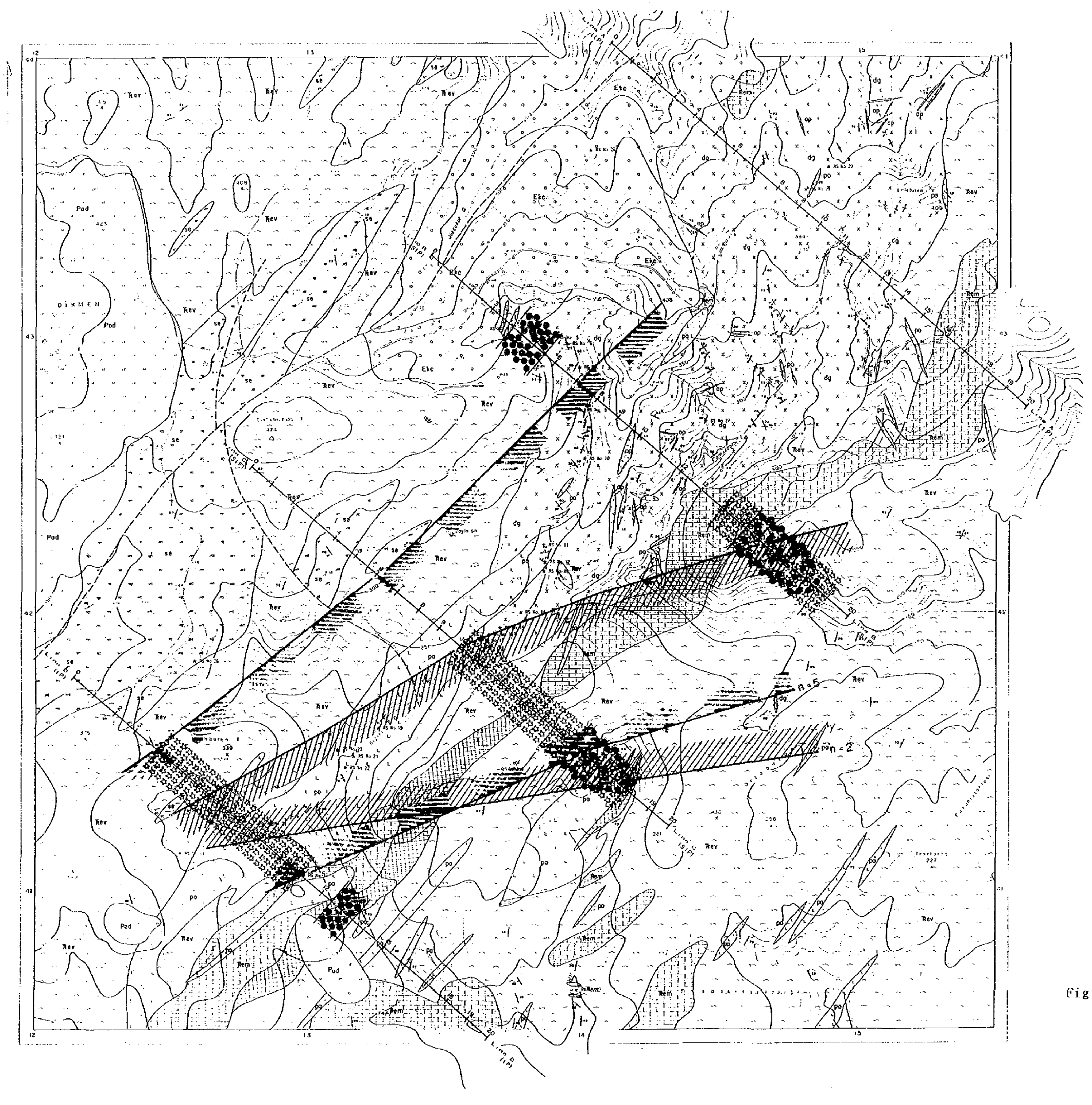


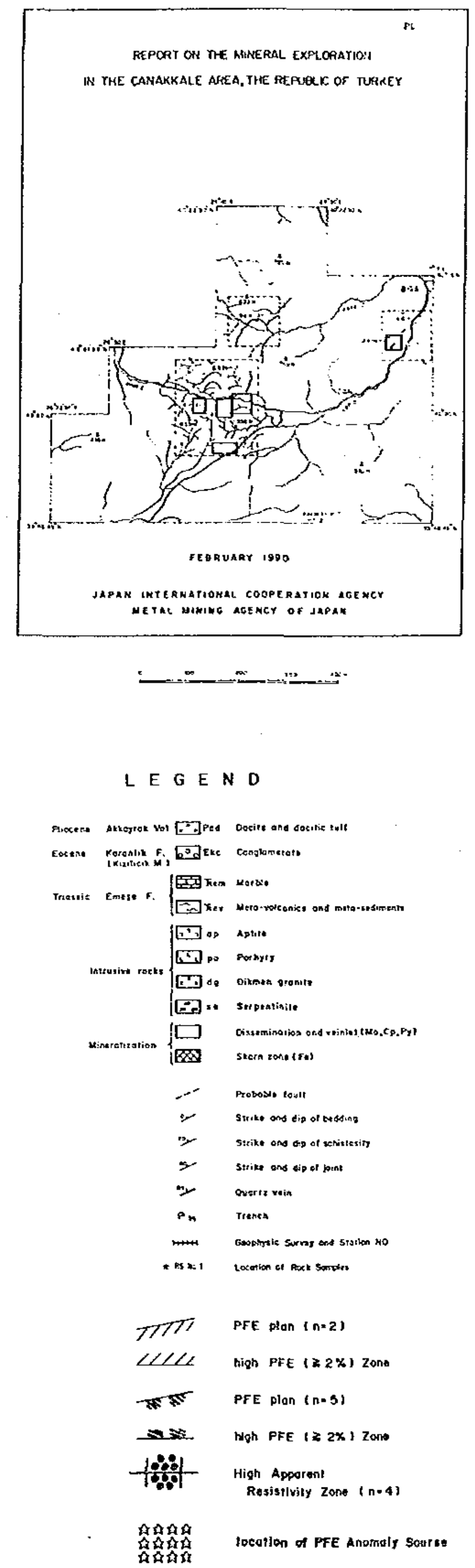


Fig. 6-31 Geophysical Interpretation Map in the Dikmen Area

## CHAPTER 6 DISCUSSION

### 6-1 Alteration Zones

A porphyry molybdenum-copper deposit associated with the intrusion of the Dikmen Granite and porphyries was discovered. The mineralization extends from the eastern side of the Dikmen Granite which extends in a NE-SW direction to the Emeşe Formation in the Sıġırirek Stream. The Dikmen Granite and porphyries which are distributed along the Sıġırirek Stream and the upstream section of Domuzdamı occur with the same direction as the Dikmen Fault. Sericitization is intense in Dikmen Granite and porphyries near porphyry molybdenite mineralization zones.

The gold mineralization found in the silicified zones of NEN-SWS direction is partially observed in the northern part of Sıġırirek Stream within the Emeşe Formation, and the silicified rocks are accompanied by quartz veinlets within the Dikmen Granite and porphyries. Auriferous localities gradually are increasing with the advance of geochemical prospecting. Generally, Kaoline is detected where gold mineralization is found.

The rocks are decloured white at Sıġırirek, and minor amounts of sulfide minerals such as molybdenite, chalcopyrite, sphalerite and pyrite occur associated with the quartz veinlets. Although invisible under the microscope, analysis (Tables 1-3 and 1-4) shows the existence of gold, arsenic, and mercury. Sericite and kaoline were identified by X-ray diffraction, indicating epithermal activity after the porphyry mineralization. The two mineralizations could be overlapping.

The porphyry mineralization extends to the lower horizons and this is expected to be a low-grade large-scale deposit. This deposit locally contains gold, silver and antimony. If gold could be found to be contained in significant amounts in the overlapped part, this would be a important future target.

### 6-2 Mineralization of the Deeper Zone

As a result of geophysical prospecting, PFE anomalies were found to be extensive downward in the eastern part of the Dikmen granite and porphyries which extend in the Sıġırirek Stream with a NE-SW direction. Therefore, it is considered that mineralization of the deeper zone extends downward from the surface with southeast dip.

By geophysical methods, the subsurface extent of mineralization from the outcrop downward was shown by delineating the low resistivity zone and FE anomalies by IP, then detailed SIP work has been provided the promising section by the interpretation of simulations.

## 6-3 Relationship between Gold and Mo-Cu Mineralization

A porphyry molybdenum-copper deposit associated with the intrusion of the Dikmen Granite and porphyries was discovered. The mineralization extends from the eastern side of the Dikmen Granite which extends in a NE-SW direction to the Emeşe Formation in the Sığırirek Stream. Molybdenite and pyrite are traced in the Sığırirek Stream within the granodiorite as disseminations, as strains along fractures and cracks, and in quartz veins as grains or groups of grains and veinlets.

On the other hand, the silicified zones with NEN-SWS direction are partially observed in the northern part of Sığırirek Stream within the Emeşe Formation. Silicification especially is traced within the metamorphosed volcanics and sedimentary rocks of the Emeşe Formation. Gold, silver, molybdenum, lead and mercury content is high in this zone. Also, the auriferous rocks were detected in the chip samples which were collected from the silicified rocks accompanied by quartz veinlets within the Dikmen granite and porphyries.

The porphyry molybdenum deposit mentioned above is expected to be a large-scale low-grade deposit as this type of mineralization is extensive in the lower portions. It contains gold, silver and antimony locally, and it may turn out to be a very important target if significant gold is found in the overlapping portion.

# CHAPTER 7 CONCLUSIONS AND RECOMMENDATIONS

## 7-1 Conclusions

Geophysical prospecting was carried out together with a detailed geological survey and geochemical prospecting. The detailed geological survey has clarified the distribution and conditions of gold occurrence, argillized zones and skarnization. The geochemical work has revealed two types of mineralization. By geophysical methods, the subsurface extent of mineralization from the outcrop downward was shown by delineating the low-resistivity zone and FE anomalies by IP; detailed SIP work provided the promising section by the interpretation of simulations.

A porphyry molybdenum-copper deposit associated with the intrusion of the Dikmen Granite and porphyry was discovered. The mineralization extends from the eastern side of the Dikmen Granite which extends in a NW-SE direction to the Emeşe Formation in the Sıgırirek Stream. The Emeşe Formation is altered, and minor amounts of sulfides such as molybdenite, chalcopyrite, wolframite, sphalerite and pyrite occur in the quartz veinlets. The analytical results show the existence of gold, arsenic, mercury and antimony. This shows that epithermal mineralization occurred after the porphyry molybdenum mineralization, and they now overlap spatially.

The porphyry molybdenum deposit above-mentioned is expected to be a large-scale low-grade deposit as this type of mineralization is extensive at depth. It contains gold and antimony locally and may turn out to be a very important target if significant gold is found in the overlapping portion.

## 7-2 Recommendations for the Third Phase

Geophysical prospecting was carried out along with detailed geological survey and geochemical prospecting. By geophysical methods, the subsurface extent of mineralization from the outcrop downward was shown by delineating the low-resistivity zone and FE anomalies by IP; detailed SIP work provided the necessary information. Drill survey should be conducted in the mineralized zone of the localities distributed in the Dikmen Granite and porphyry.

# PART Ⅶ CONCLUSIONS AND RECOMMENDATIONS

# PART VII CONCLUSIONS AND RECOMMENDATIONS

## CHAPTER 1 CONCLUSIONS

During the second phase, geological and geochemical surveys were conducted in the Arlık Stream, Karaibrahimler, Kestane Mountain, Piren Hill and Dikmen Areas. Further geophysical prospecting was carried out in the Dikmen, and drill survey in the Arlık Stream and Piren Hill. Compiled maps of those areas were shown Figures 1-15 and 1-16, list of geological and geochemical characteristics in the Table 1-13, summary of five areas are as follows:

Table 1-13 List of Geological and Geochemical Characteristics

| Characteristics of Geology and Geochemistry | Survey Area | | | | |
|---|---|---|---|---|---|
| | Arlık Dere | Karaib-rahimler | Kestane Dagı | Piren Tepe | Dikmen |
| Type of Mineralization | Epithermal Type | | | | Porphyry Mo |
| Country Rock of Ore Horizon | Şapçı Volcanics | | | | Dikmen G. Porphyry |
| Clay Minerals | Kaoline, alunite, pyrophyllite | | | | Sericite |
| Silicified Zone:Massive | ○ | × | ○ | ○ | – |
| Vein | ○ | ○ | × | ○ | ○ |
| Scale($km^2$) | 1.5 | – | 0.8 | 4.7 | – |
| Number of Samples (N) | 282 | 98 | 140 | 207 | 269 |
| Au (max) ppb | 3050 | 490 | 3660 | 2060 | 4600 |
| Au (average) ppb | 14 | 7 | 13 | 7 | 6 |
| Mo (average) ppm | 4 | 2 | 3 | 5 | 7 |
| Number of Samples more than 50 ppb(A) | 68 | 14 | 35 | 32 | 56* |
| Frequency (A/N)% | 24 | 14 | 25 | 15 | 21 |
| Heavy Mineral Study | ● | ● | – | ● | – |
| Detection of Gold Grains | common | abundant | – | few | – |
| Potential | high | low | high | high | high |

*:Including sample more than 100ppm Mo
○ : predominant × : not observed ● : collected samples

(1) Arlık Dere: Silicified and argillized zones occur in Şapçı Volcanics and part of Kirazlı Conglomerate. The Kocataş silicified zones occurring in Şapçı Volcanics were evident to 100m in MJTC-5 and 6, after which Kirazlı Conglomerate was intersected, but the SartaŞ silicified zones continued for at least 150m in MJTC-4. Altered zones with limonite are predominant on the outcrops, but pyrites are not observed. Of the results of the drill survey, the following are significant: fine-grained pyrites are developed in the section underneath the surface, limonitic silicified zones with open spaces (caves) were found by drill hole MJTC-4 and the low-grade auriferous zones continued from near surface to bottom in hole MJTC-4. Therefore, it is

considered that the potential of gold deposits is high.

Generally, auriferous mineralization in the silicified body did not extend further downward, and silicified veins were observed in the periphery of the silicified zones. Thus it is considered that their shapes are "jellyfish-like" in geologic section.

(2) Karaibrahimler: The Şapçı Volcanics and Kirazlı Conglomerate have suffered hydrothermal alteration in the vicinity. Altered zones with limonite and hematite are predominant on the outcrops, and pyrites are rarely observed because of oxidation. It is considered that the Şapçı Volcanics becomes thin because of proximity to the basement rocks. Silicified veins occur in Şapçı Volcanics and Kirazlı Conglomerate and are exposed rock from lower levels of the formation after erosion of the upper levels.

(3) Kestane Dağı: The Şapçı Volcanics and Kirazlı Conglomerate have suffered hydrothermal alteration in this vicinity. In particular, the Şapçı Volcanics have suffered strong silicification and argillization. Altered zones with limonite and hematite are predominant on the outcrops, and pyrites are usually not observed due to oxidation. Silicified bodies which form the hills consist of massive, porous and brecciated parts. Silicified veins were not observed in the periphery of silicified bodies. Thus it is considered that their shapes are "mushroom-like" in geologic section.

(4) Piren Tepe: The geology consists of Şapçı Volcanics in this vicinity. The original rocks cannot be distinguished in the altered zones. The volcanic rocks become thick with distance from the geologic basement. Altered zones with limonite and hematite are predominant on the outcrops, and pyrites are not observed because of oxidation.

Gold anomalies were detected in the silicified zones located in the southern part of the large alteration zone. The zones extend in an E-W direction in the vicinity of Piren Hill. The auriferous zones, which occur in limonitic clay such as those in fault zones, were detected by drill hole MJTC-2. Silicified zones are considered to be "jellyfish-shaped" in geologic section.

(5) Dikmen: Geophysical prospecting was carried out together with a detailed geological survey and geochemical prospecting. The detailed geological survey has clarified the distribution and conditions of gold occurrence, argillized zones and skarnization. The geochemical work has revealed two types of mineralization. By geophysical methods, the subsurface extent of mineralization from the outcrop downward was shown by delineating the low-

resistivity zone and FE anomalies by IP; detailed SIP work provided the promising section by the interpretation of simulations.

A porphyry molybdenum-copper deposit associated with the intrusion of the Dikmen Granite and porphyry was discovered. The mineralization extends from the eastern side of the Dikmen Granite which extends in a NW-SE direction to the Emeşe Formation in the Sığırirek Stream. The Emeşe Formation is altered, and minor amounts of sulfides such as molybdenite, chalcopyrite, wolframite, sphalerite and pyrite occur in the quartz veinlets. The analytical results show the existence of gold, arsenic, mercury and antimony. This shows that epithermal mineralization occurred after the porphyry molybdenum mineralization, and they now overlap spatially.

The results of the second phase work summarized above in (1)～(4), indicate the possibility of large-scale low-grade gold deposits in the alteration zone near the basement rocks. The porphyry molybdenum deposit mentioned in (5) also is expected to be a large-scale low-grade deposit as this type of mineralization is extensive at depth. It locally contains gold and antimony, and it may turn out to be a very important target if significant gold is found in the overlapping portion.

## CHAPTER 2 RECOMMENDATIONS FOR THE THIRD PHASE

It is recommended that the following work be conducted in the promising areas delineated above (Figure 1-17).

In the four localities of Zone B, epithermal gold mineralization is anticipated because of the gold showings of the alteration zones which were identified by geological and geochemical surveys. The hydrothermal gold mineralization is expected to extend both horizontally and vertically. Here, detailed geological survey clarified the distribution and extent of the alteration zone and heavy mineral investigation in the vicinity located the position of the gold mineralization. On the basis of these findings, inclined drilling should be carried out in order to clarify the state of subsurface mineralization.

Arlık Dere: The auriferous zones have been detected in Kocataş, Sartaş and Güvemalanı Hills; these localities belong to the concession of MTA. The drilling survey should be continued in these localities because the auriferous zones were intersected by drill hole MJTC-4.

Karaibrahimler: The silicified zones were not predominant because the upper portions of altered zones had been eroded. As the possibility of detection of gold deposits is low, the survey should be completed with the second phase.

Kestane Dağı: The concession of the Kestane Mountain area has been purchased by Tüprag Co. has its head office in Istanbul and which has commenced joint exploration with a private West German company. Geochemical prospecting (soil sampling and trench) and geophysical survey (resistivity method) was carried out in 1989. Therefore, the survey should be completed with the second phase.

Piren Tepe: Gold anomalies were detected in the silicified zones which are located in the southern part of the large alteration zone. Also, the zone extends in an E-W direction in the vicinity of the Piren Tepe. The auriferous zone was found by drill hole MJTC-2 in the Davulgılı silicified zones belonging to the concession of MTA. During the third phase, drilling survey should be carried out in the southeastern part of the Piren silicified zones

Dikmen: Geophysical prospecting was carried out along with detailed geological survey and geochemical prospecting. By geophysical methods, the subsurface extent of mineralization from the outcrop downward was shown by delineating the low-resistivity zone and FE anomalies by IP; detailed SIP work provided the necessary information. Drill survey should be conducted in the mineralized zone of the localities distributed in the Dikmen Granite and porphyry.

Etili: Etili locates in the southeast area of Zone B. Silicified zones are predominant in the Şapçı Volcanics which are widely distributed in the vicinity. A hot spring near Etili village has been used as a bath for medical purposes. Gold grains have been detected in the soil samples collected from nearby the hot spring (Table 6 of Appendix). Etili Area is considered to be a promising area, and a drill survey should be carried out after the geological survey and geochemical prospecting.

## REFERENCES


Abe,I., Suzuki,H., Isogami,A. and Goto,T.(1986):Geology and Development of the Hishikari Mine, Mining Geology, Vol.36, p.117-130 (in Japanese with English abstract).

Behçet Akyürex and Yılmaz Soysal(1980):Biga Yarımadası ve Güneyinin -1/100,000 Ölçekli Kompilasyonu, Report of MTA(unpublished).

Dey,A.and Morison,H.F.(1973) : Electromagnetic coupling in frequency and time domain induced polarization surveys over multilayered earth, Geophysics, Vol. 38, P.380-405.

ERSDAC(1988):ERSDAC-In Search of Mineral Wealth of the Mother Earth from Space-Earth Resources Satellite Analysis Center(ERSDAC), p.16

Hayba,D.O., Bethke,P.M., Heald,P. and Foley,N.K.(1985):Geologic, Mineralogic, and Geochemical Characteristics of Volcanic-Hosted Epithermal Precious-Metal Deposits, Geology and Geochemistry of Epithermal Systems, Vol.2, p.129-167

Hallof,P.G.and Pelton,W.H.(1980):The removal of inductive coupling effects from spectral IP data,.SEG.50th Annual International Meeting in Houston

Hallof P.G. and Klein,J.D.(1982) : Electrical parameters of volcanogenic mineral deposits,.S.E.G.52nd Annual International Meeting

Hedenquist,J.W.(1987) : Mineralization associated with volcanic-related hydrothermal systems in the Circum-Pacific Basin. In Transactions of the Fourth Circum Pacific Conference on Energy and Mineral Resources.

Higgs,R.(1962):Kartaldag Gold Prospect, Çanakkale(memorandum).

Henley,R.W.(1985):The Geothermal Framework of Epithermal Deposits, Geology and Geochemistry of Epithermal Systems, Vol.2, p.1-24

Hohmann,G.W.(1973): Electromagnetic coupling between grounded wires at the surface of a two layered earth, Geophysics, Vol.38, P.854-863

Ishihara,S.(1977):The magnetite-series and ilmenite-series granitic rocks, Mining Geology,27, p.293-305

Ishihara,S.(1986):Gold Deposits of Philippines, Type and Model of Ore Genesis, Geology News, No.384, p.6-21 (in Japanese).

Izawa,E.(1985) : Alteration Zone and Clay Mineral of Epithermal Gold-Silver Deposits, Discussion on Geothermal System, Special Issue, Gold-silver Ore of the Japan, No.3, The Mining and Metallugical Institute of Japan, p.133-154 (in Japanese)

Izawa,E.(1986) : Symposium on Mineral Deposit Modeling(Manila)-with special reference to models for hydrothermal gold deposits., Mining Geology, Vol.36, p.237-241 (in Japanese).

Mason,B.(1966):Principle of geochemistry(third edition), John Wiley & Sons,

Inc. New York.
Matsushita,Y.(1987):Gold Deposit of Hot Spring Type and Geothermal System, Geology News, No.390, p.20-43 (in Japanese).
Maucher,A.(1960):Report on Gold Occurrence in Çanakkale(memorandum).
MMAJ(1986) : Gold Deposits of the World, Information Center of Metal Mining Agency of Japan, p.65-109 (in Japanese).
MMAJ・ERSDAC(1986) : Report on Research and Development of Remote Sensing Technology for Natural Resources Satellite Data Analysis, Metal Mining Agency of Japan(MMAJ) and Earth Resources Satellite Analysis Center (ERSDAC), p.76-94 (in Japanese).
Molly,E.W.(1958):Türkiye batısı altın mineralizasyonu(memorumdum).
MTA(1964):Iron Ore Deposits of Turkey, No.118
MTA(1965):Barite and Fluorite Deposits of Turkey, No.126
MTA(1965):Tungsten and Molybdenum Deposits of Turkey, No.128
MTA(1970):Arsenic, Mercury, Antimony and Gold Deposits of Turkey, No.129
MTA(1970):TÜRKIYE METALOJENİSİ, 1:2,500,000 Ölçekli Türkiye Metalolenik Haritasının İzahı, No.144
MTA(1972):Lead, Copper and Zinc Deposits of Turkey, No.133
Nagasawa,K.(1981):Characteristic Clay Minerals occurred in Gold-silver Deposits, Mining Geology, Special Issue, No.10, p.227-233 (in Japanese)
Pelton,W.H.,Ward,.S.H., Hallof, P.G., Sill,W.R., and Nelson,P.H.(1978) : Mineral discrimination and removal of inductive coupling with Multifrequency IP, Geophysics, Vol.43,P.598-609
Shikazono,N.(1981) : The Chemical Compositions and These Factor of Control of Electrum occurred in Black Ore Deposits and Epithermal-type Vein Deposits, Mining Geology, Special Issue, No.10, p.259-267 (in Japanese with English abstract).
Shoji,T(1986) : Relation with Gold-silver Vein Deposits and Adularia, Special Issue, Gold-silver Ore of the Japan, No.3, The Mining and Metallugical Institute of Japan, p.113-132
Takeda,H.& Imamura,R.(1979) : Photogeological Interpretation for Construction Engineer, Kyouritsu Shuppan, p.72
Turhan,A.(1968):Çanakkale H17-$C_1$ nolu paftanın, Koru-Balcılar Köyleri civarının jeoloji etüdü(unpublished).
Urabe,T(1985):Gold Deposits in the state of Nevada, their type and model, Geology News, No.373, p.25-37 (in Japanese).
Urashima,Y., Saito, M. and Sato,H.(1981) : Iwato Gold Deposits, Special Issue of Mining Geology, No.10, p.1-14 (in Japanese with English abstract).
Wakimoto,K., Tarumizu,K. and Tanaka,Y(1984) : Statistic Interpretation using personal Computer, Kyouritsu Shuppan, p.160-175 (in Japanese).

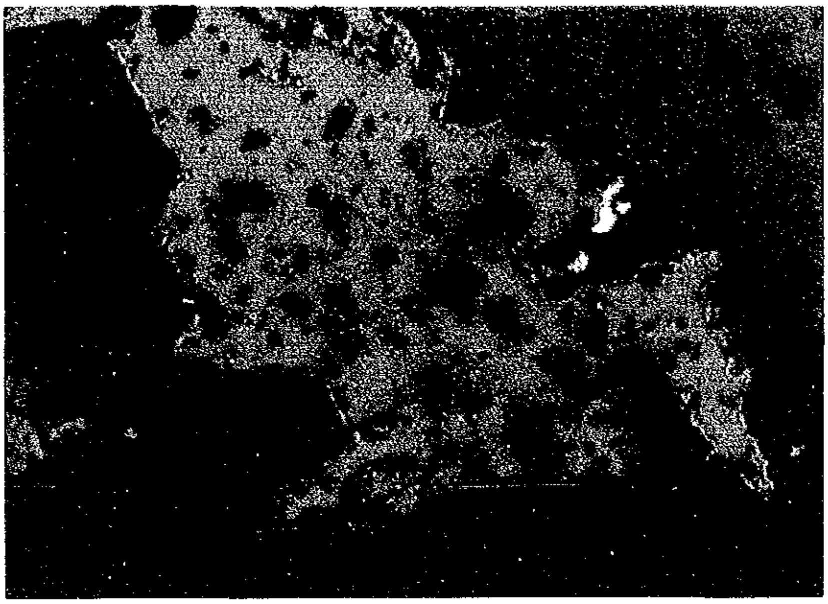

Sample No. : K382
Locality : Dikmen
Rock Name : Cu-Pb ore

Sp : sphalerite
Co : covelline
Qz : quartz

0 0.3mm

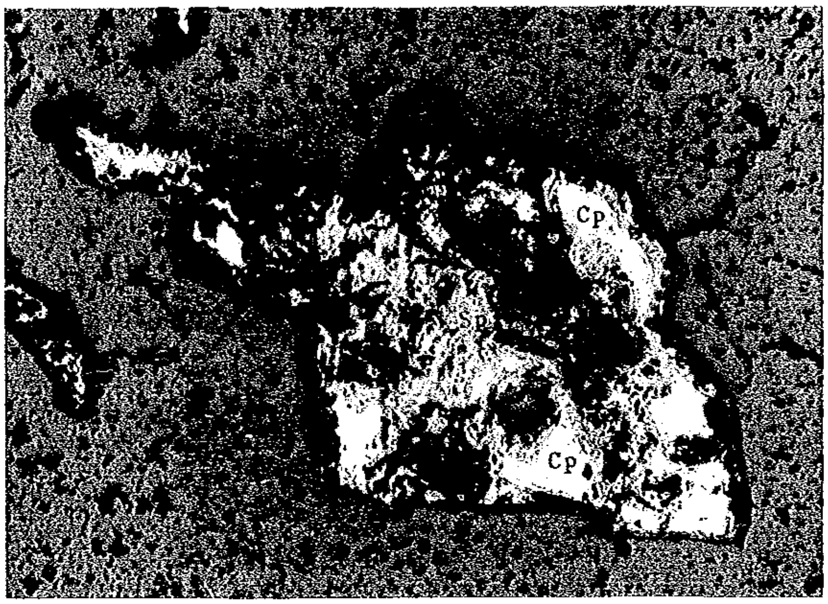


Sample No. : M363
Locality : Dikmen
Rock Name : Mo-Py ore

Sp : sphalerite
Cp : chalcopyrite
Co : covelline
Qz : quartz

0 0.3mm


Sample No. : T358
Locality : Dikmen
Rock Name : Cu ore

Sp : sphalerite
Py : pyrite
Qz : quartz

0 0.3mm

Photo. 1 Microscopic photograph (Polished Section)

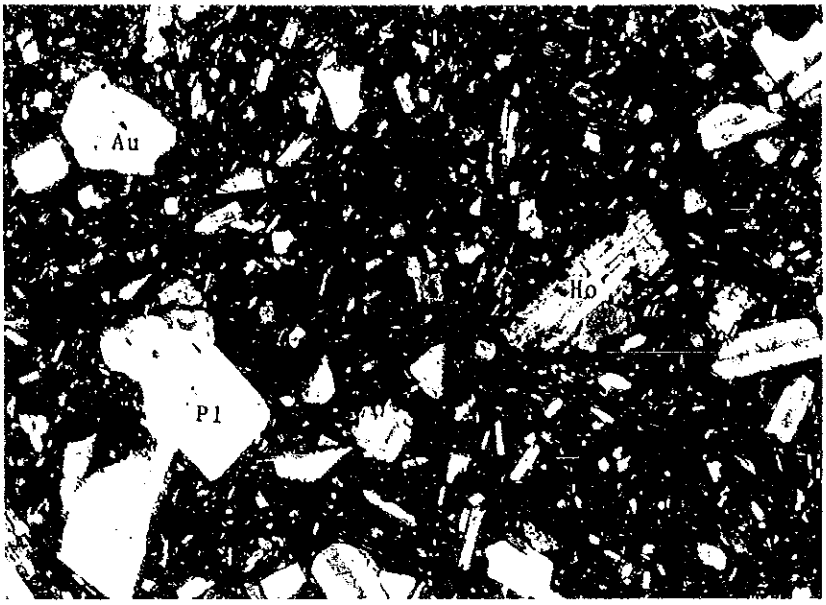


Sample No. : S405
Locality : Arlık Dere
Rock Name : Andesite
(Şapçı Volcanics)

Au : augite
Ho : hornblende
Pl : plagioclase

0 0.1mm

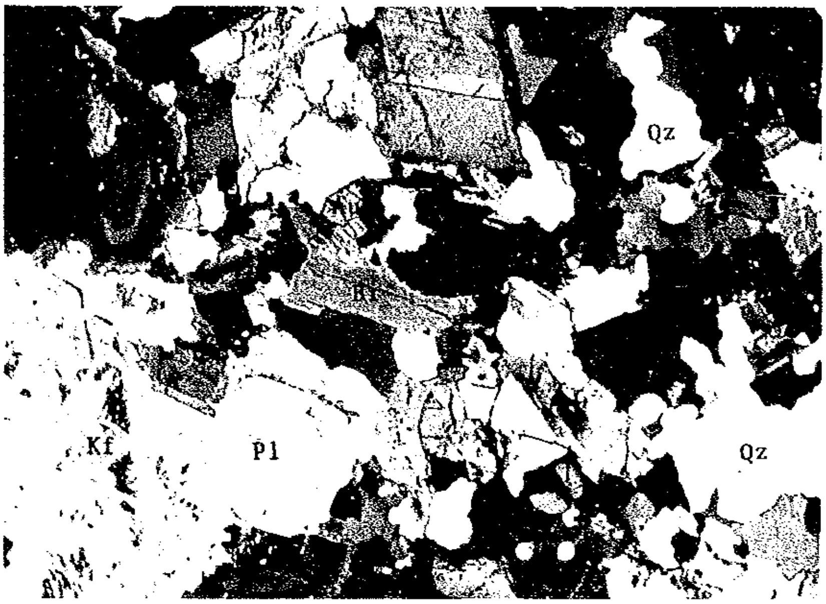


Sample No. : Y309
Locality : Dikmen
Rock Name : Granodiorite

Au : augite
Bi : biotite
Pl : plagioclase
Kf : potashic feldspar
Qz : quartz

0 0.1mm

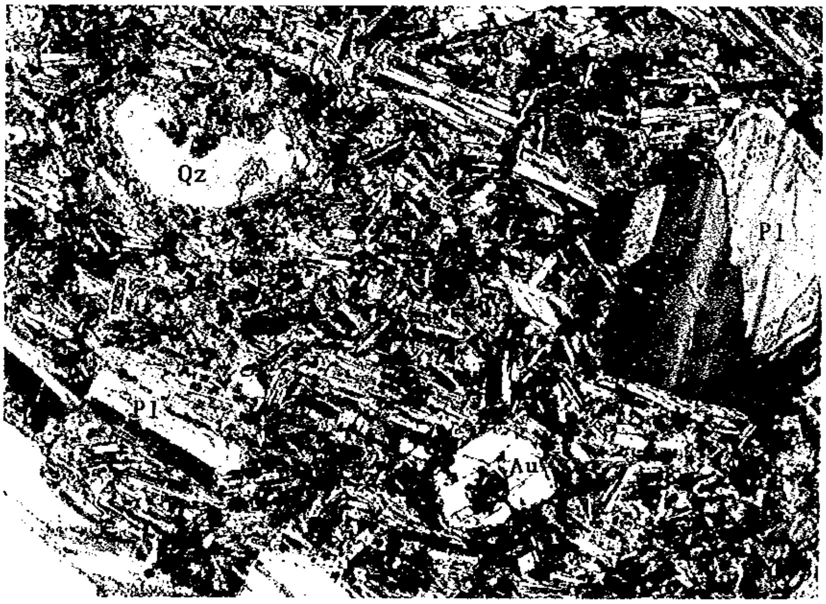


Sample No. : 156
Locality : MJTC-1,126mm
Rock Name : Andesite
(Şapçı Volcanics)

Au : augite
Qz : quartz
Pl : plagioclase

0 0.1mm

Photo. 2 Microscopic photograph (Thin Section)